AFWAL-TR-80-4052

(2) LEVEL II

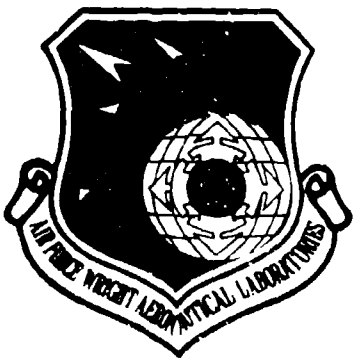

TIME-DEPENDENT ENVIRONMENTAL BEHAVIOR OF GRAPHITE/EPOXY COMPOSITES

K. G. KIBLER
GENERAL DYNAMICS CORPORATION
P. O. BOX 748
FORT WORTH, TX 76101

MAY 1980

TECHNICAL REPORT AFWAL-TR-80-4052
Final Report for period 1 August 1977 – 31 January 1980

Approved for public release; distribution unlimited.

MATERIALS LABORATORY
AIR FORCE WRIGHT AERONAUTICAL LABORATORIES
AIR FORCE SYSTEMS COMMAND
WRIGHT-PATTERSON AIR FORCE BASE, OHIO 45433

NOTICE

When Government drawings, specifications, or other data are used for any purpose other than in connection with a definitely related Government procurement operation, the United States Government thereby incurs no responsibility nor any obligation whatsoever; and the fact that the government may have formulated, furnished, or in any way supplied the said drawings, specifications, or other data, is not to be regarded by implication or otherwise as in any manner licensing the holder or any other person or corporation, or conveying any rights or permission to manufacture, use or sell any patented invention that may in any way be related thereto.

This report has been reviewed by the Office of Public Affairs (ASD/PA) and is releasable to the National Technical Information Service (NTIS). At NTIS, it will be available to the general public, including foreign nations.

This technical report has been reviewed and is approved for publication.

J. M. Whitney

J. M. WHITNEY, Project Engineer
Mechanics & Surface Interactions Br.
Nonmetallic Materials Division

S. W. Tsai

S. W. TSAI, Chief
Mechanics & Surface Interactions Br.
Nonmetallic Materials Division

FOR THE COMMANDER

F. D. Cherry

F. D. CHERRY, Chief
Nonmetallic Materials Division

"If your address has changed, if you wish to be removed from our mailing list, or if the addressee is no longer employed by your organization please notify AFWAL/MLBM, W-PAFB, OH 45433 to help us maintain a current mailing list".

Copies of this report should not be returned unless return is required by security considerations, contractual obligations, or notice on a specific document.

AIR FORCE/56780/26 September 1980 -- 200

(9) Final technical report 1 Aug 77 - 31 Jan 80

SECURITY CLASSIFICATION OF THIS PAGE (When Data Entered)

(19) **REPORT DOCUMENTATION PAGE**

READ INSTRUCTIONS BEFORE COMPLETING FORM

(18) 1. REPORT NUMBER: AFWAL-TR-80-4052 ✓	2. GOVT ACCESSION NO.: AD-A091028
3. RECIPIENT'S CATALOG NUMBER:	
(6) 4. TITLE (and Subtitle): Time-Dependent Environmental Behavior of Graphite/Epoxy Composites	5. TYPE OF REPORT & PERIOD COVERED: Technical - Final 1 Aug. 1977 - 31 Jan 1980
	6. PERFORMING ORG. REPORT NUMBER:
7. AUTHOR(s): (10) K. G./Kibler	8. CONTRACT OR GRANT NUMBER(s): (15) F33615-77-C-5109 NEW
9. PERFORMING ORGANIZATION NAME AND ADDRESS: General Dynamics, P. O. Box 748 ✓, Fort Worth, TX 76101	10. PROGRAM ELEMENT, PROJECT, TASK AREA & WORK UNIT NUMBERS: (16) 2419 03 04 (17) 03
11. CONTROLLING OFFICE NAME AND ADDRESS: (11) Materials Laboratory, Air Force Wright Aeronautical Laboratories, AFSC, Wright-Patterson AFB, OH 45433	12. REPORT DATE: May 1980 (12) 15
	13. NUMBER OF PAGES: 140
14. MONITORING AGENCY NAME & ADDRESS (if different from Controlling Office):	15. SECURITY CLASS. (of this report): Unclassified
	15a. DECLASSIFICATION/DOWNGRADING SCHEDULE:

16. DISTRIBUTION STATEMENT (of this Report)

Approved for public release; distribution unlimited.

17. DISTRIBUTION STATEMENT (of the abstract entered in Block 20, if different from Report)

18. SUPPLEMENTARY NOTES

19. KEY WORDS (Continue on reverse side if necessary and identify by block number)

Composite, Viscoelasticity, Graphite-Epoxy, Time-Dependent Behavior, Polymeric Materials, Time-Temperature-Humidity Superposition, Environmental Creep Testing.

20. ABSTRACT (Continue on reverse side if necessary and identify by block number)

Experimental and analytical investigations have been conducted to determine the individual and combined effects of temperature and absorbed moisture on the time-dependent mechanical response of unidirectional and cross-plied graphite-epoxy composites. Tensile creep response was measured at room temperature and four elevated temperatures (up to the glass transition region of the materials) for dry specimens and for specimens moisture-saturated (continued)

DD FORM 1 JAN 73 1473 EDITION OF 1 NOV 65 IS OBSOLETE

SECURITY CLASSIFICATION OF THIS PAGE (When Data Entered)

at 75% and 95% relative humidity. Results were obtained for two material systems: Narmco T300/5208 and Hercules AS/3502. The stress levels used were demonstrated to be within the range of linear viscoelastic response. Superposition techniques were used to determine compliance master curves from the results for individual temperature and moisture condition, and quasi-elastic conversion was employed to extract relaxation modulus behavior. Expansional strains due to temperature and moisture were measured. From measured principal properties, laminate response was predicted using time-stepped elastic analyses for the environments considered. Analytical procedures for transient and nonuniform temperature and moisture conditions were formulated. An analytical method for minimizing residual stresses during cure was developed, and sample results for the present materials are presented. Observations and recommendations resulting from these investigations are included in this final report.

FOREWORD

This final technical report describes the work performed under Contract No. F33615-77-C-5109, Project No. 2419/0304, from 1 August 1977 to 31 January 1980. The program was sponsored by the Materials Laboratory, Air Force Wright Aeronautical Laboratories, Air Force Systems Command, Wright-Patterson Air Force Base, OH 45433, with Dr. J. M. Whitney, AFWAL/MLBM, as Project Engineer.

Dr. K. G. Kibler, the General Dynamics' Fort Worth Division Program Manager, acknowledges the guidance of Dr. W. G. Knauss (California Institute of Technology), and Drs. R. A. Schapery and Y. Weitsman (Texas A & M University) in this program. Many technical personnel at General Dynamics contributed to this program, including Messrs. T. S. Creasy, J. E. Halkias, J. D. Reynolds, W. S. Robinson, J. H. Fruit, G. W. Matlock, R. L. Jones, E. D. Dawson, W. S. Margolis, J. W. Head, R. L. Ratzlaff, J. R. Eisenmann, F. C. Nordquist, H. C. Hoffman, and Ms. J. R. DeZern.

TABLE OF CONTENTS

TABLE OF CONTENTS (Continued)

LIST OF ILLUSTRATIONS

LIST OF ILLUSTRATIONS (Continued)

LIST OF ILLUSTRATIONS (Continued)

LIST OF TABLES

SECTION I

1. INTRODUCTION

The use of graphite-epoxy composites for aerospace structural applications has evolved as a result of their mechanical properties, such as high strength-to-weight ratio, and their tailorability of design, relative to conventional materials. The composite constituent materials are usually assumed to respond to external inputs in a linearly elastic manner, and this feature is reflected in the common analytical methodologies used. It must be recognized, however, that composites do exhibit a significant amount of time, temperature, and moisture dependent behavior, particularly in service-type environments. In fact, the problem of time influences the behavior of these materials in several ways; e.g., the time of exposure to environment, the age of the material, and the time (duration) of a particular loading condition.

Although much research has been conducted on the viscoelastic behavior of polymers and the particulate-filled composites, only limited investigations on the time-dependence of fibrous composites had been accomplished through 1975 (Ref. 1-7, e.g.) Recent years have witnessed rapidly expanding activities directed more specifically at time-dependent behavior of advanced composite materials systems of particular interest for aerospace applications (Ref. 8-11). These works have established that although the behavior of fibrous composites is in general not linearly viscoelastic, there is often a considerable range of input (temperature, humidity, load) where linear response may at least be a very appropriate approximation.

The overall objective of this program was to determine analytically and experimentally the coupled and uncoupled effects of temperature and absorbed moisture on the time-dependent mechanical properties of unidirectional and laminated graphite-epoxy composites.

The scope of these investigations included experimental creep and stress relaxation measurements on two material systems; the development of analytical methodologies to predict time-

dependent mechanical response; an assessment of the effects of non-uniform moisture distribution on mechanical properties; and the development of an analytical procedure for optimizing cure cycles to reduce residual stress.

The technical investigations to fulfill these objectives were conducted in six interrelated experimental and analytical tasks, which may be briefly described as follows:

- o Specimen Preparation and Baseline Data - fabrication, quality assurance, environmental conditioning of unidirectional and laminated tensile coupons of two material systems; and measurement of tensile stress-strain curves in the principal material directions at room temperature and elevated temperature for specimens dry and with two prescribed moisture contents.

- o Time-Dependent Data - measurement of creep and stress relaxation response in the principal material direction at room temperature and four elevated temperatures for dry specimens and for those conditioned to two prescribed moisture contents, followed by room temperature residual strength tests.

- o Expansional Strains - measurement of longitudinal and transverse expansional strains due to temperature and moisture, including dry and wet glass transition temperature determinations.

- o Analytical Methodology - development of analytical procedures to predict the time-dependent mechanical behavior of laminae and laminates, including the effects of residual stresses.

- o Effects of Non-Uniform Moisture Distribution - experimental and analytical assessment and demonstration of the effects of non-uniform moisture distribution.

- Cure Cycle Optimization - development of an analytical procedure to minimize residual stresses induced during the cure cycle.

These investigations, and their inter-relationships, are schematically outlined in Figure 1.

The present work summarizes these investigations to obtain generic information on the time-dependent mechanical behavior of graphite-epoxy composites used in aerospace structures. Results are presented for two material systems: Narmco T300/5208 and Hercules AS/3502, both presently used in F-16 aircraft production. Experimental and analytical results are described for the individual and coupled effects of temperature and absorbed moisture on the tensile static and creep properties of unidirectional and cross-plied composites. Mechanical response was measured at room temperature and several elevated temperatures (up to the glass transition region of the materials) for dry specimens and for specimens saturated at 75% and 95% relative humidity.

Superposition techniques were used to determine time-temperature-moisture master curves from the results for individual temperature and moisture conditions. These experimental characterizations were then used with conventional or slightly modified analytical techniques to predict time-dependent laminate response, in order to ascertain the magnitude and importance of time, temperature, and humidity effects on structural composites.

Figure 2 briefly summarizes the test environments used for static and creep testing, while Figure 3 demonstrates the overall features of the test/prediction scheme employed.

In the following sections are described the procedures and results for each of the tasks indicated previously in Figure 1.

OBJECTIVE: Determine analytically and experimentally the coupled and uncoupled effects of temperature and absorbed moisture on the time-dependent properties of graphite-epoxy composites.

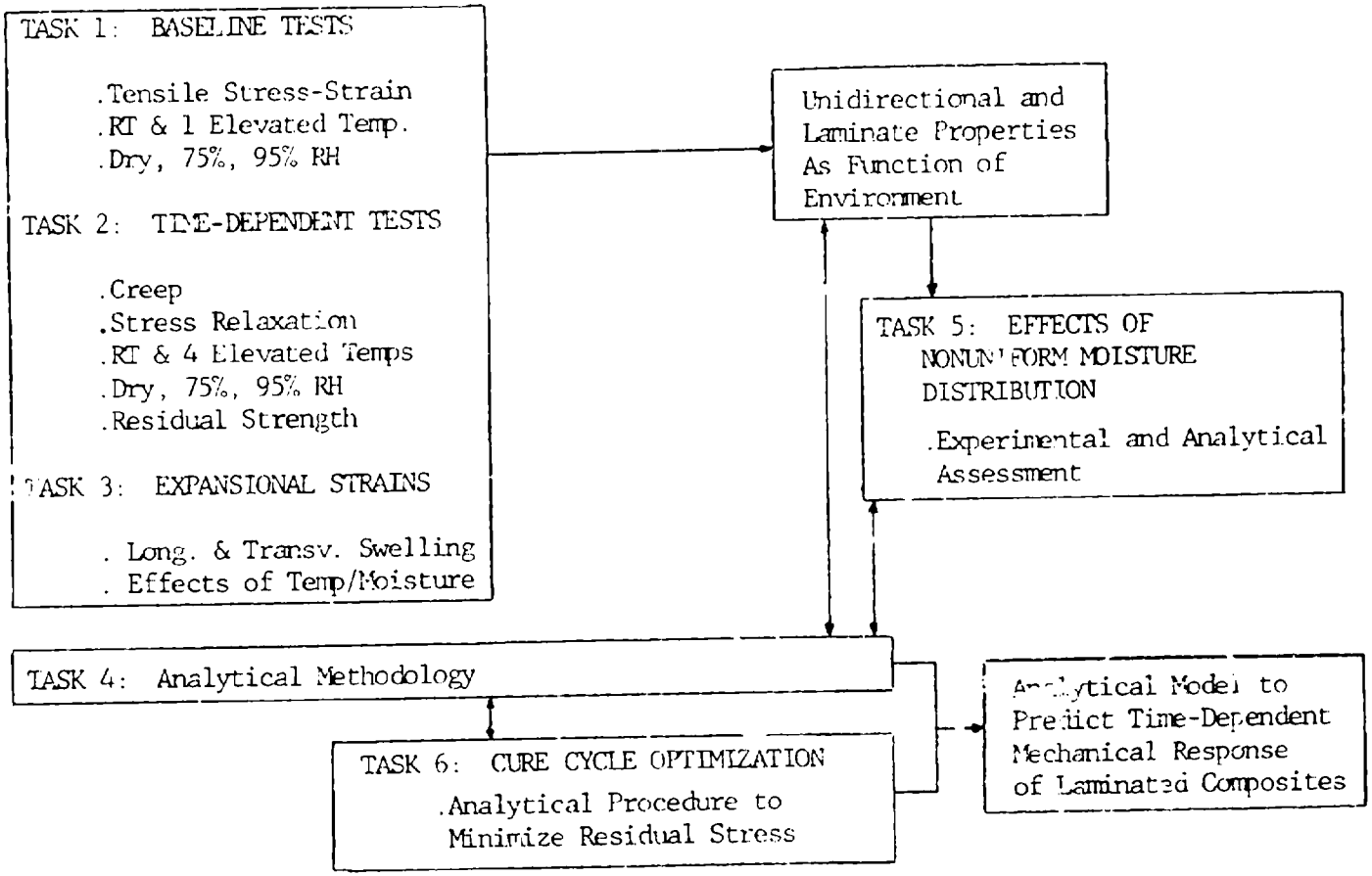

Figure 1. Program Plan

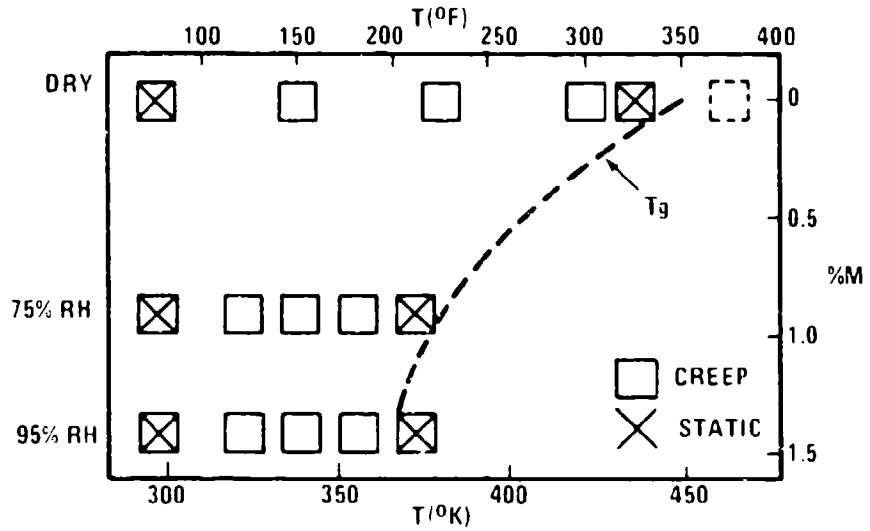

Figure 2 Test Matrix

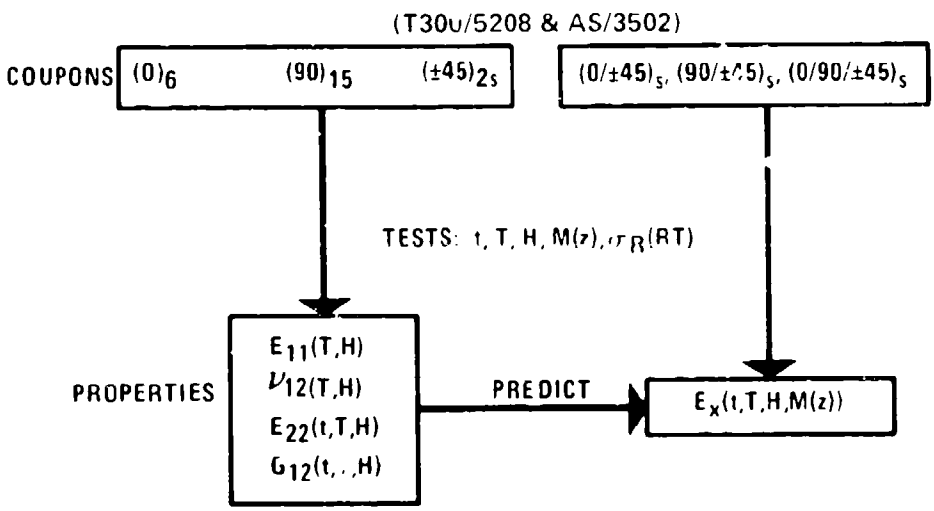

Figure 3 Time-Dependent Tests/Predictions

SECTION II

2. BASELINE DATA

Summary details are provided in this section of the material characteristics; specimen preparation, inspection, and conditioning; and the baseline tensile stress-strain results. Complete baseline tensile data are reported in Appendix A to this report.

2.1 Materials

All experiments performed in this program utilized coupons fabricated from two material systems: T300/5208 (Narmco) and AS/3502 (Hercules). Both materials are currently used by General Dynamics in F-16 production. As will be seen from the results to be presented throughout this report, these materials systems are similar in their physical characteristics and mechanical behavior.

Figure 4 shows a typical liquid chromatographic scan of the two resin systems and demonstrates their similar chemical characteristics. The as-received Hercules material tends to exhibit less of the reaction product than Narmco's material. This suggests that Hercules may use a somewhat greater amount of the high-viscosity minor epoxy and thus does not need to advance the material as far as Narmco does to achieve the same viscosity.

2.2 Specimen Preparation

All specimens and coupons used in this program were accepted, processed, and inspected in accordance with standard General Dynamics' material and processing specification as briefly outlined in Appendix B. Except for thermal- and moisture-expansion specimens and moisture travelers, the coupons were of the designs shown in Figure 5 All coupons mechanically tested were instrumented with 2 axial gages on opposite sides of the specimen as indicated in Figure 5. In each set of replicates for $(0)_6$ and $(\pm 45)_c$ tests, a transverse gage was also used for obtaining Poisson ratio data.

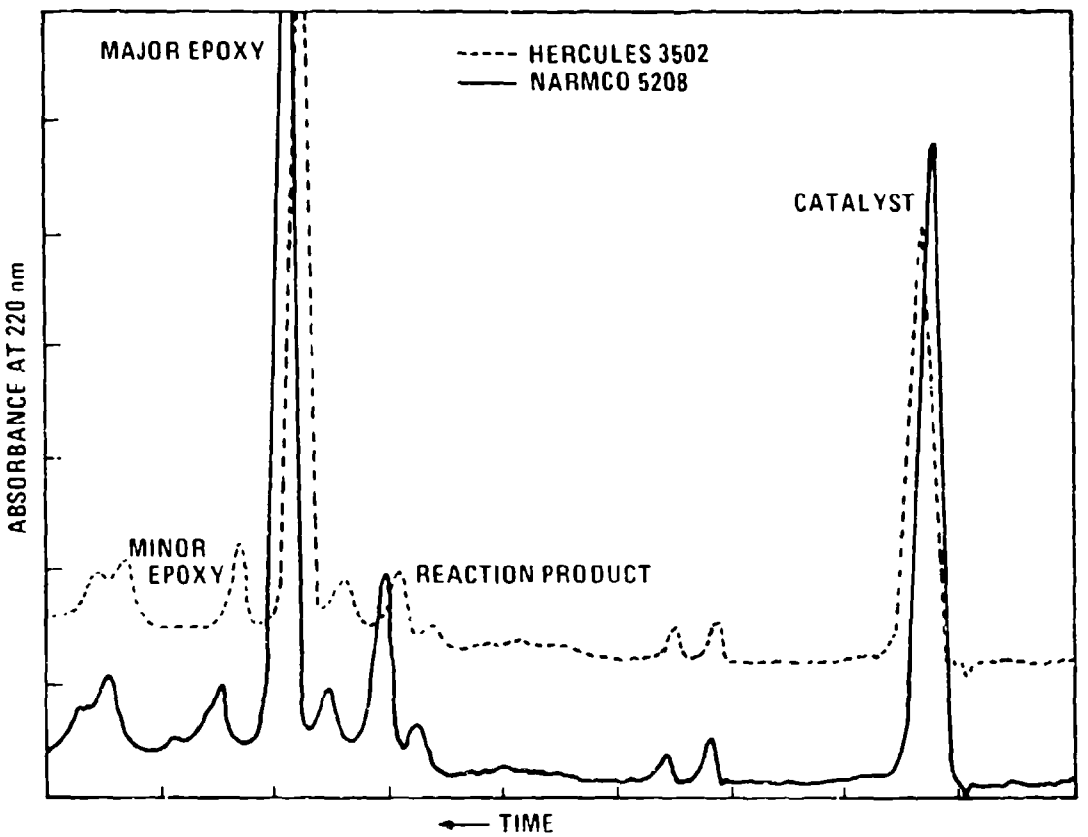

Figure 4 Liquid Chromatograms of Hercules 3502 and Narmco 5208

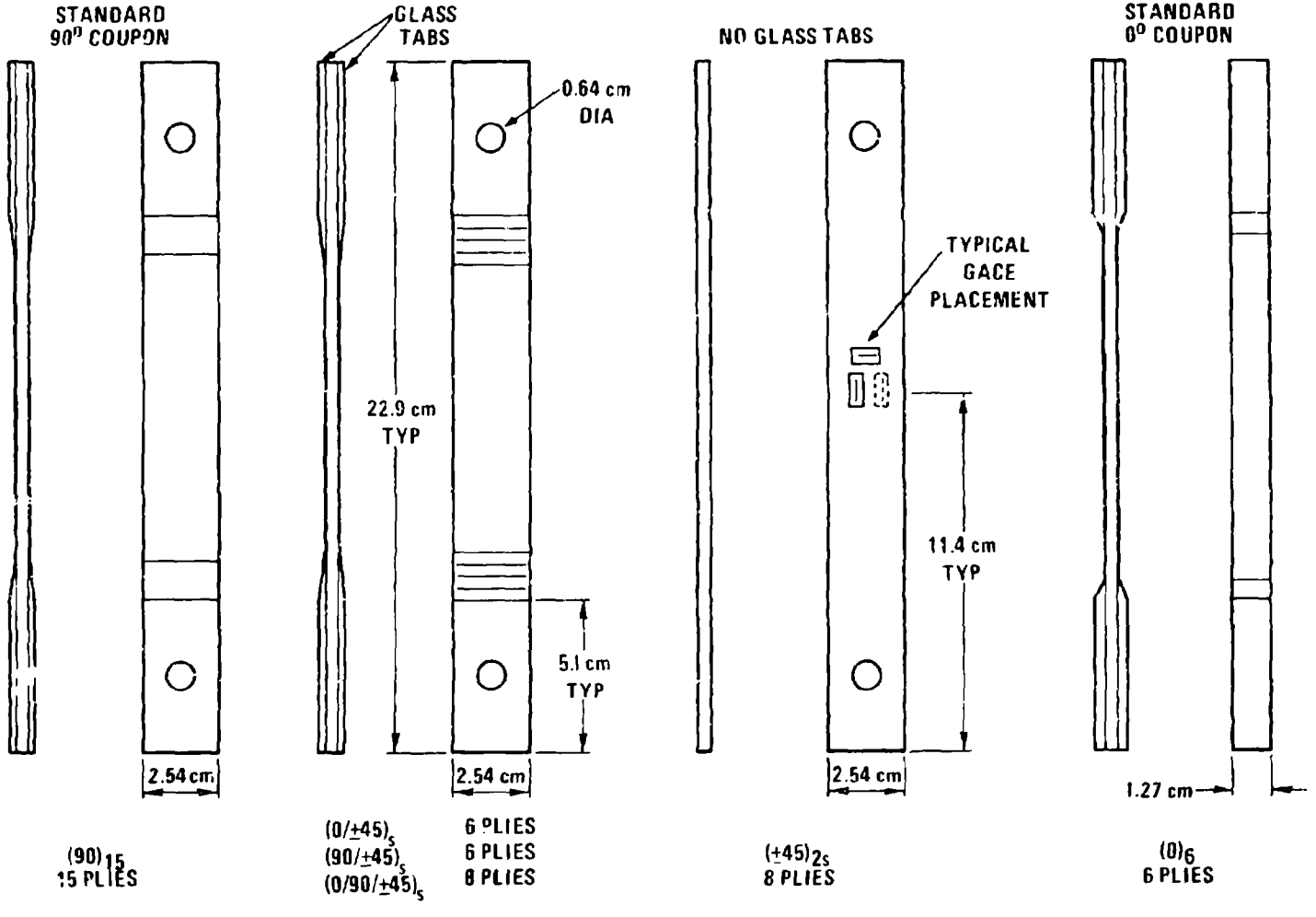

Figure 5. Coupon Configurations

A summary of the test coupons for mechanical response and their utilization is indicated below:

- o Unidirectional Composite Properties
  - Baseline, Creep/Relaxation, Residual Strength: $(0)_6$, $(90)_{15}$, $(\pm 45)_{2S}$
- o Laminated Composite Properties
  - Baseline, Creep/Relaxation, Residual Strength: $(0/\pm 45)_S$, $(90/\pm 45)_S$, $(0/90/\pm 45)_S$
- o "Thick" Specimen Properties
  - Effects of Non-Uniform Moisture Distrition: $(90/\pm 45)_{4S}$, $(\pm 45)_{6S}$

All materials were cured per General Dynamics' specification which culminates with a 2-hour hold at 453°K (355°F) with 5.9×10^5 N/m^2 (85 psi) pressure, followed by a subsequent post-cure for 6 hours at 453°K.

As previously noted, the quality assurance provisions for materials and processing were conducted as outlined in Appendix B. Inspection of specimens per that plan did reveal irregularities in certain sets of $(90/\pm 45)_c$ and 0° coupons. New coupons were subsequently fabricated. The tensile data presented in Appendix A indicate that problems still existed with some of the unidirectional coupons. Since the 0° coupons are highly sensitive to end tab misalignments, we believe that end grip features account for most of the test variabilities. Since the primary purpose of the baseline tensile data was to aid in choosing stress/strain levels for the time-dependent tests, the end grip problems were likely not a factor for the remainder of the program since subsequent tests were conducted well below the region of tensile ultimate properties.

Table I summarizes the typical thickness variations noted for four different layups of each material. Our past experience had indicated that more thickness variation occurs in systems

using the AS fiber compared to T300, and this observation was borne out by the measurements given in the table. Both materials were, however, within our nominal ply thickness requirement, 0.14 ± .001 cm (.0055 ± .0004 in.).

TABLE I. Typical Thickness Variation In Test Coupons

Layup	Thickness/Ply (cm)	
	T300/5208	AS/3502
$(0)_6$	.0140-.0147	.0123-.0147
$(\pm 45)_{2S}$	.0141-.0148	.0134-.0146
$(90)_{15}$	.0135-.0141	.0122-.0142
$(\pm 45)_{6S}$	.0134-.0139	.0127-.0132
Mean Thickness/Ply	.0141 cm (.0055 in)	.0134 cm (.0053 in)
Standard Deviation	.0005 cm (.0002 in)	.0010 cm (.0004 in)

Table II summarizes resin content, specific gravity and fiber volume, V_f, for the cured coupons. In all cases except those labeled "$(0)_6$ large", the measurements were conducted on test tabs cut from the panels used for tensile coupon fabrication. The large $(0)_6$ panels were especially fabricated to provide the sizable number of unidirectional specimens (normally 3 cm. square) used for moisture-induced swelling measurements. Two separate determinations of resin content were made on 24-ply tabs to obtain an estimate of the through-the-thickness resin content gradient.

2.3 Environmental Conditioning

For each coupon type tested in this program, results were obtained under dry and wet (saturated to uniform moisture content at two different humidities) conditions. Coupons for dry tests were initally desiccated for several days at moderately elevated temperatures (322-339°K), then stored in desiccant at RT until test.

TABLE II. DRY RESIN CONTENT AND SPECIFIC GRAVITY FOR T300/5208 AND AS/3502 SPECIMENS

LAYUP	T300/5208 RESIN CONTENT (%)	T300/5208 SPECIFIC GRAVITY	T300/5208 V_f	AS/3502 RESIN CONTENT (%)	AS/3502 SPECIFIC GRAVITY	AS/3502 V_f
$(0)_6$ (large)	27.04	1.602	.668	24.83	1.649	.684
$(0)_6$	25.63	1.619	.688	25.52	1.652	.680
$(90)_{15}$	25.28	1.600	.683	25.15	1.639	.678
$(\pm 45)_{2S}$	27.68	1.581	.653	27.07	1.627	.655
$(0/\pm 45)_S$	26.89	1.599	.668	25.21	1.640	.678
$(90/\pm 45)_S$	26.40	1.591	.669	23.38	1.658	.702
$(0/90/\pm 45)_S$	26.14	1.586	.670	24.96	1.636	.678
$(\pm 45)_{6S}$ (bag)	26.48	1.615		26.70	1.631	
(mold)	27.56	1.591		25.66	1.664	
$(90/\pm 45)_{4S}$ (bag)	26.63	1.594		26.19	1.626	
(mold)	26.53	1.597		25.62	1.633	
Mean	$26.52 \pm 0.75\%$		.671 $\pm .011$	$25.55 \pm 1.02\%$		.679 $\pm .014$

Wet coupons were moisture-conditioned to saturation at 339°K (150°F) in 75% and 95 RH. The latter humidity was selected to provide the greatest amplification of moisture effects without immersion conditioning. The 75% RH represents a worst-case service condition. These specimens were supported on racks in the humidified stagnant air space above saturated salt solutions of lead nitrate (95% RH) and sodium chloride (75% RH). Coupon end tabs were wrapped with aluminized tape to retard moisture ingress during conditioning. As previously indicated in Figure 2, typical saturation moisture contents for these two conditions were 1.0-1.2% and 1.4-1.5% by weight. Section IV details the moisture absorption characteristics of these materials.

2.4 Baseline Tensile Tests

After appropriate environmental conditioning was completed, coupons to be tested were strain-gaged, then reconditioned (if wet) as necessary. Micro-measurements CEA-06-250UW-350 foil gages (350 ohms), .64 cm (.25 in) long, were bonded to the coupons with Eastman 910 adhesive for RT tests, and with M-Bond 600 for all elevated temperature and wet tests. This latter adhesive requires baking at 450°K (350°F) for ½ hour for cure. After this bake, the wet coupons were then reconditioned for three days in the appropriate humidity chamber to re-establish the outer-plys' moisture level lost in the bake.

All baseline tensile tests were performed with an Instron tester controlled by a Hewlett-Packard Model 8050B computer. The system includes a 10-channel scanner for strain gage reading, a 10-channel actuator scanner of control of the load machine, and a B & F signal conditioner for the strain gage inputs. The load and strain inputs are processed by the computer and output via thermal printer and plotter. A typical sample output for this program is indicated in Figure 6.

Due to the relatively short time required for typical tensile tests (several minutes), provision was not made to retard moisture egress from the wet specimens during these tests. In examining the wet baseline tensile data, then, one must note that some coupon dryout does occur during the test.

For each moisture condition (dry or wet), baseline tensile tests were conducted at room temperature (RT) and one elevated temperature (ET). The elevated temperature was chosen to be

GENERAL DYNAMICS
FORT WORTH DIVISION

PAGE 1
MAY 15,1978

TIME-DEPENDENT/BASELINE DATA
TENSILE TEST AT 325 F DRY
77021-15 T.R.#804240
+/-45 DEG.IN TENSION
SPECIMEN NO.15-7

NO.	STRESS PSI	CHAN#2 STRAIN UIN/IN	CHAN#3 STRAIN UIN/IN	AVERAGE STRAIN UIN/IN	MODULUS PSI	TRANSVERSE STRAIN UIN/IN
1	28	10	61	35		1
2	775	297	470	384		0
3	1439	622	688	655	2.45E+06	0
4	1924	854	832	843	2.50E+06	-1
5	2496	1107	1034	1070	2.51E+06	-1
6	2996	1348	1225	1287	2.46E+06	-2
7	3439	1555	1393	1476	2.44E+06	-2
8	3917	1763	1609	1686	2.41E+06	-2
9	4401	1937	1857	1897	2.40E+06	-2
10	4948	2137	2144	2141	2.24E+06	-2
11	5633	2453	2477	2465	2.17E+06	-2
12	6332	2805	2848	2827	1.93E+06	-1
13	7072	3216	3261	3238	1.86E+06	-1
14	7799	3656	3707	3682	1.64E+06	-1
15	8553	4155	4202	4178	1.58E+06	-2
16	9280	4694	4752	4723	1.33E+06	-1
17	9979	5298	5349	5323	1.24E+06	-1
18	10643	5938	5996	5967	1.03E+06	-1
19	11238	6634	6695	6664	9.39E+05	-1
20	11806	7387	7459	7423	7.48E+05	-1
21	12283	8195	8271	8233	6.66E+05	-1
22	12712	9059	9138	9099	4.96E+05	0
23	13086	9955	10036	9996	4.55E+05	0
24	13446	10895	10979	10937	4.30E+05	0
25	13764	11861	11939	11900	3.30E+05	0
26	14062	12844	12905	12874	3.18E+05	0
27	14346	13831	13885	13858	3.09E+05	0
28	14595	14854	14880	14867	2.92E+05	0
29	14816	15893	15897	15895	2.76E+05	1
30	15017	16943	16907	16925	1.95E+05	1
31	15238	18010	17934	17972	2.03E+05	1
32	15425	19102	18959	19030	1.94E+05	0
33	15605	20206	19992	20039	1.88E+05	0
34	15723	21311	20994	21153	1.72E+05	1
35	15854	22476	22025	22251	1.63E+05	0
36	15944	23682	23116	23399	7.83E+04	0
37	16027	24920	24247	24583	7.41E+04	0
38	16062	26150	25749	25949	5.61E+04	-1
39	16110	27616	1047980	27404	4.97E+04	1
40	16124	1046850	1047980	1056140	1.34E+01	1
41	16013	1046790	1047980	1056140	-9.42E+01	1

EXTRAPOLATED STRAIN= 32048 UIN/IN
AT MAXIMUM STRESS = 16341 PSI
THICKNESS= 0.0455IN. AREA= 0.0456SQ.IN.
INSTRON LOAD 745POUNDS

FILE NO. 4

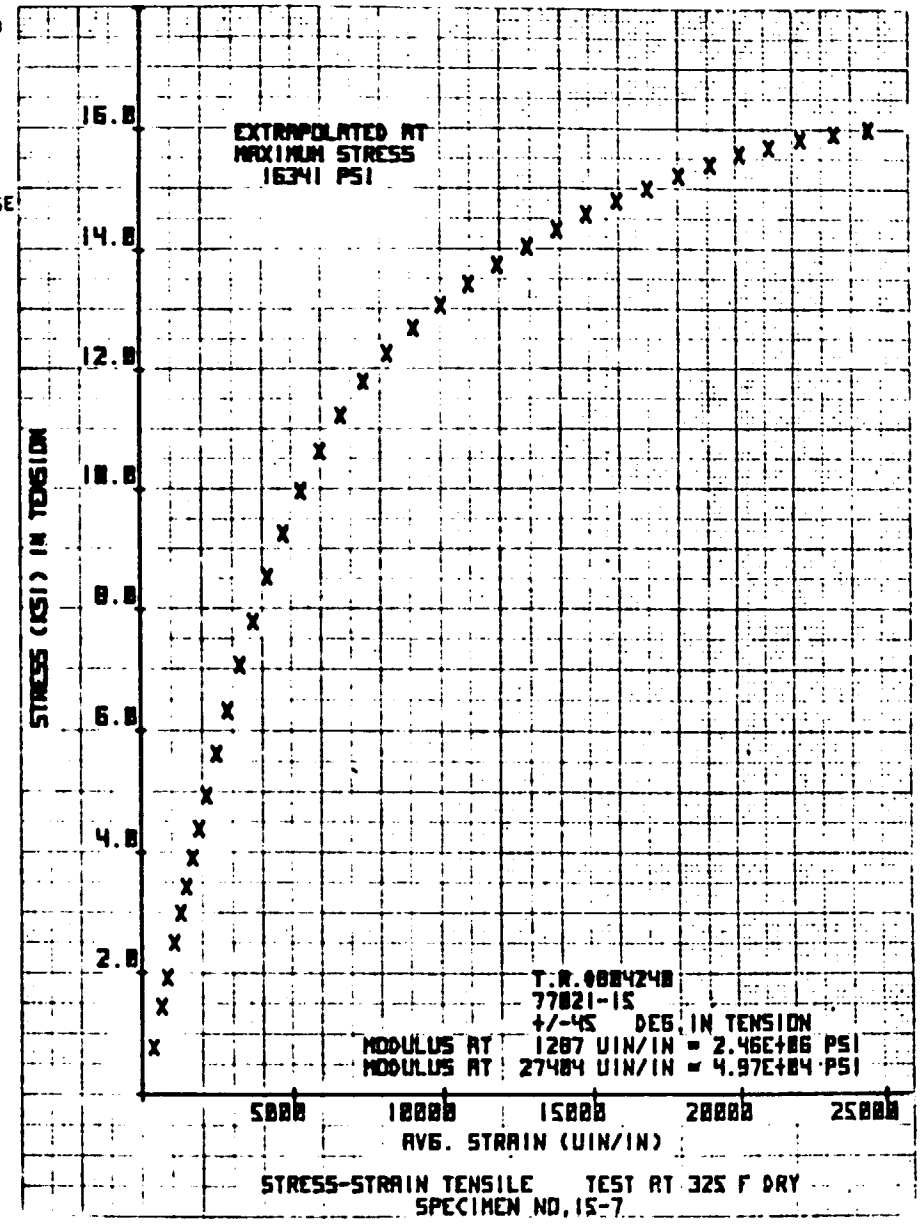

Figure 6. Sample Stress–Strain Output

near the (dry or wet) glass transition temperature (Tg) of the materials, and to cause a decrease of matrix-dominated tensile properties to about 70% of the RT values. Figure 7 demonstrates that this goal was achieved at our selected temperatures of 436°K (325°F) dry and 372°K (210°F) wet.

A tabular summary of tensile strength retention relative to RT dry conditions is given in Table III. One notes that slight problems still persisted with even the refabricated sets of (0) and (90/±45) coupons, since the RT dry values were low compared to other test conditions. In general, however, the reduction in ultimates due to temperature and moisture content are fairly typical. Subsequent time-dependent tests (Section III) used stress/strain levels which were typically 20-30% of ultimates.

A complete listing of the baseline tensile properties for all coupons for this task and the following one are presented in Appendix A.

Two results related to time dependence were obtained during baseline testing, and we will comment briefly on those findings. Figure 8 presents Poisson's ratio data for both materials from all the baseline tensile tests. These plots of transverse strain vs. longitudinal strain demonstrate that ν_{12} is essentially constant over the entire range of temperature and humidity (and strain) used here. This provides strong evidence early in the program for the time-independence of ν_{12}.

During the later stages of baseline tensile testing of wet coupons, we also initiated a modification of the tests to obtain stress-relaxation data. In these cases, we programmed the Instron tester to ramp at constant crosshead speed to a preselected strain level (typically 20% of ultimate) and hold there for 30-60 minutes. During the hold, all stress/strain values were printed at regular intervals to observe the relaxation of the coupons. After the selected hold time was complete, the ramp to failure was completed.

Two interesting results were obtained from these tests: (1) The hold period appeared to have no influence on the eventual ultimate properties measured, so no baseline data was lost in this process; and (2) we were able to obtain stress-relaxation results for the unidirectional coupons which were adequate to verify the time-independence (as expected) of E_{11} and ν_{12}. On the basis of these results, then, we did not perform any creep compliance measurements on the $(0)_6$ coupons. The $E_{11}(t) \approx E_{11}$

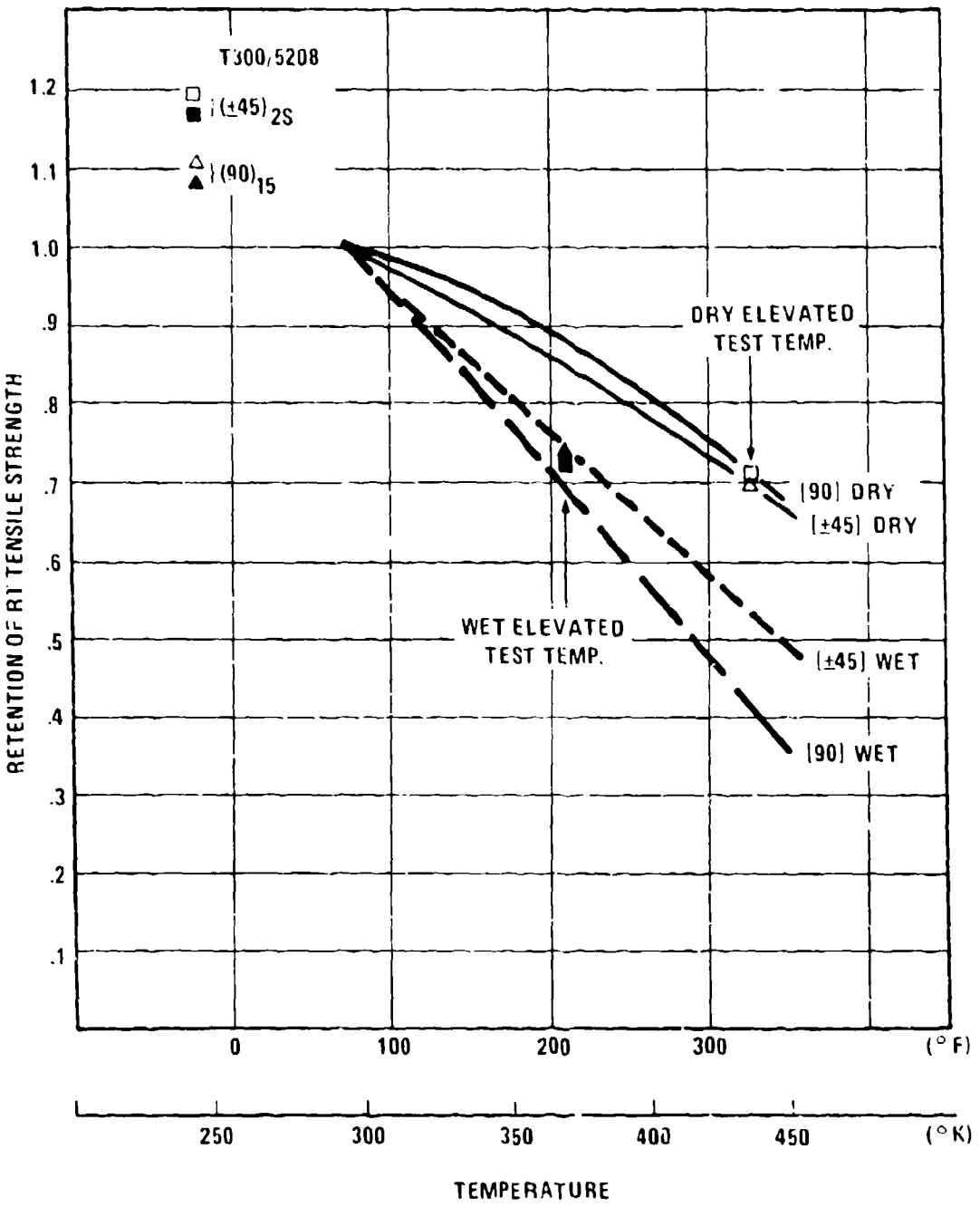

Figure 7. Retention of Matrix-Dominated Tensile Properties At Elevated Temperature for T300/5208

TABLE III. TENSILE STRENGTH RETENTION (RELATIVE TO RT DRY)

		RT 75%RH	RT 95%	[illegible]	372°K 75%RH	372°K 95%RH
T300/5208	$(0)_6$	.90	.88	.78	.87	1.05
	$(90)_{15}$	.56	.56	.71	.42	.33
	$(\pm 45)_{2S}$	.99	.99	.70	.73	.74
	$(0/\pm 45)_S$	.81	.78	1.01	.76	.88
	$(90/\pm 45)_S$	1.57	1.20	.98	.96	.89
	$(0/90/\pm 45)_S$	.94	.90	.93	.88	1.02
AS/3502	$(0)_6$	1.06	1.14	1.02	1.04	1.03
	$(90)_{15}$	.61	.64	.82	.45	.36
	$(\pm 45)_{2S}$	.93	.95	.77	.79	.87
	$(0/\pm 45)_S$	1.00	.87	.94	1.01	1.03
	$(90/\pm 45)_S$	1.13	1.13	.91	.85	.83
	$(0/90/\pm 45)_S$	.91	.90	.95	.92	.92

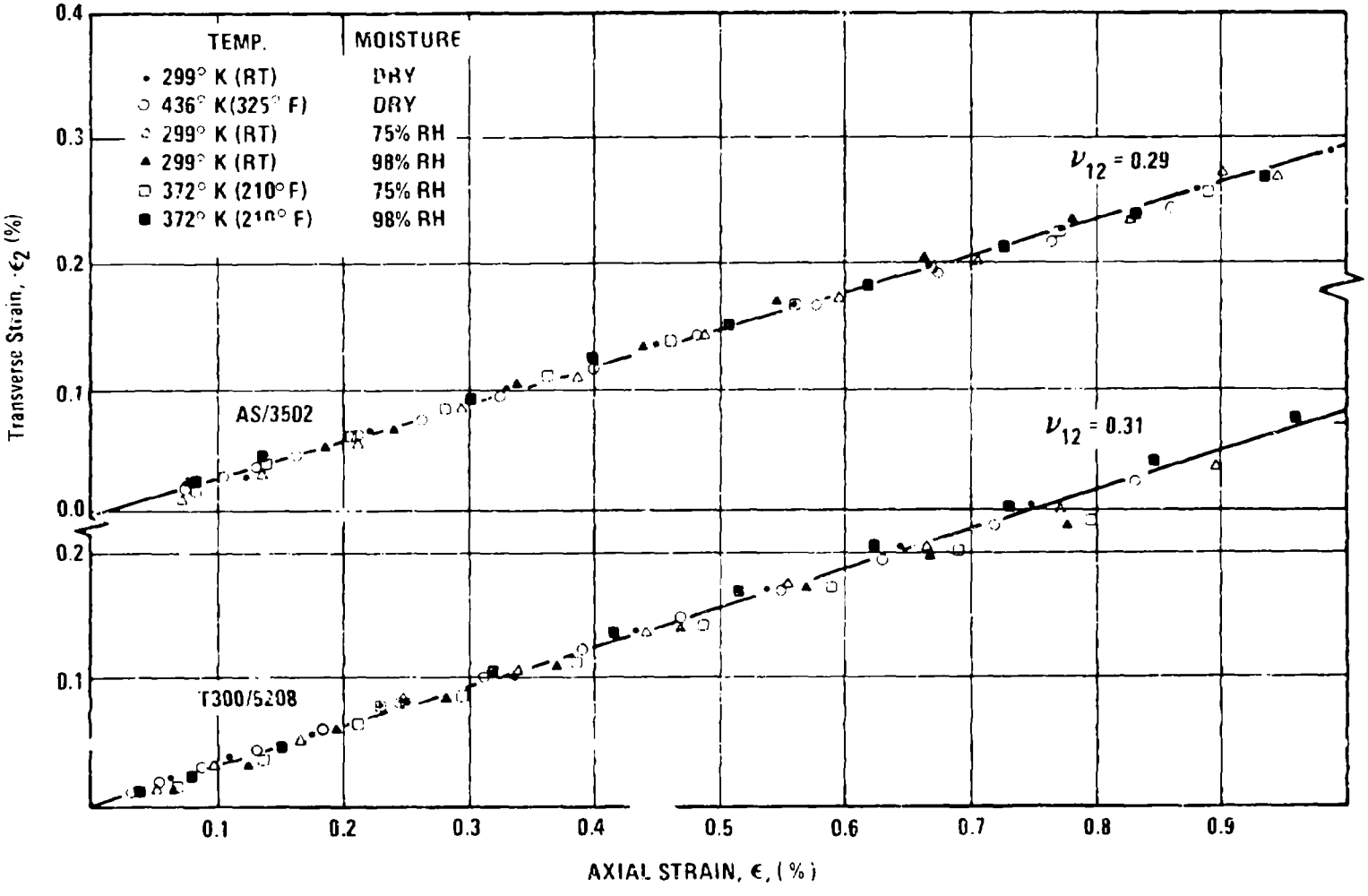

Figure 8. Poisson Ratio for Unidirectional $(0)_6$ Coupons

results from these hold experiments are presented in Section III. One should note however, that those tests on wet coupons were conducted at RT with no provision for moisture maintenance in the coupons. Even though the measured moisture loss in these thin specimens was about 20%, the E_{11} and ν_{12} principal moduli appear constant.

One word of caution should be interjected regarding the use of such stress-relaxation data. Proper consideration must be given to the relaxation effects which occur during the initial ramp to the constant (hold) strain value. This is readily accomplished by not including the data obtained during the early stages of the hold interval. That is, the relaxation which occurs during the first time interval, approximately three times the duration of the ramp, is not representative of the true stress relaxation.

SECTION III

3. TIME-DEPENDENT RESULTS

The objective of this task was to measure the time-dependent mechanical response for both material systems under a variety of temperature/humidity conditions. As previously indicated in Section I, these tests were conducted on dry coupons and on coupons conditioned to a uniform moisture content at 75% and 95% RH. At each of these humidity conditions, five test temperatures were used, from room temperature up to the glass transition region for the materials.

Although most of the experimental results in this section are presented as time-dependent moduli, the majority of our experiments were constant load creep compliance measurements. Since we set out to obtain a linearly viscoelastic characterization of the materials, we indeed found that quasi-elastic conversion (i.e., $E(t) \simeq S(t)^{-1}$) gave very good results as expected, so the moduli presented here are reciprocal compliances.

From these creep compliance results for the various layups tested, we thus obtained both unidirectional (principal) properties and laminate properties. E_{11} and ν_{12} were obtained from tests on $(0)_6$ coupons; $E_{22}(t)$ from $(90)_{15}$ coupons; and $G_{12}(t)$ from $E_R(t)$ and $\nu_{xy}(t)$, the longitudinal modulus and Poisson's ratio, respectively, of a $(\pm 45)_{2S}$ coupon.

From the individual creep measurements on each layup at various temperature/humidity conditions, master curves were constructed using the procedure diagrammed in Figure 9. The individual temperature/humidity results were horizontally shifted on a log compliance-log time plot until a smooth "master curve was obtained. Since our tests were all conducted in linear regions of material response, and since this procedure generally yielded reasonable and repeatable results, we made no attempt at vertical shifting of the data. Although others (Ref. 8) have performed vertical shifts based on arguments, e.g., from rubber elasticity, we saw no compelling reason to do so in this case, since our data were quite tractable without such shifting.

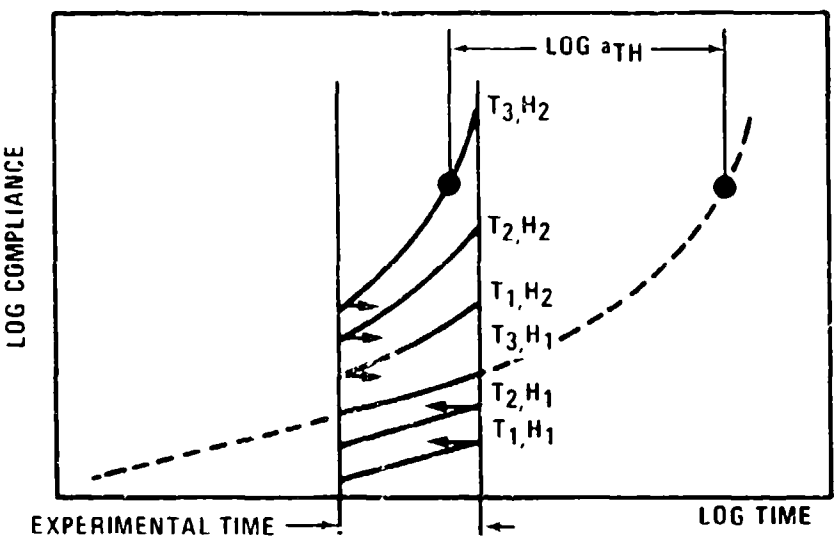

Figure 9 Superposition Procedure

In the following subsections, we provide details about our experimental procedures and present specific experimental results for the coupons tested. Some of these results do relate closely to our Analytical Methodology task. We reserve for that section (V) those specifics which treat the prediction of time-dependent response.

3.1 Experimental Procedures

Tests, primarily tensile creep, were conducted on all coupons under the temperature and moisture conditions previously diagrammed in Figure 2. As indicated by the dotted square in that figure, we initially planned to use 464°K (375°F) as our highest dry test temperature. After conducting some early testing at that temperature and experiencing various premature coupon failures, we lowered that selected test temperature to 436°K (325°F), somewhat below the dry T_g of the material.

Early in the program we experimented with various types of time-dependent testing in order to compare the respective results. Figure 10 shows a typical example of such results. Using three different 90° coupons of T300/5208, we measured both stress relaxation (by two different methods) and creep compliance. These data, all plotted as moduli, are compared in Figure 10. For the tests shown, the largest disagreement in results was about 4%.

The choice of experimental method and apparatus for the bulk of the time-dependent tests was driven by several requirements: total number of specimens to be tested, number of replicates per test, and maintenance of moisture in the wet specimens during test. The experimental creep apparatus is shown schematically in Figure 11.

This test set up utilized a whiffle-tree fixture to accomplish simultaneous loading of four specimens (3 replicates plus one dummy). The strain in each of the replicate specimens was monitored with two strain gages on opposite sides of the specimen. The average of the two gage outputs for each specimen was plotted on a strip chart recorder. For analysis, the plotted strains from the three specimens were averaged, and the average tabulated vs. time. In the case of ±45 coupons, one of the replicate specimens was sometimes monitored with an additional gage (transverse) in order to extract the Poisson ratio ν_{xy}.

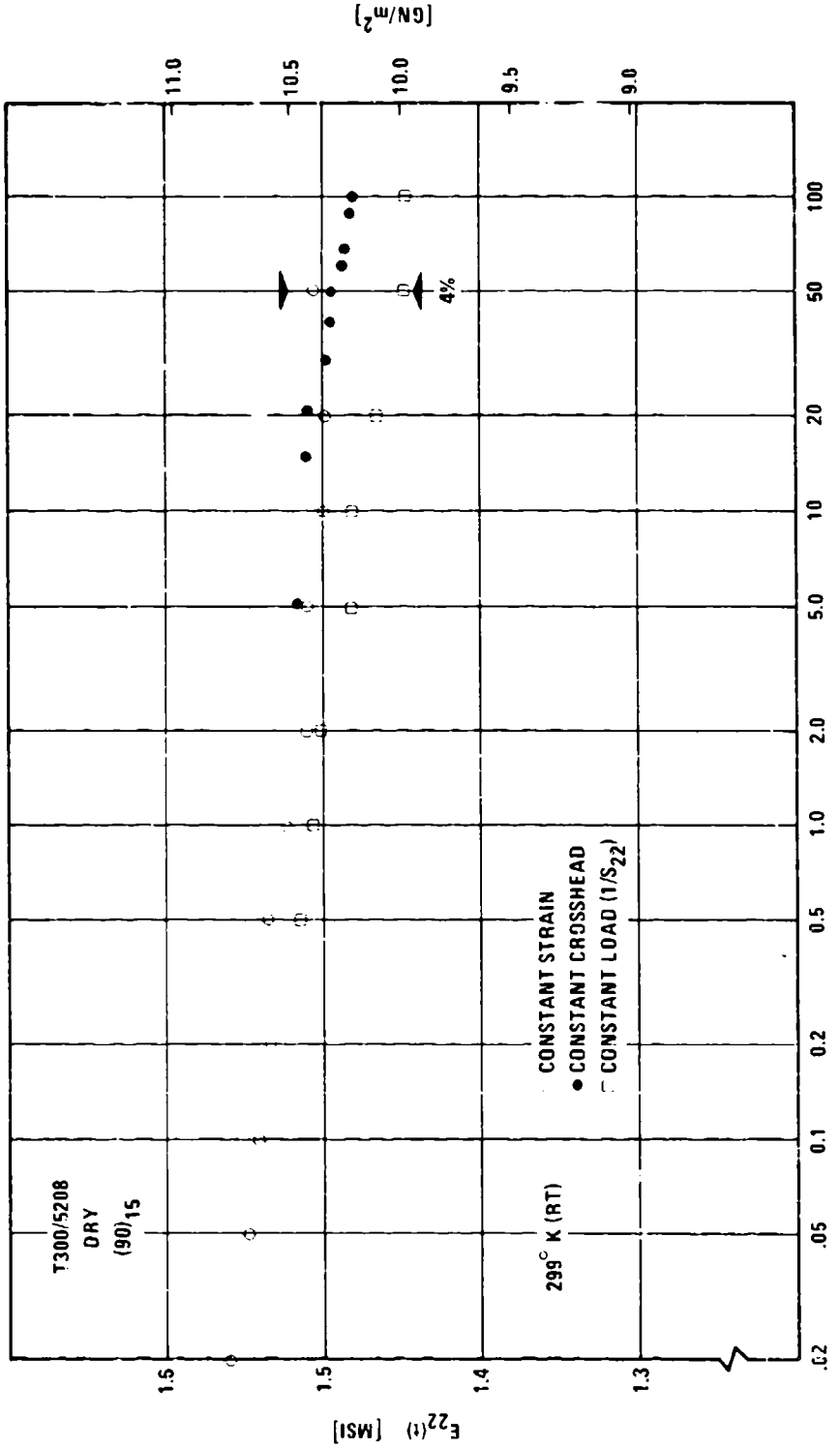

Figure 10 $E_{22}(t)$ at 299°K (RT) and 339°K (150°F) for Dry T300/5208

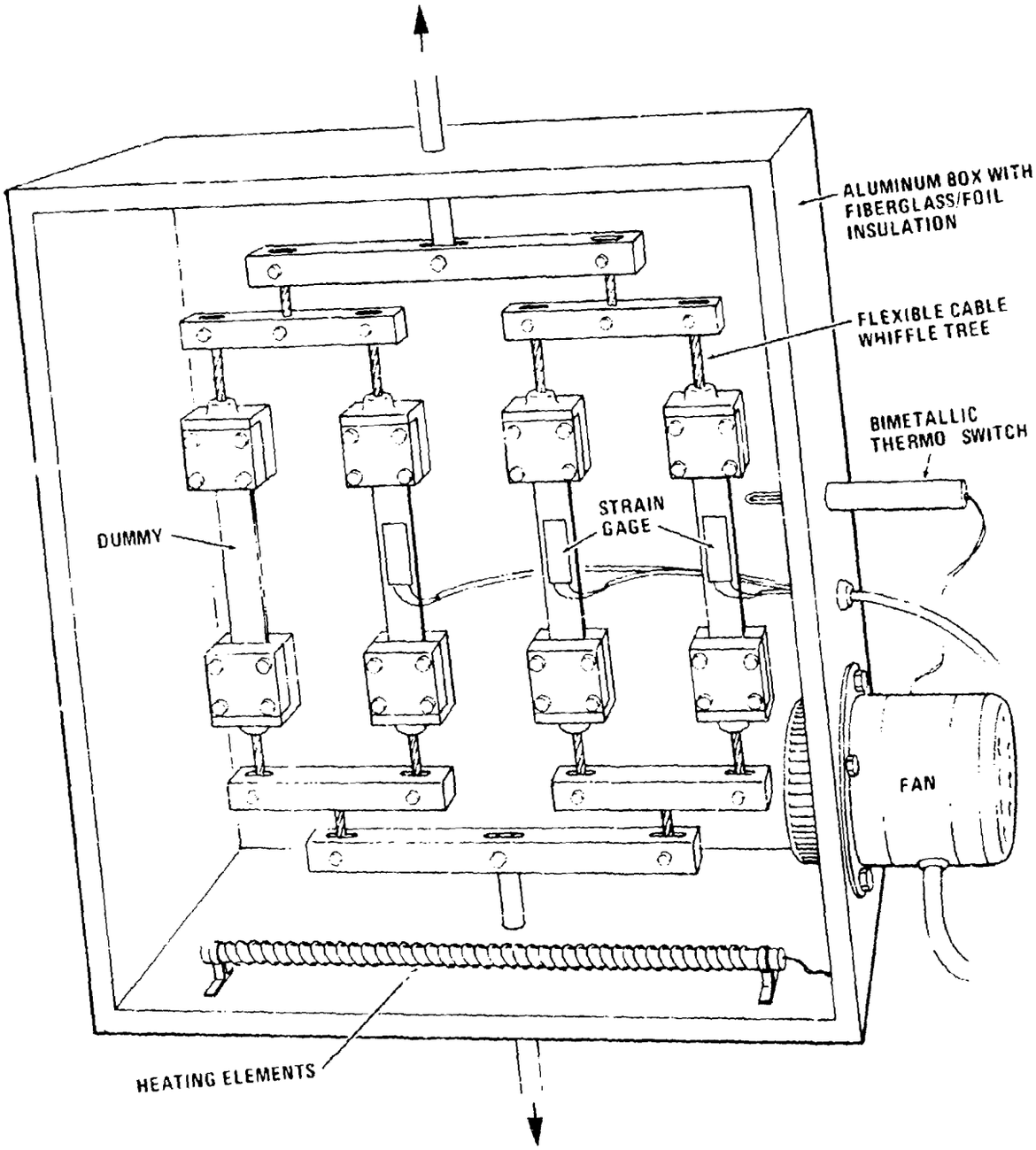

Figure 11. Test Configuration for Creep Experiments

For dry tests, an oven was placed about the fixture, with a tray of desiccant, and the temperature was continuously monitored by a thermocouple placed on one of the specimens.

For wet tests, we accomplished a somewhat innovative procedure whereby the specimens were continuously immersed in liquid. Immersion heaters and impellers were used for temperature uniformity. One of the paramount problems existing in usual wet test techniques is the maintenance of moisture in previously conditioned wet specimens and/or accounting for dryout during the test. This is not an insurmountable problem in the case of tensile tests, where the test times are typically of a few minutes duration. In the present case however, our planned tests were to be 100 minutes, so moisture egress was a major consideration.

As discussed in Section IV, the wet glass transition temperatures for these coupons were all measured to be in the vicinity of the boiling point of water. This fact allowed us to immerse the coupons in water mixtures and still test at temperatures very near the glass transition range. The immersion fluids selected for these tests were mixtures of ethylene glycol and water. The mixtures were selected on the basis of Raoult's law (Ref. 12, e.g.) to provide effective vapor pressures of water equivalent to that at which the coupons were initially conditioned, i.e., 75% or 95% RH. Such a procedure may be expected to work reasonably well when the liquid added to the water has a high boiling point.

During all the creep testing, the moisture content of the specimens was monitored by periodic weight measurement of a moisture traveler specimen, of the same type as, and submerged with the creep coupons. During a typical test duration on one set of replicates, three days, the traveler indicated only slight moisture pickup (usually less than 10% increase).

Strain gages used during these immersion tests were the same type as described previously in Section II. For these immersion tests, however, we coated the gages with Aqua Seal, an elastomeric product sold by Kearney National, Inc. Although this does not inhibit moisture uptake, it did retard moisture effects on the gages for a sufficient time to complete a given series of tests. In separate tests conducted on aluminum coupons gaged, coated, and immersed in the same manner as our graphite-epoxy specimens, we verified that reliable strain readings were being obtained. Although gage problems would typically initiate after 5-10 days of testing, this was well outside our usual 3-day test sequence for five temperatures on one set of specimens.

The typical creep testing sequence consisted of 100 minutes of creep at a given temperature, followed by a recovery period with no-load while the temperature was raised and stabilized to the next value. There are two time intervals during such experiments which should be considered: the time immediately following load application, and the recovery time between successive loadings.

In the first case, one should note that true compliance measurements are obtained only after a time interval, typically 3-5 times the loading interval, due to relaxation during loading. Our initial creep strain readings were recorded at 0.5 minutes after loading. The 100 minute creep duration thus gives us slightly over two decades of response, which was acceptable for later forming master curves since we obtained data at five separate test temperatures.

In the second case, the recovery time should normally be about three times the creep interval for the specimen to approach its initial condition. This feature is readily ascertained, however, from successive identical creep experiments. For our purposes, we allowed the coupons to recover for a time equal to the creep interval (at the creep temperature) then raised the temperature to the next higher test value. By the time the chamber had equilibrated at the higher temperature, (e.g., 60-100 minutes), the coupons had sufficiently recovered for the next test.

Since our intent for this program was to obtain a complete linearly viscoelastic characterization for these materials, we devoted considerable attention to determining the cycle-to-cycle repeatability of the experiments and the range of linear behavior. During this process we assessed the possible requirements for mechanical "break-in" of the coupons prior to actual creep experiments.

Various workers (e.g., Ref. 3 and 9) have noted the need to condition these fibrous composites mechanically before attempting to obtain reproducible time-dependent data. We examined such requirements by low rate strain cycling (0.05% per second) hysteresis, and by cycle-to-cycle (constant load) creep recovery results. Although in some cases a different response was noted for the first cycle compared to subsequent cycles, this was not uniformly the case. We adopted a precautionary procedure, therefore in which, prior to the creep experiments, the coupons were subjected to 3-5 load/unload cycles (~1 min each) using a 10% higher load than planned for the actual creep experiment. Following this cycling, a 30-minute recovery period was allowed prior to initiation of the creep experiments.

A typical cycle-to-cycle repeatability test is indicated in Figure 12, where we also assessed the range over which the tensile relaxation modulus of a ± 45 coupon remains constant. For a strain range of 0.1-0.2%, the variation between maximum and minimum E_R at a given time is about 5%. Such a range is probably within the typical specimen to specimen variability. If we include the E_R data at 0.3% strain, the variation between minimum and maximum results increases only slightly to about 7%. If, however, we examine the $E_R(t)$ results over a strain range of 0.1-0.4%, the variation at a given time increases to around 15%. These results would tend to indicate that for RT dry specimens, the material is linearly viscoelastic up to about 0.3% strain, which is roughly 30% of the strain ultimate under these conditions. The stress corresponding to this strain level is about 60 MN/m^2 (8.75 ksi), which corresponds to about 35-40% of ultimate stress.

Stress levels for all creep tests were set at typically 25-35% of ultimate values for each temperature/moisture condition. For a given sequence of test temperatures at a particular moisture condition, the creep load was systematically lowered at each higher test temperature in order that the creep strains remained approximately constant.

Verification of linear response was obtained by superposition of creep-recovery results (Ref. 7) as shown for a typical case in Figure 13 where a comparison is made between measured and extrapolated compliance at equivalent times in the respective creep and recovery periods.

3.2 Unidirectional Properties

In this subsection, we describe the experimental results from which principal properties for these two material systems are derived.

3.2.1 Results for $(0)_6$ Coupons

For measurements of properties along the fiber direction, we initially set out to screen the $(0)_6$ results with Instron constant-crosshead displacement tests. By this screening we attempted to verify quickly that mechanical response in the fiber direction was not sensitive to time effects, and thus reduce testing of these coupons to allow more experimental time for testing matrix-dominated response.

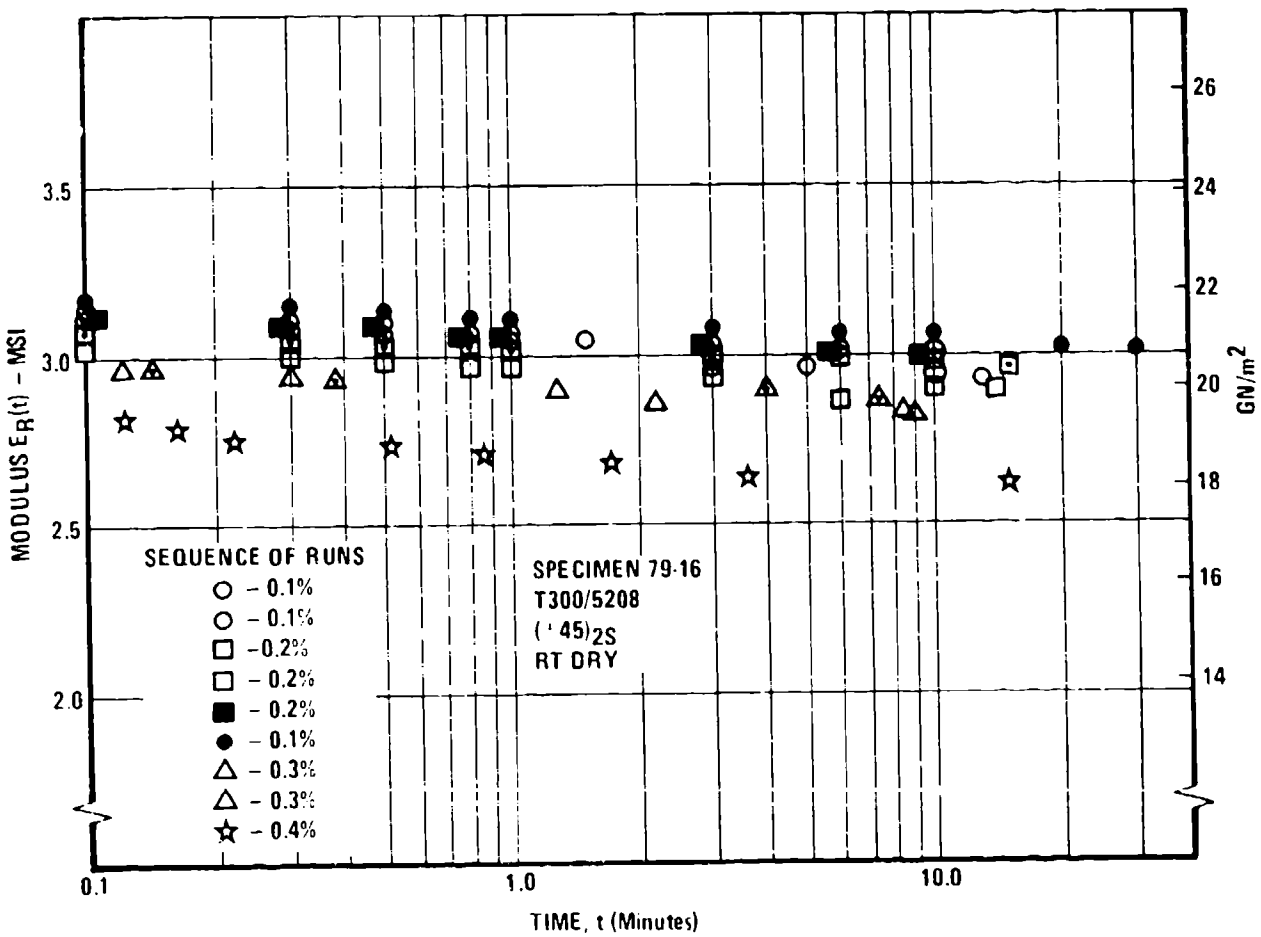

Figure 12 Relaxation Modulus for T300/5208 (RT Dry), $(\pm 45)_{2S}$

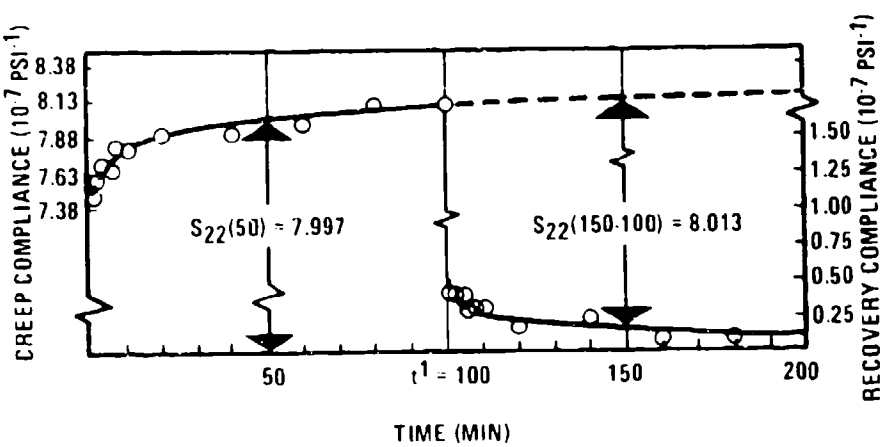

Figure 13 Linear Viscoelasticity of T300/5208 $(90)_{16}$: 95%RH, 150°F

Figure 14 shows typical $E_{11}(t)$ and $\nu_{12}(t)$ results obtained for the two materials under RT/wet conditions. In this case, no provision was made for maintaining moisture in the coupons during the tests, so one might expect to observe slight property changes during the experimental time simply due to moisture content changes. This was generally not the case, as can be noted in the figure. Although a fair degree of specimen-to-specimen variability was noted for the materials tested (typically 124-138 GN/m^2 for E_{11} and 0.28-0.33 for ν_{12}), there appears to be no sensitivity to time for the moisture-conditioned specimens tested at RT.

In Figures 15 and 16, respectively, are shown the results for one of the materials, AS/3502, when tested dry over the entire range of experimental temperatures. In the case of the Poisson ratio (Figure 16), there appears to be a slight increase with time at some of the temperatures. This effect was not reproducible, however, as can be noted by comparing the two different data sets shown for the 436°K (325°F) temperature.

On the basis of tests such as these, then, we conclude that the principal moduli E_{11} and ν_{12} are time-insensitive, in agreement with other work such as Ref. 8 for example. A recent paper (Ref. 13) on the time-insensitivity of Poisson's ratio for an unfilled adhesive lends considerable support to this viewpoint.

3.2.2 Results for $(\pm 45)_{2S}$ Coupons

Tensile creep results on $(\pm 45)_{2S}$ coupons were used to derive compliance, and thus relaxation modulus ($E_R(t)$), master curves. From these results for $E_R(t)$, shear modulus data were extracted using the relationship

$$G_{12}(t) = \frac{E_R(t)}{2(1+\nu_{xy}(t))} \qquad (1)$$

Typical tensile creep results for one of the materials, AS/3502 are given in Figure 17. Using the procedure previously noted in Figure 9, master compliance curves were extracted by simple horizontal shifting of the data.

We have initially planned to provide an analytical description of our data by assuming that the compliance could be represented by a power law in time, i.e.,

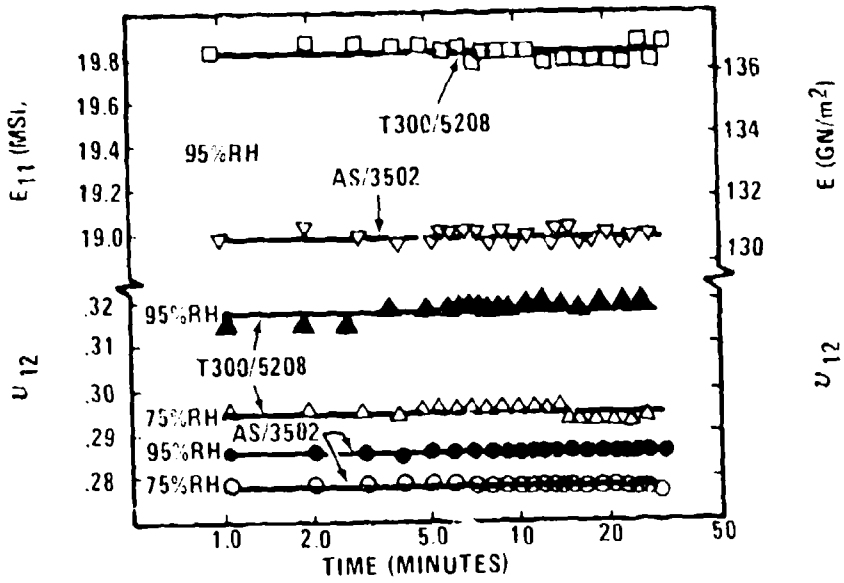

Figure 14 Typical ε_{11} and ν_{12} for RT Wet $(0)_6$ Coupons

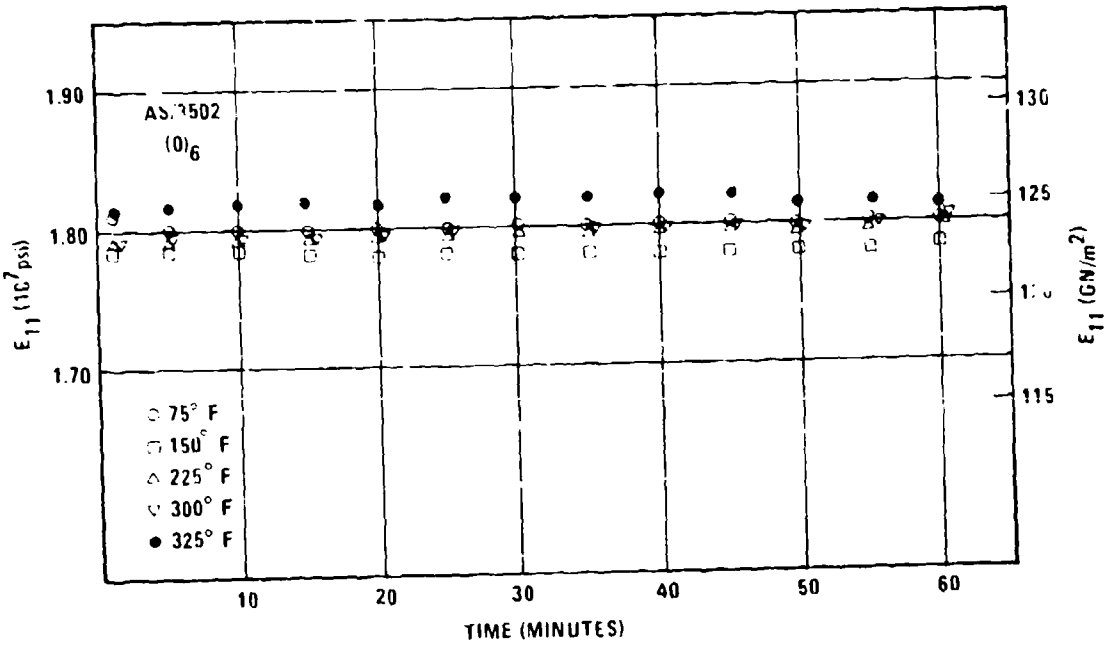

Figure 15 Relaxation Modulus for $(0)_6$ AS/3502

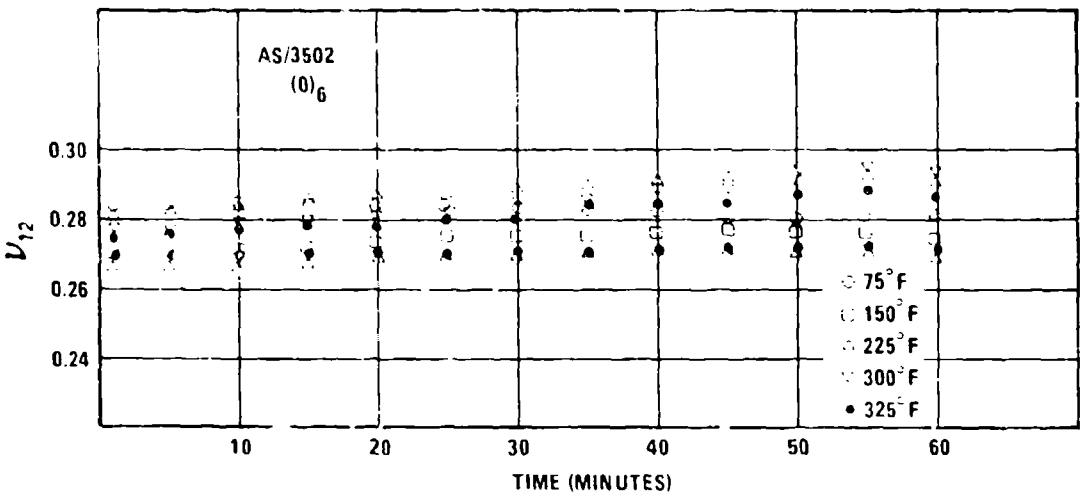

Figure 16 Major Poisson Ratio for $(0)_6$ AS/3502

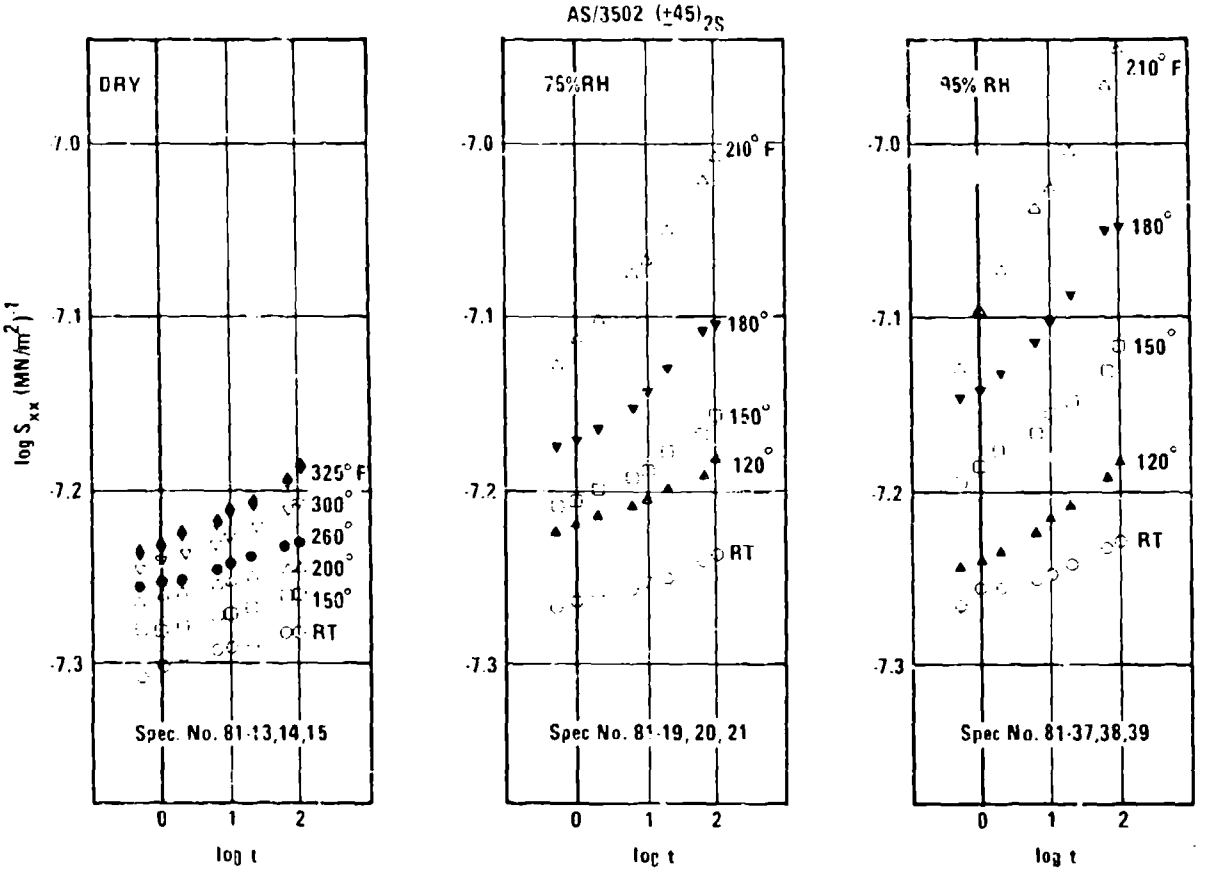

Figure 17 Creep Compliance Results for $(\pm 45)_{2S}$ AS/3502

$$D(t) = D_o + D_1 t^n \qquad (2)$$

where D(t) represents the measured tensile compliance, and both D_o and D_1 are temperature dependent. Other previous work on fibrous composites (e.g., Ref. 7 and 10) demonstrated that such a description is quite useful.

Repeated attempts by us to apply Eq. (2) however, met with only limited success in that we were not able to find a single n-value which appeared to describe satisfactorily the data at all temperatures. In those cases where the description appeared good, the derived n-value tended to be quite small, e.g., about 0.05, whereas work on a similar material, AS/3501-6, in Ref. 10 derived $n \simeq 0.2$.

Lou and Schapery (Ref. 3) found that recovery curves are particularly useful for determining the exponent n, so we also employed that approach. Due to the rather weak time-dependence of the present materials, the recovery strains are quite small, typically 0.001-0.005% at RT dry, and there was considerable scatter in our data. Although n values around 0.05 were again indicated, no consistent value could be obtained. At the suggestion of Dr. Knauss, then we simply adopted the "visual" superposition procedure previously noted. All master curves were thus formed by horizontal shifting on log-log plots.

Results from such a procedure for $(\pm 45)_{2S}$ specimens are given in Figures 18 and 19. The data points in Figure 18 are taken from the 100-minute dry creep tests for T300/5208 at different test temperatures, while the dashed curve represents similar data for the AS/3502 material. It is interesting to note (1) the quite similar behavior for the two materials; (2) the relatively weak time-dependence for dry materials, and (3) the near linearity over roughly seven decades in time. The log-log slopes for both materials are similar (about 0.01) and in excellent agreement with independent results obtained at Texas A&M (Ref.14) on the AS/3502 material.

The shift factors a_T are plotted in the inset to Figure 18 in a conventional Arrhenius-type form, i.e., log a_T vs. reciprocal Kelvin temperature. If one forces a straight line through the log a_T data to extract an apparent activation energy, the results tend to range about 20-25 k cal/mole, which is reasonable for these types of materials.

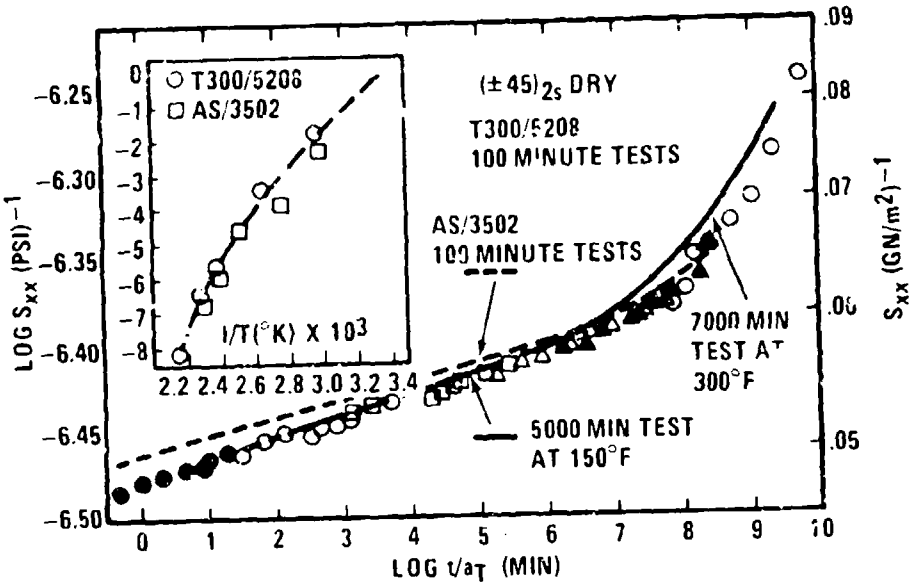

Figure 18 Creep Compliance Master Curve for Dry (±45)

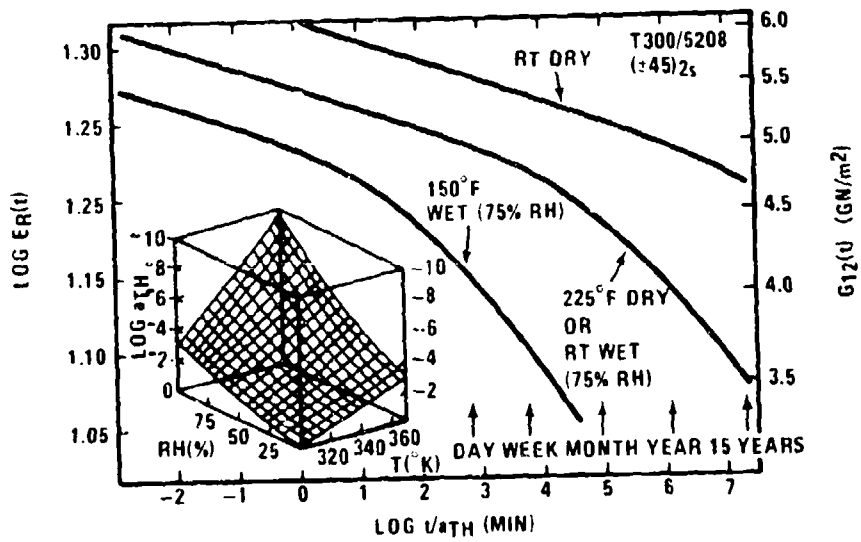

Figure 19 Relaxation Moduli for Dry (±45)

This type of straight graphical shifting is similar to that used by Crossman, et al. (Ref. 15) on HMF 330C/934 relaxation modulus data. If one uses the roughly linear portions of Crossman's relaxation modulus master curve, the magnitude of the log-log slope there is approximately 0.02, similar to our value noted above.

In order to provide some assessment of these master curves derived from superposition of short-term results, we conducted two longer-time tests on the T300/5208 material. These results are shown as the solid curves in Figure 18, and represent a 5000 minute test at 339°K (150°F) and a 7000 minute test at 422°K (300°F). These results are positioned in time with the log a_T values previously derived. The agreement between the longer tests and the superposed short-time tests is quite good.

Turning now to our results for wet coupons saturated at 75% and 95% RH, we employed the same graphical shifting procedures as were used for the dry data. We assumed here that the moisture content for a given coupon was constant for all test temperatures, although there was typically a moisture increase in the specimens during the immersion tests of about 10% (relative to the initial moisture content). This represents a rather small perturbation on the overall results.

Figure 19 summarizes the wet (and dry) results for the T300/5208 material. The AS/3502 behavior was nearly identical, as previously noted. In order to form the combined wet/dry master curves, we have assumed that moisture-only and moisture plus temperature results are superposable in time exactly in the same manner as temperature-only results. This implies that shifting due to moisture and to temperature are separable in the sense that

$$\text{Log } a_{TH} = \log a_T + \log a_H. \qquad (3)$$

Although there is no a priori reason why (3) should hold, the smoothness of our shifted curves and the overall consistancy and reproducibility of results demonstrate its usefullness in the present case.

In Figure 19 we have employed a reduced time scale which extends roughly out to a usual aircraft service life, about 15 years. Within that time frame are shown three different plots of the master curve for the ±45 modulus (reciprocal of compliance) The top curve uses RT dry conditions as the reference and demonstrates only small modulus changes over an aircraft lifetime.

Realizing that no aircraft may be expected to spend a service life at RT dry conditions, the other two solid curves in the figure show the shift in response which occurs if, respectively 380°K (225°F) dry (or equivalently RT wet), or 334°K (150°F) wet conditions are taken as reference. In the latter case, we see that rather dramatic changes in shear modulus may be expected in times of the order of a month.

The inset to Figure 19 presents the log a_{TH} shift surface for a range of temperature and humidity conditions. Although the humidity-induced effects are not dramatic at room temperature, the combined effects of elevated temperature and moisture may be considerable.

In producing this shear modulus time dependence, we have used Eq. (1) and a time-insensitive Poisson ratio of $\nu_{xy} = 0.72$. Figure 20 shows typical ν_{xy} measurements from creep experiments at various temperatures. The two separate measurements at 350°K shown indicate that the variability in results may be at least ±3%. Thus although a slight upward trend in ν_{xy} may be noted in the figure, most measurements fall within or near the standard deviation of the mean there indicated. We have accordingly taken $\nu_{xy} = 0.72$ throughout, and the overall consistency of results would appear to support both this value and its insensitivity to time. A change in ν_{xy} of ±0.1 only results in a shear modulus variation of about ±5%, so again the effect is not great.

3.2.3 Results for $(90)_{15}$

Figures 21 and 22, respectively, show the E_{22} master curves derived from tensile creep compliance measurements on our two material systems. The data in either the dry or the wet case seem to conform nicely to smooth master curves, and the shift factors derived from graphical shifting (horizontal only) are quite similar for the two materials.

One interesting feature of the dry master curves in Figure 21 is their adherence to log-log linearity over the 10-11 decades of reduced time represented there. The overall slope on this log-log plot is in the range [.008-.010], which is quite similar to the ±45 master curve slope. Complementary data obtained at Texas A&M agree in magnitude to within typically 6% and have an equivalent slope.

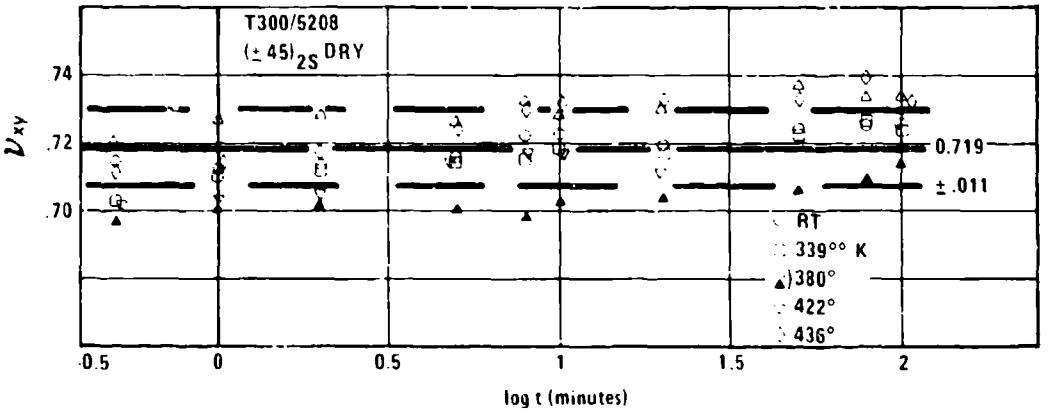

Figure 20 Poisson Ratio for Dry $(\pm 45)_C$ T300/5208

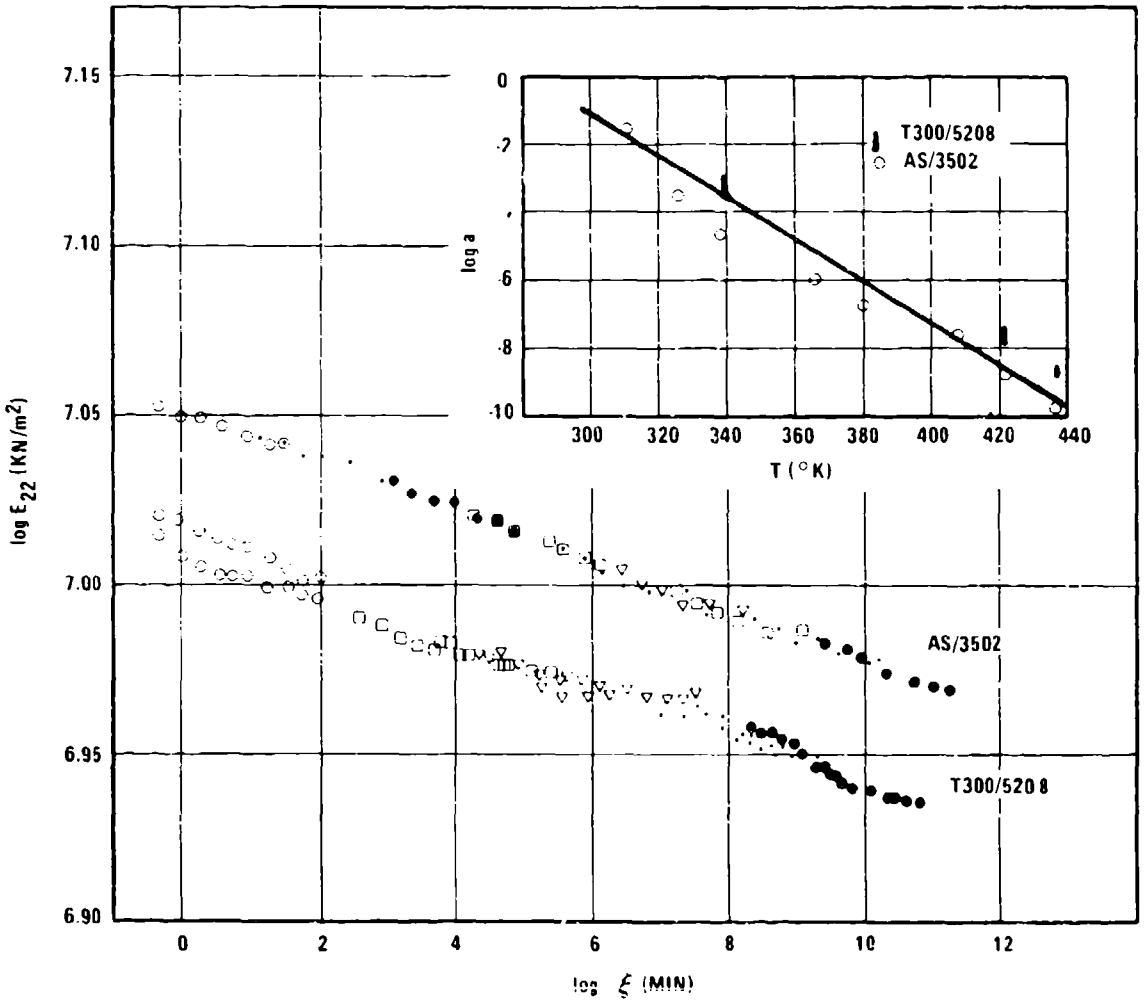

Figure 21 Dry E_{22} Master Curves

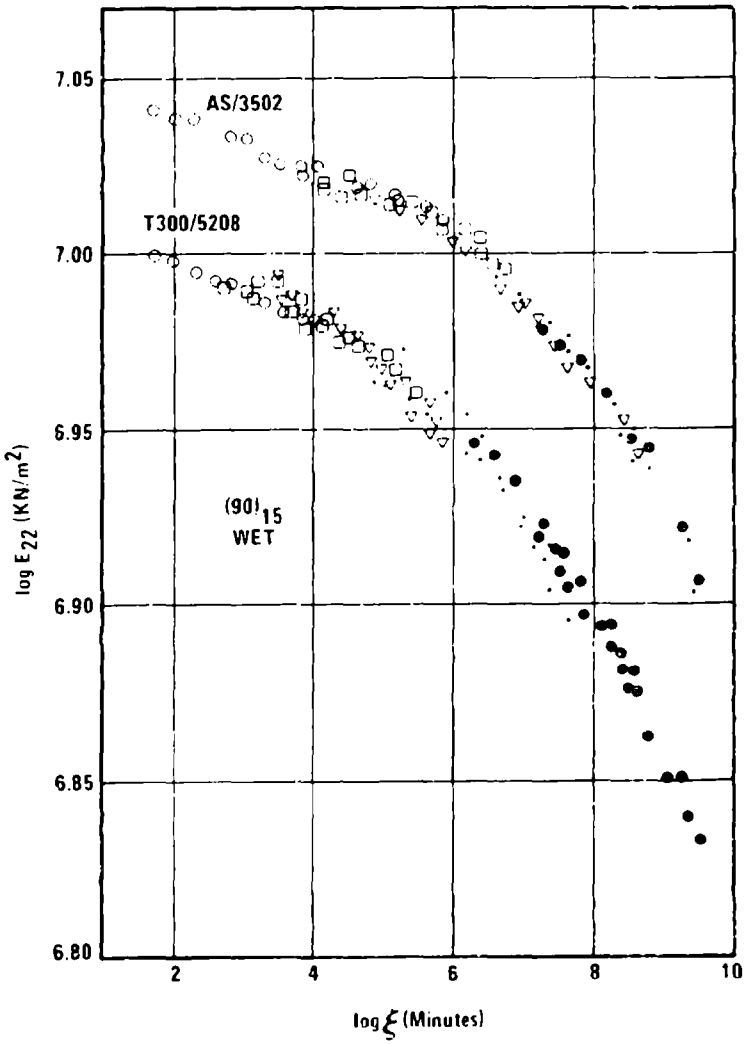

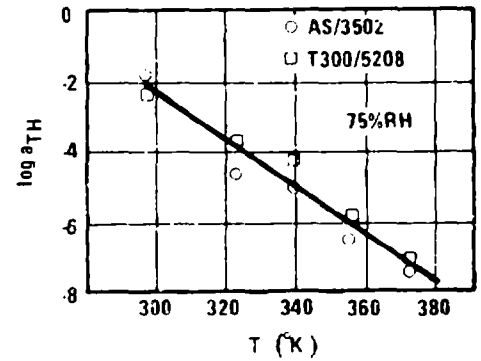

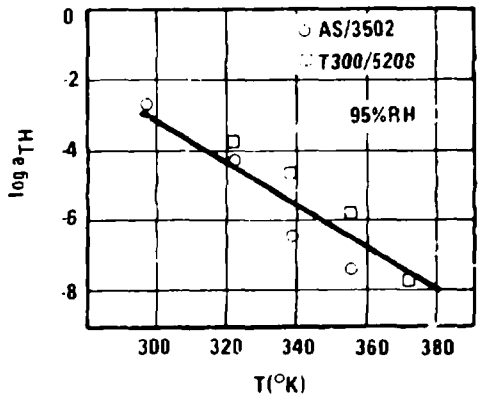

log a_{TH} (RT,DRY)=0

Figure 22 Wet E_{22} Master Curves

If one attempts to superpose the wet and dry data, however, curves of the type shown in Figure 23 result. One sees that when no vertical shifting is used, a severe difference both in the wet and dry master curves occurs at a reduced time of about 10^6 minutes. It is somewhat difficult to reconcile this result with the previously derived wet/dry master curves for shear modulus.

Due to the proclivity of 90° coupons to damage, we undertook an investigation to determine whether any damage (specifically, edge cracks) was evident in typical specimens of these types which had seen extensive histories of time and temperature at load. Several T300/5208 coupons (both ±45 and 90 types) were edge polished and examined on a bench metallograph. Although all the coupons had previously been subjected to many 100-minute creep cycles at various temperatures, no evidence of damage was found.

Surface replicates of the edges were then made while the coupons were subjected to small tensile loads in order to open any cracks which might have healed during the previous examination and handling. Again, no damage was noted. The specimens were then placed in a heated vacuum chamber overnight to eliminate any residual moisture which might have been absorbed during creep cycling. Replicas were again made under load, as before, but no cracking was evident. Finally the 90° specimens were subjected to several creep cycles at stresses between 20 and 30% of ultimates, and for times up to 16 hours (at 350°K). Periodic replicas failed to reveal any edge damage.

On the basis of these limited damage investigations, we concluded that there were probably no gross differences in the specimen integrity which could reasonably account for the differences in the master curve data.

Dr. Schapery of Texas A&M raised questions about possible physical aging effects (Ref. 16) in these materials which might account for long term stiffness changes due to free volume changes. Such a mechanism could possibly account for the differences in the long-term behavior of the dry 90° coupons compared to the dry 45°, since one expects the residual stresses in the specimen to inhibit aging effects.

We thus repeated the creep experiments on 90° coupons, but with one important change compared to our previous procedure. Prior to each creep run, the specimen was heated to around 450°K (350°F), its previous cure temperature, with no load applied.

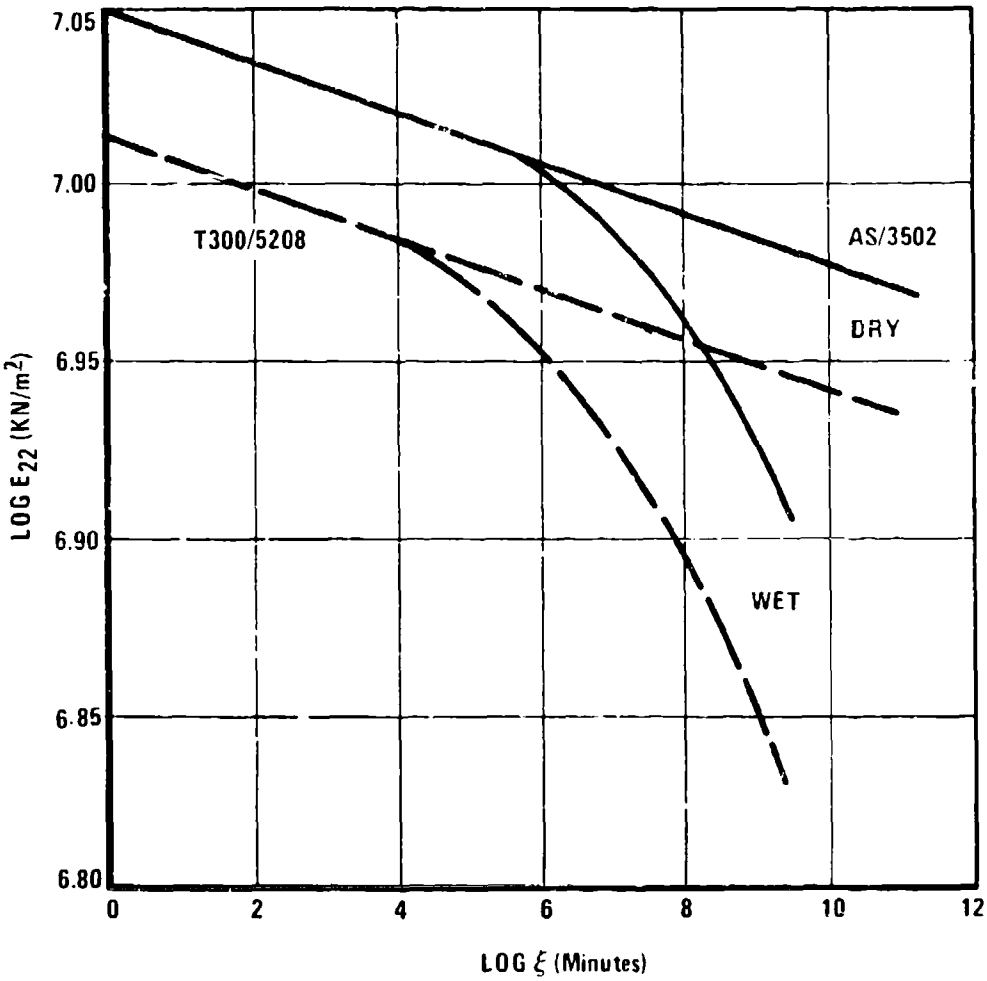

Figure 23 Combined Wet/Dry E_{22} Master Curves

According to Struik (Ref. 16), such a procedure should effectively erase the material's memory of its age, i.e., become "unaged". The modulus results obtained from such specimens are shown in Figure 24.

Two features are very important in Figure 24. Firstly, the long-time/high-temperature behavior shows a marked departure from log-log linearity, in contrast to the dry data shown in Figures 21 or we, and in general agreement with the ± 45 data. Secondly, the master curves for the two materials shown in Figure 24 were obtained with two different sets of shift factors (log a_T). In the T300/5208 case, the master curve was formed with G_{12}-derived shift factors. For the AS/3502, the actual 90° data shown were visually shifted to obtain the best smooth curve. The discrepancy is evident.

It is not particularly satisfying to find that $G_{12}(t)$ and $E_{22}(t)$ master curves have different shift factors, if the time-dependence is logically believed to be matrix controlled. Figure 25 demonstrates, for the T300/5208 material, that G_{12}-derived shift factors are applied to the E_{22} results, then the long-time results for wet and dry (unaged) coupons superpose equivalently on the same master curve (as was the case for wet and dry G_{12} results).

In Figure 26, we repeat the T300/5208 data from Figure 25, and show the individual-temperature results for AS/3502, shifted with the same log a_T values as used for the T300/5208. It does not appear implausible, given the error bars indicated (from repeated runs) that all the 90° data shifts in the same manner as the $\pm 45^\circ$ results.

The apparent effects noted in these 90° data which we have ascribed to physical aging certainly bear further investigation. Residual stresses will always be present to different extents in different layups, and these stresses will be affected by the time-temperature-moisture-environment. It may be very important to ensure that the effective ages of specimens used in comparison tests are in fact comparable.

3.2.4 Summary of Shift Factors

In Figure 27 are shown the time-temperature-humidity shift factors derived from graphical log-log shifting of the ± 45 results and the 90° results, independently. All shift factors given there are referenced to RT dry conditions. In each case shown, the

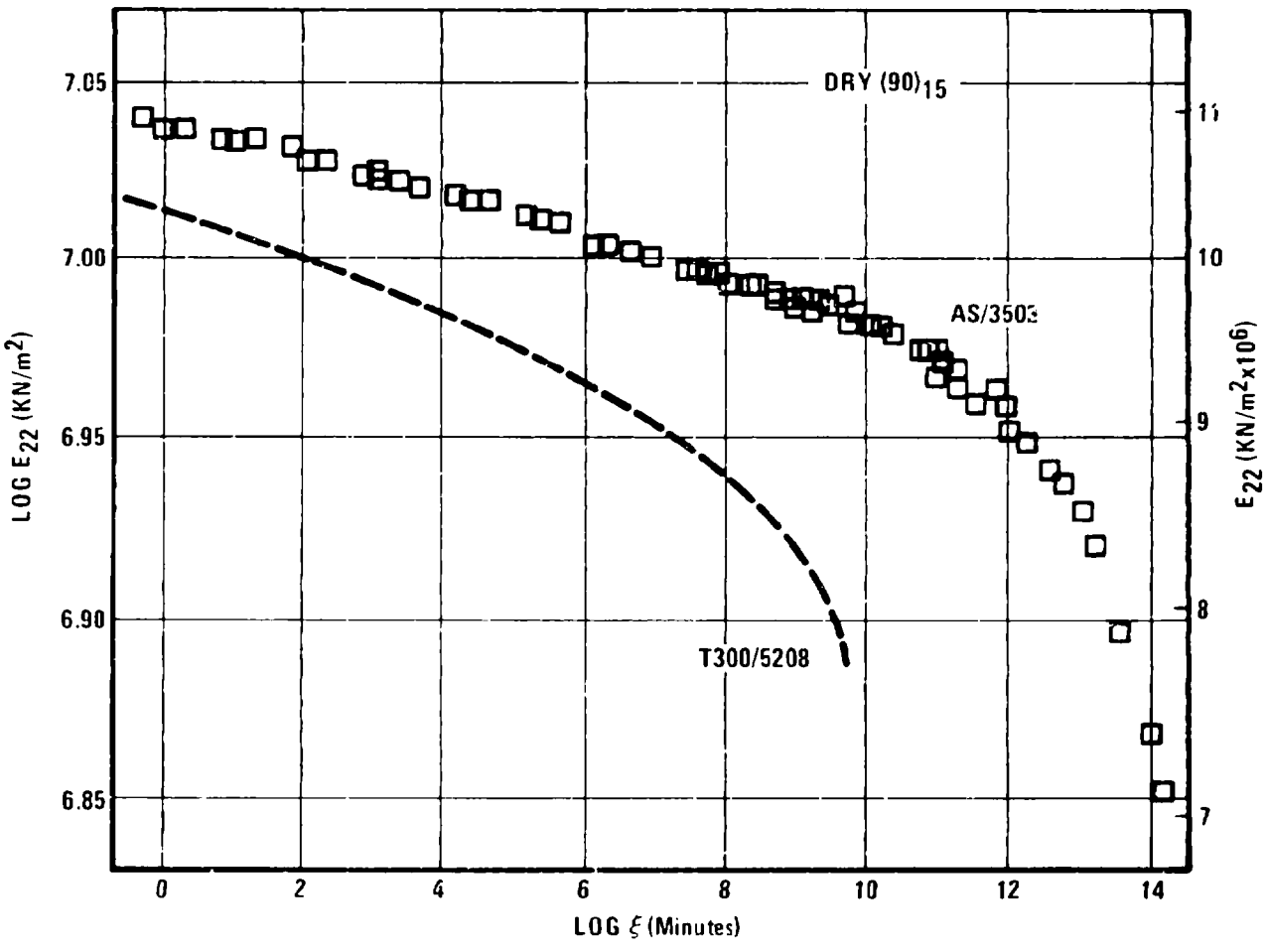

Figure 24 E_{22} MASTER Curves for "Unaged" Materials

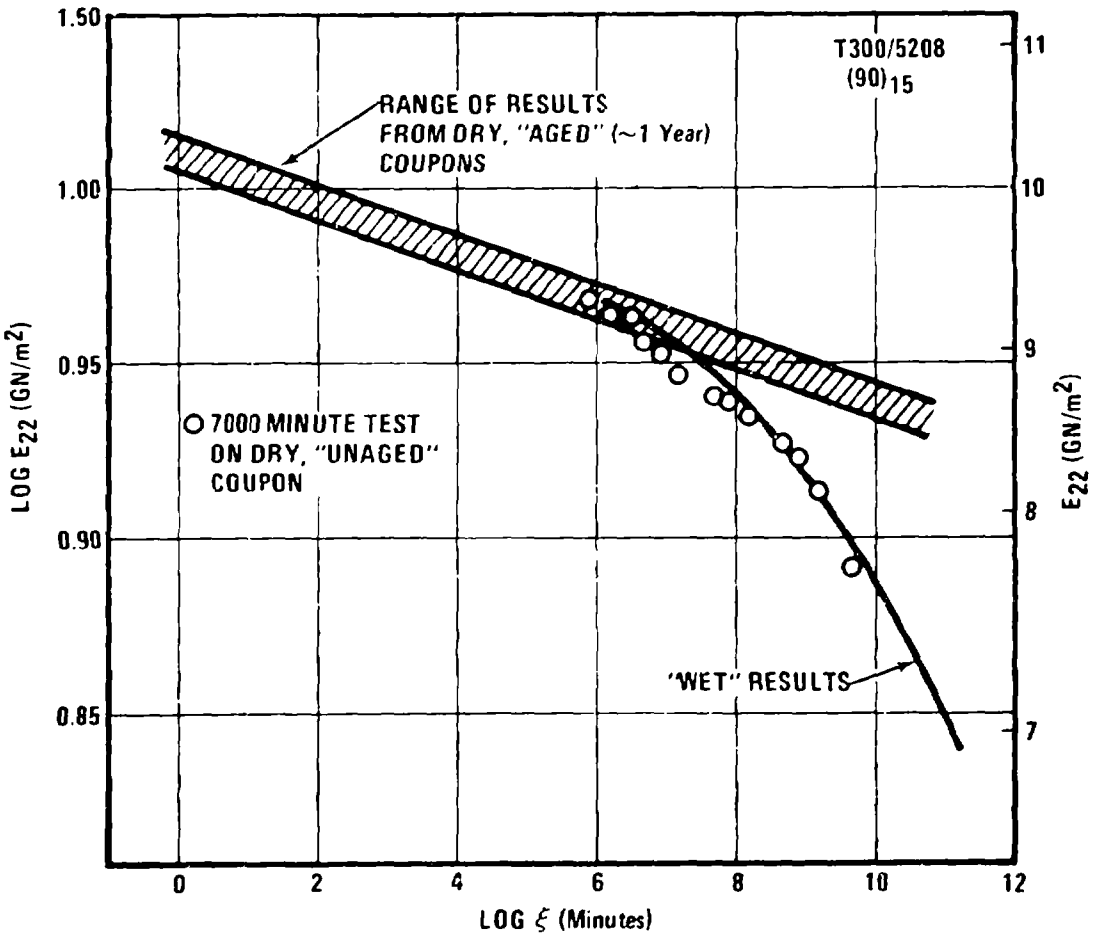

Figure 25 Long-Term Test Results Shifted with a_T from +45's

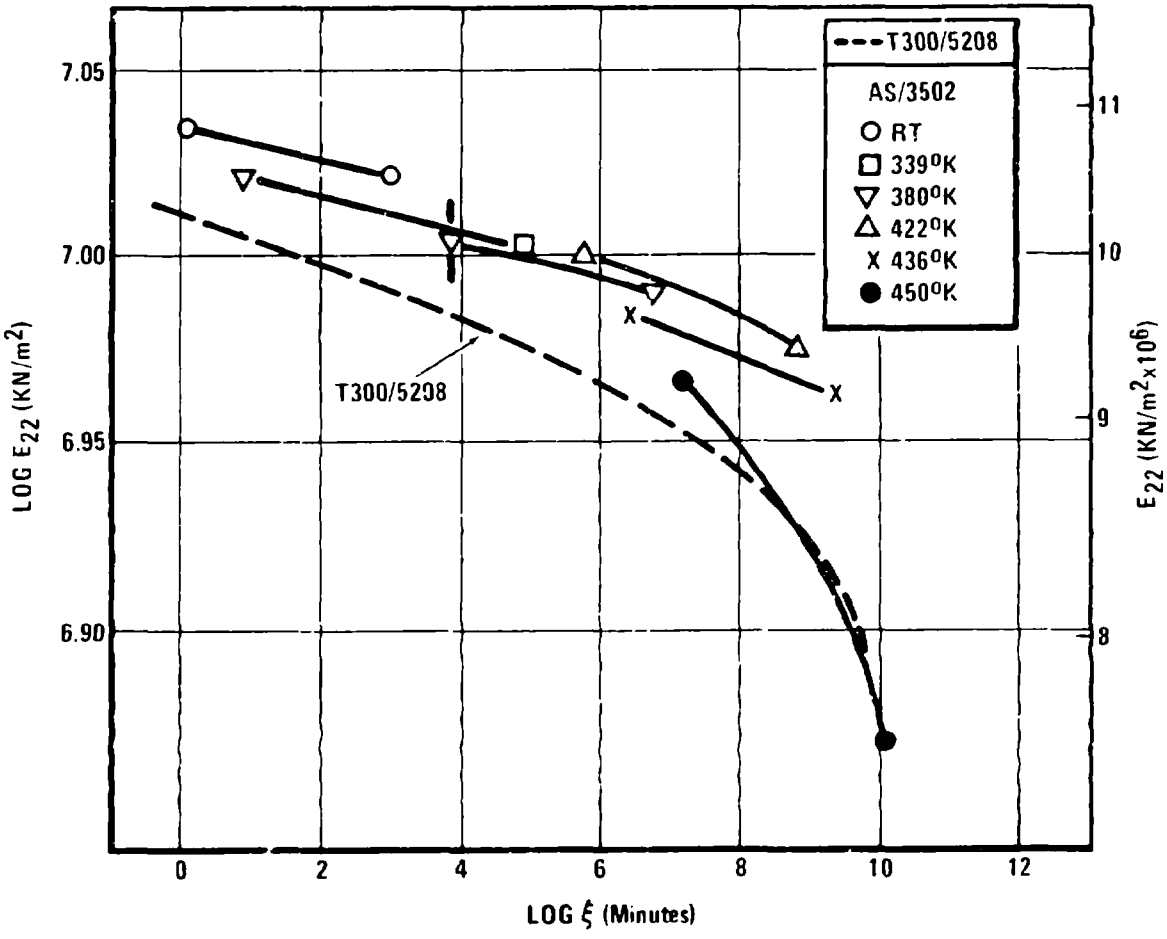

Figure 26 Dry E_{22} Results Shifted with a_T from ±45's

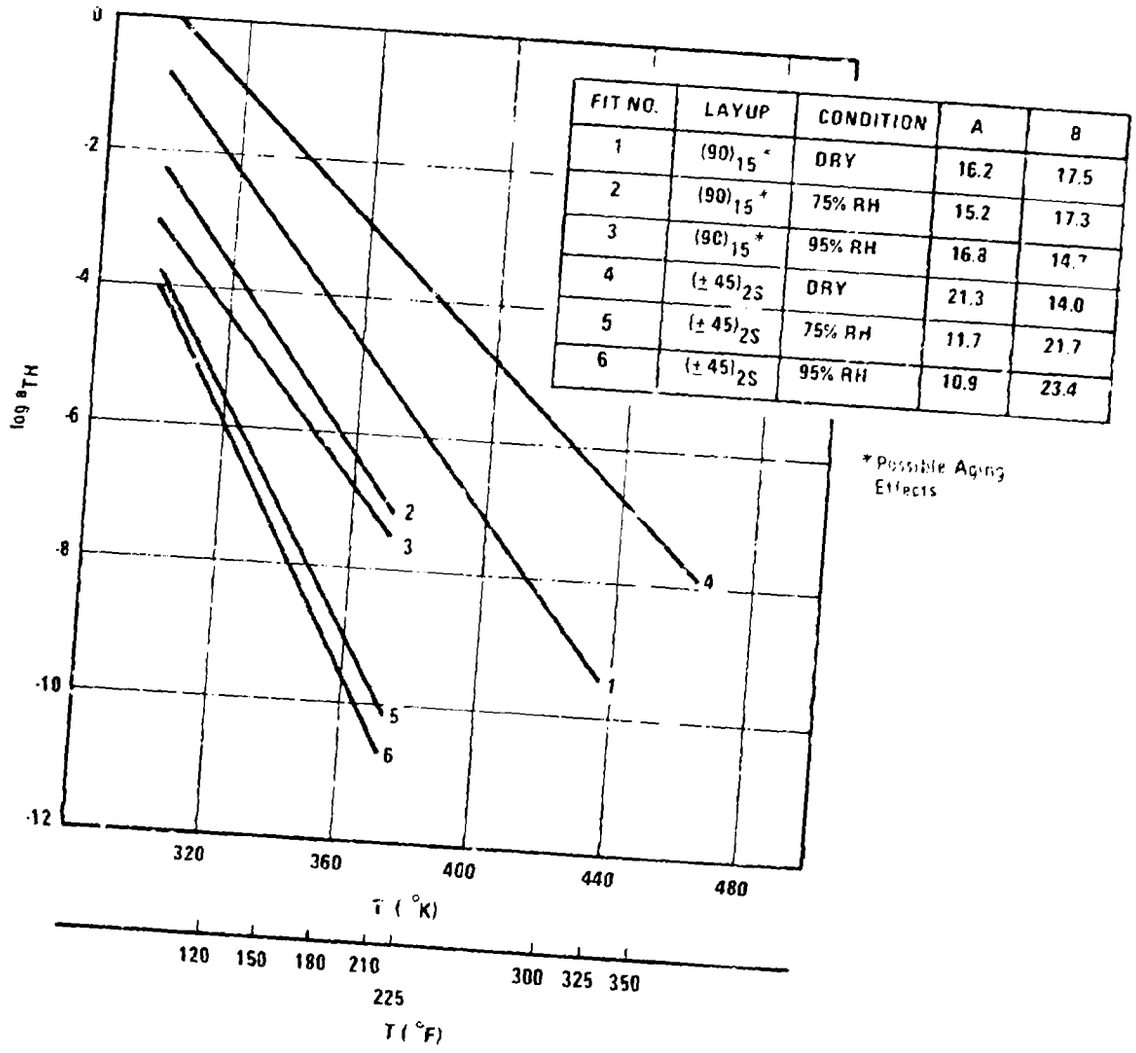

FIT NO.	LAYUP	CONDITION	A	B
1	$(90)_{15}$ *	DRY	16.2	17.5
2	$(90)_{15}$ *	75% RH	15.2	17.3
3	$(90)_{15}$ *	95% RH	16.8	14.7
4	$(\pm 45)_{2S}$	DRY	21.3	14.0
5	$(\pm 45)_{2S}$	75% RH	11.7	21.7
6	$(\pm 45)_{2S}$	95% RH	10.9	23.4

* Possible Aging Effects

Figure 27 Time-Temperature-Humidity Shift Factors

results for the two materials tested have all been included to obtain the fitted curves shown of the form

$$\log a_{TH} = -\frac{T}{A} + B. \qquad (4)$$

We include all six curves to document our overall results. As noted in the previous subsection, however, we would tend to recommend that the $\pm 45^{o}$ coupon shift factors be used for all data. Due to the scatter of some of the 90^{o} results, this practice would not be inconsistent with our overall results, and it does offer the more analytically-reasonable result that all time dependent results, being traceable to matrix effects, are described by a single set of shift factors.

3.3 Laminate Properties

In our tests on laminate tensile compliance, very weak time dependence was observed for coupons with any fibers parallel to the load direction. For example, in an AS/3502 $(0/\pm 45)_S$ laminate tested dry, the total change in measured compliance at $436^{o}K$ was about 4% over a 100-minute creep cycle while, for comparison, a similar test on a ± 45 coupon yielded a roughly 12% change over the same time interval.

Wet tests on the fiber-dominated laminates yielded about the same time-dependent results as the dry. In repeated runs under the same environment for a $(0/\pm 45)_S$ laminate, we found a variation of 4% for RT dry and about 5% for RT wet. Thus, the measured changes in compliance during 100 minutes were typically the same as the test-to-test variability.

In Figure 28, for example, are shown dry test results on a $(0/90/\pm 45)_S$ laminate. Little, if any time dependence is noted, and the change in short time compliance from RT to $464^{o}K$ ($375^{o}F$) is only 6%. Although the compliance in Figure 28 changes in a regular way from the lowest to highest test temperature, that particular result was probably fortuitous, since the run-to-run variation, as previously noted, was 4-5%. The 6% change indicated in the figure is in fact roughly the same as the modulus variation noted in 0^{o} lamina tension tests over this temperature range during lamina design data testing at General Dynamics.

In order to remain cognizant of the experimental variability and its relationship to apparent time dependence, in Figure 29 are plotted "master" curves for two fiber dominated laminates under dry conditions. The data envelopes shown there include

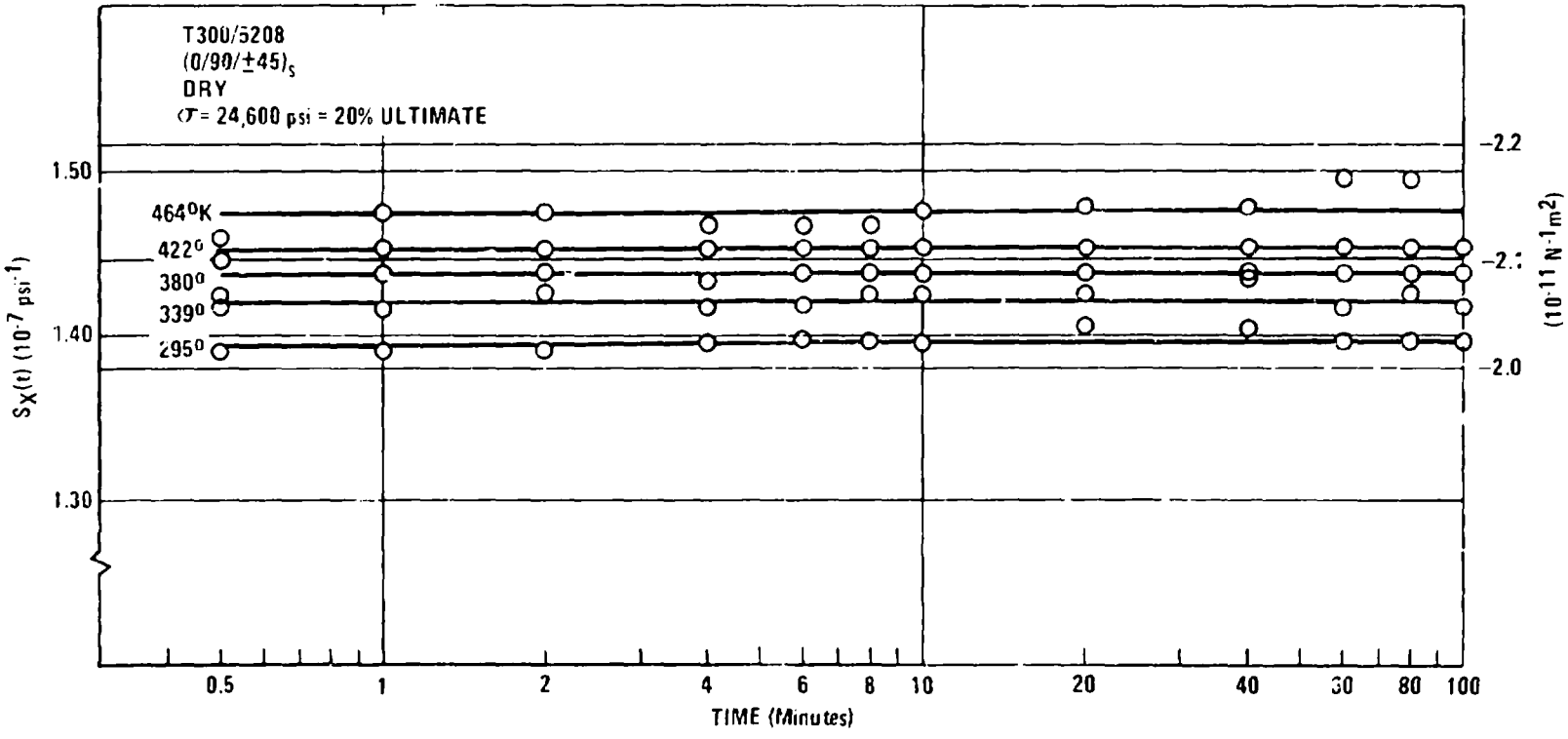

Figure 28 $S_X(t)$ for $(0/90/\pm45)_s$ T300/5208

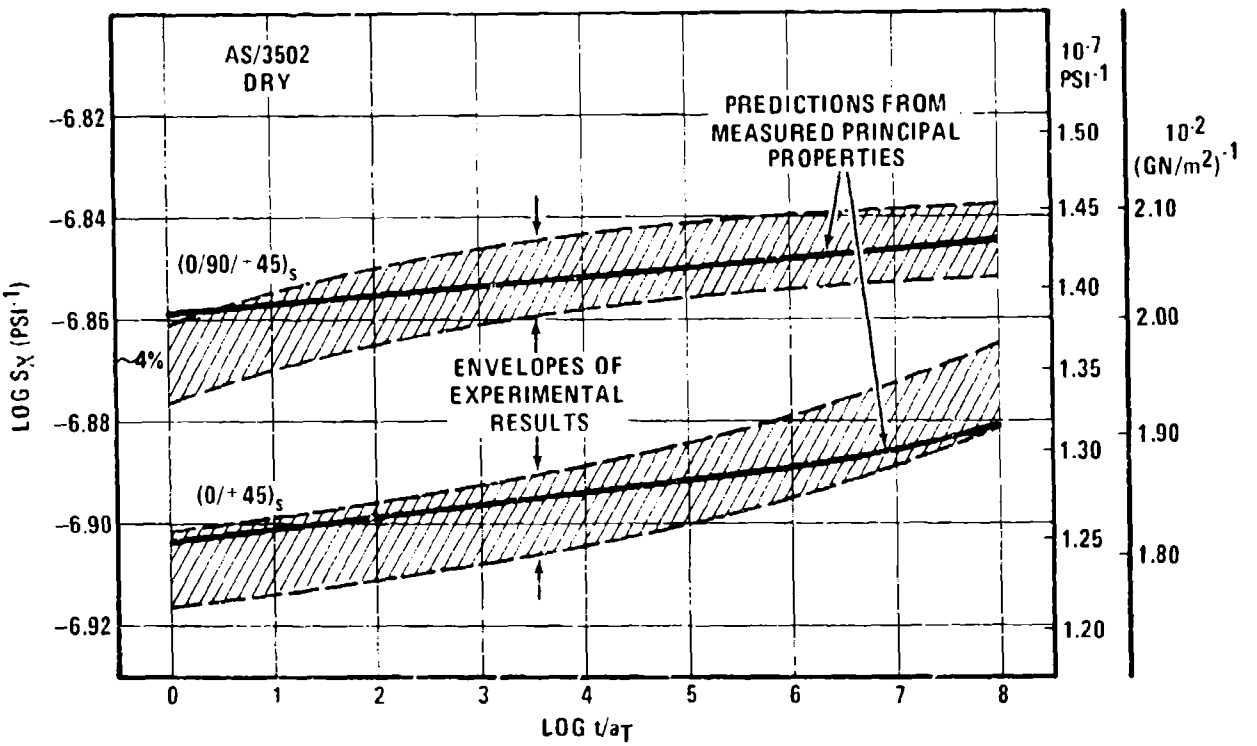

Figure 29 Measured and Predicted Compliance for Dry $(0/\mp 45)_S$ and $(0/90/\mp 45)_S$

nearly all tests on these laminates at all temperatures, and the elevated temperature results have been horizontally shifted in time using the log a_T values derived from the G_{12} results. Also included in that figure are predictions using measured principal properties in an elastic lamination code, with the curves simply calculated stepwise in time. The predictions fall reasonably within the scatter band of data over the entire range of reduced time indicated.

The experimentally-derived master curve, and a similar prediction, for a matrix-dominated laminate, both wet and dry, are shown in Figure 30. Again, the shift factors derived from the ±45 data were used. We observe that the experimental master curve is quite smooth, and the prediction is very good over the entire range. We will discuss this particular laminate prediction in somewhat more detail in Section V.

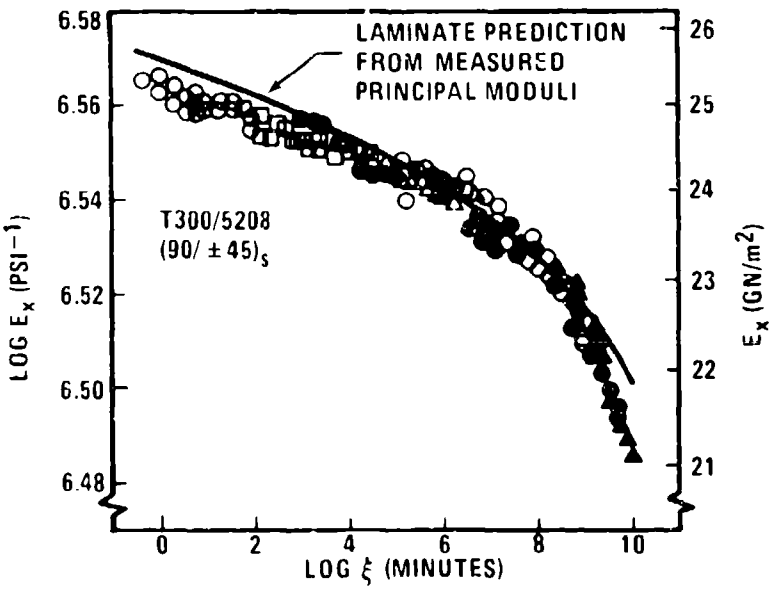

Figure 30 Measured and Predicted Laminate Response

3.4 Residual Strengths

Residual strengths were measured under ambient conditions on approximately 50 specimens which had been creep-tested under various conditions, and these results are shown in Tables IV and V for the two materials.

There is really little generalization which can be made of these results. Realizing that in all cases the changes between residual and baseline properties are only slight, if any, the comments indicated in Table VI might be made.

TABLE VI RESIDUAL STRENGTH TRENDS

Layup/Condition	Trend(Residual Properties Compared to Baseline)
(90) wet	Some reduction
($\pm$45) dry	No change
(90/$\pm$45) dry	Slight increase
wet	Slight decrease
(0/$\pm$45) dry, wet	Slight increase
(0/90/$\pm$45) dry	Slight decrease
wet	Slight increase

TABLE IV RESIDUAL STRENGTH DATA
AS/3502

LAYUP	MOISTURE CONDITION*	STRESS ULTIMATE MN/m^2	STRESS ULTIMATE KSI	STRAIN ULTIMATE %	STRESS ULTIMATE MN/m^2	STRESS ULTIMATE KSI	STRAIN ULTIMATE %
$(90)_{15}$	95%	21(3) [7]	3 [1]	.17(3)	28(3) 3 [.07]	4 .5	.26(3) .02
$(0/\pm45)_S$	DRY	648(2) [41]	94 [6]	1.41(2) [.03]	585(3) [75]	85 [11]	1.04(3) [.14]
	75%	614(3) [62]	89 [9]	1.21(3) [.14]	587(4) [33]	85 [5]	1.10(4) [.06]
	95%	600(3) [76]	87 [11]	1.20(3) [.07]	507(4) [37]	73 [5]	.96(3) [.11]
$(90/\pm45)$	DRY	207(3) [7]	30 [1]	.98(3) [.06]	188(5) [13]	27 [2]	.82(5) [.09]
$(0/90/\pm45)_S$	DRY	483(2) [14]	70 [2]	.98(2) [.03]	536(4) [42]	78 [6]	1.10(4) [.09]
	95%	510(2) [41]	74 [6]	1.11(2) [.09]	481(3) [32]	70 [5]	.94(3) [.07]

* All specimens were tested at all standard creep test temperatures prior to residual strength tests.
(#) Number of specimens tested.
[ ] Standard deviation

TABLE V RESIDUAL STRENGTH DATA
T300/5208

LAYUP	MOISTURE CONDITION*	RESIDUAL STRENGTH STRESS ULTIMATE MN/m²	RESIDUAL STRENGTH STRESS ULTIMATE KSI	RESIDUAL STRENGTH STRAIN ULTIMATE %	BASELINE STRENGTH (RT) STRESS ULTIMATE MN/m²	BASELINE STRENGTH (RT) STRESS ULTIMATE KSI	BASELINE STRENGTH (RT) STRAIN ULTIMATE %
$(90)_{15}$	75%	27(3) [.2]	4 [.03]	.31(3) [.01]	27(4) [6]	4 [1]	0.24 [.06]
		15(1) -	2 -	.16(1) -			
$(\pm 45)_{2S}$	DRY	159(3) [2]	23 [.3]	1.71(1) -	161(4) [6]	23 [1]	1.17 [.12]
	DRY - 2 TEMP	156(2) [4]	23 [.6]				
	DRY - 3 TEMP	158(1) -	23 -				
$(0/\pm 45)_S$	DRY	575(3) [21]	83 [3]	1.06(1) -	593(5) [30]	86 [4]	1.03(5) [.05]
	75%	579(3) [64]	84 [9]	1.05(3) [.12]	483(4) [43]	70 [6]	.92(4) [.07]
$(90/\pm 45)_S$	DRY	209(3) [10]	30 [1]	.91(3) [.05]	148(4) [6]	21 [1]	.63(4) [.02]
	75%	172(3) [6]	25 [1]	.80(3) [.05]	233(4) [112]	34 [16]	1.07(4) [.55]
		168(3) [6]	24 [1]				
	95%	152(3) [3]	22 [.5]	.72(3) [.01]	178(3) [6]	26 [1]	.80(3) [.04]
$(0/90/\pm 45)_S$	DRY	427(3) [34]	68 [5]	.93(3) [.06]	515(1)	75	1.02(1)

3.5 Stress-Strain vs. Strain Rate

As a slight addition to the originally-planned test program, we conducted a brief experimental analysis of the effects of strain rate on tensile stress-strain testing. Instron stress-strain to failure tests were run on $(\pm 45)_{2S}$ coupons of T300/5208. Specimens were tested at RT, 380°K (225°F), 422°K (300°F), and crosshead rates of 0.00085 cm/sec (0.02 in/min), .002 (.05), .004 (.1), .0085 (.2), .02 (.5), .04 (1), and 0.085 (2). Although only one coupon per condition was tested, it was felt that useful trends might be observed, since the inherent time-dependence of the material should be expected to modify the observed tensile behavior at various strain rates, particularly at elevated temperature.

As expected, considerable scatter in the results was evident due to our use of only one coupon per condition. The following trends in the results are suggested, however.

- o There appeared to be a slight increase in stress ultimate as the strain rate increases.
- o Strain ultimates were quite erratic, but a peak appeared around .004 cm/sec crosshead rate, followed by a valley at somewhat higher rates, then a slight increase at the highest rates.
- o The Poisson ratio ν_{xy} appeared relatively constant, although with considerable scatter, under all test conditions.
- o At low stresses, say about 13.8 MN/in^2 (2000 psi), the longitudinal modulus tended to increase as the strain rate decreased.

Although these results were quite sketchy due to the limited amount of data, one should observe that caution need be exercised in the application of tensile stress-strain data for matrix-dominated coupons. Changes in measured properties do occur as the testing rates change. Thus, for example, if baseline tensile properties are to be used to set parameters for a fatigue test, the baseline rates and environment should duplicate the planned fatigue parameters as closely as possible.

SECTION IV

4. EXPANSIONAL STRAINS

In this section, we present our experimental results on the longitudinal and transverse strains observed in the two material systems due to moisture and temperature effects.

4.1 Moisture Absorption

In order to obtain moisture-induced swelling strains, unidirectional $(0)_6$ specimens were conditioned at four constant humidities at room temperature. For comparison purposes, however, additional absorption measurements were conducted on these specimens at 322°K (120°F) and 339°K (150°F) and at RT on samples of all layups used in this program. Samples for all these uptake-swelling measurements were typically 3 cm (1.2 in) square.

Specimens were conditioned in appropriate temperature chambers over saturated salt solutions, where the relative humidities achieved are as indicated in Table VII below for exposures at 339°K (150°F).

TABLE VII CONDITIONING PARAMETERS

Solution	RH(%)
KF	21
CrO_3	46
NaCl	74
$Pb(NO_3)_2$	93

The variation in humidity with temperature for these solutions is not particularly significant. The lead nitrate solution possibly shows the greatest variation, rising from 93% at 339°K to 97.5% RH at RT. We will ordinarily refer to this highest humidity used as 95%, which represents the average of this observed range.

Moisture uptake results for these graphite-epoxy materials are shown in Figures 31 - 33. After initial drying to an equilibrium weight value, the specimens were periodically weighed with a Mettler Model BA28/BE20/CT10 automatic digital balance. Three replicates were used for each data point. For one conditioning case (RT/97% RH) we exposed identical unidirectional specimens of both materials in two different chambers to assess conditioning variabilities. The maximum difference in weight gain observed in these "identical" experiments was slightly over 10% (e.g., 1.0 $\pm$ 0.1% moisture by weight) which is not atypical for such experiments, even though the standard deviation in resin content is only about $\pm$3%.

We may observe from these figures that the moisture absorption characteristics for the two material systems are quite similar, although the T300/5208 specimens generally tend to exhibit a slightly higher (~10%) weight gain than the AS/3502. We also note from Figure 31 that the addition of elevated temperature (339°K) causes roughly a 10% increase in moisture pickup, even though the effective humidity is somewhat lower at that higher temperature.

Figure 34 compares the moisture uptake under identical conditions for two different 6-ply layups of AS/3502. The saturation levels are the same, but, as might be expected, slight differences in rate occur for the differing stacking sequences.

A summary of the apparent maximum moisture content, $M_m(\%)$, as a function of relative humidity is given in Figure 35. We have in the past experienced difficult in obtaining reliable and reproducible results at very low humidities. The 21% RH data shown there are no expection. Those specimens were not weighed until about 250 days into the exposure in order to avoid the long re-equilibration times noted after opening the low-humidity chambers. Those results were will inconsistent with the other measurements, and were not included in the curve fit shown.

The anomalous diffusion behavior, particularly after long exposure times, which has been noted by some (e.g., Ref. 17 and 18), does not seem apparent in our present results.

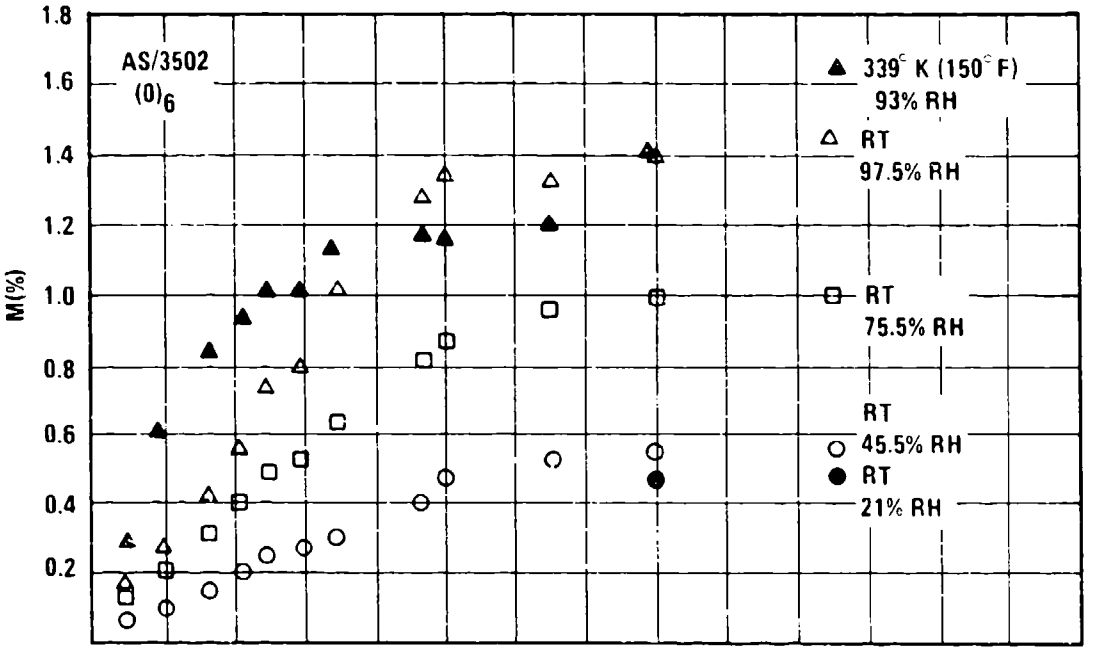

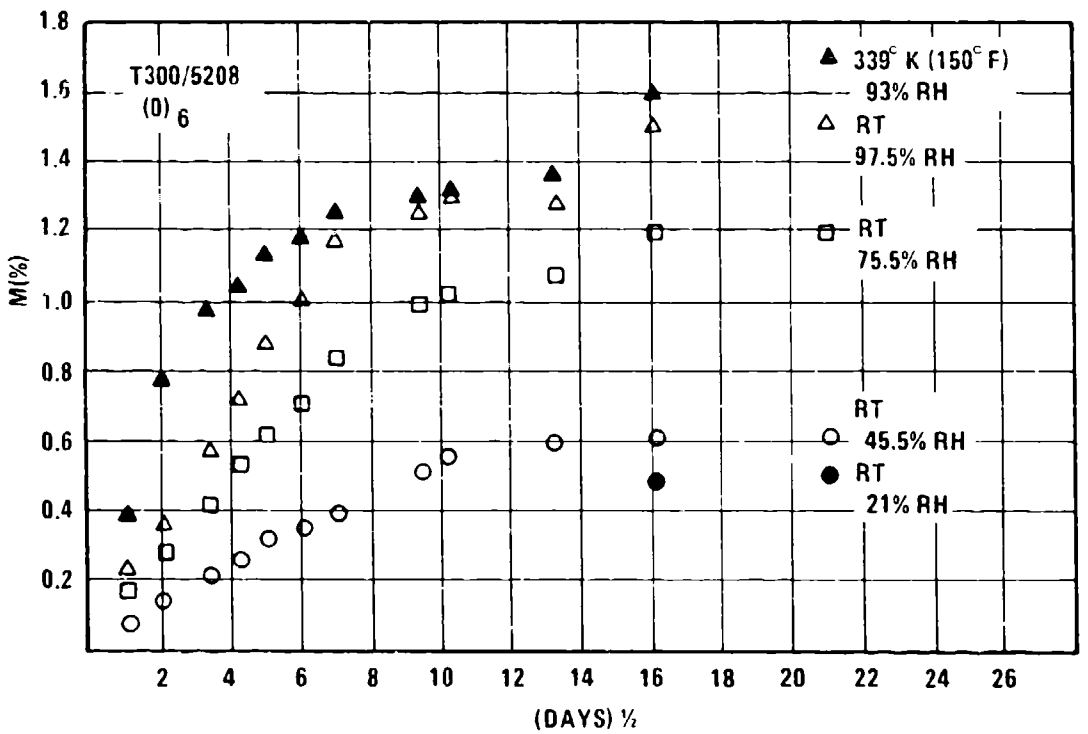

Figure 31 Moisture-Induced Weight Gain for $(0)_6$ Coupons

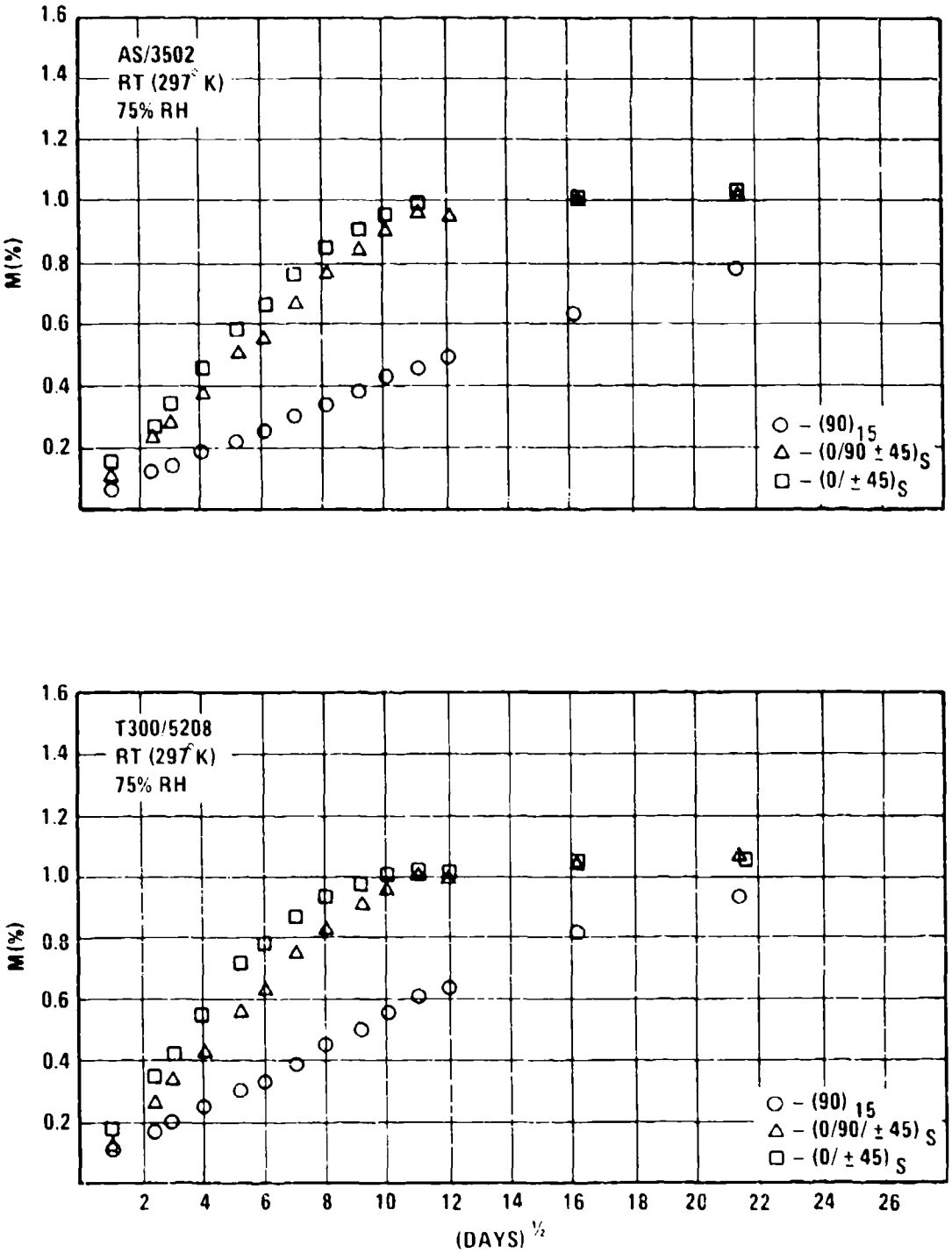

Figure 32 Moisture-Induced Weight Gain at 297° K (RT), 75% RH, for Various Laminates

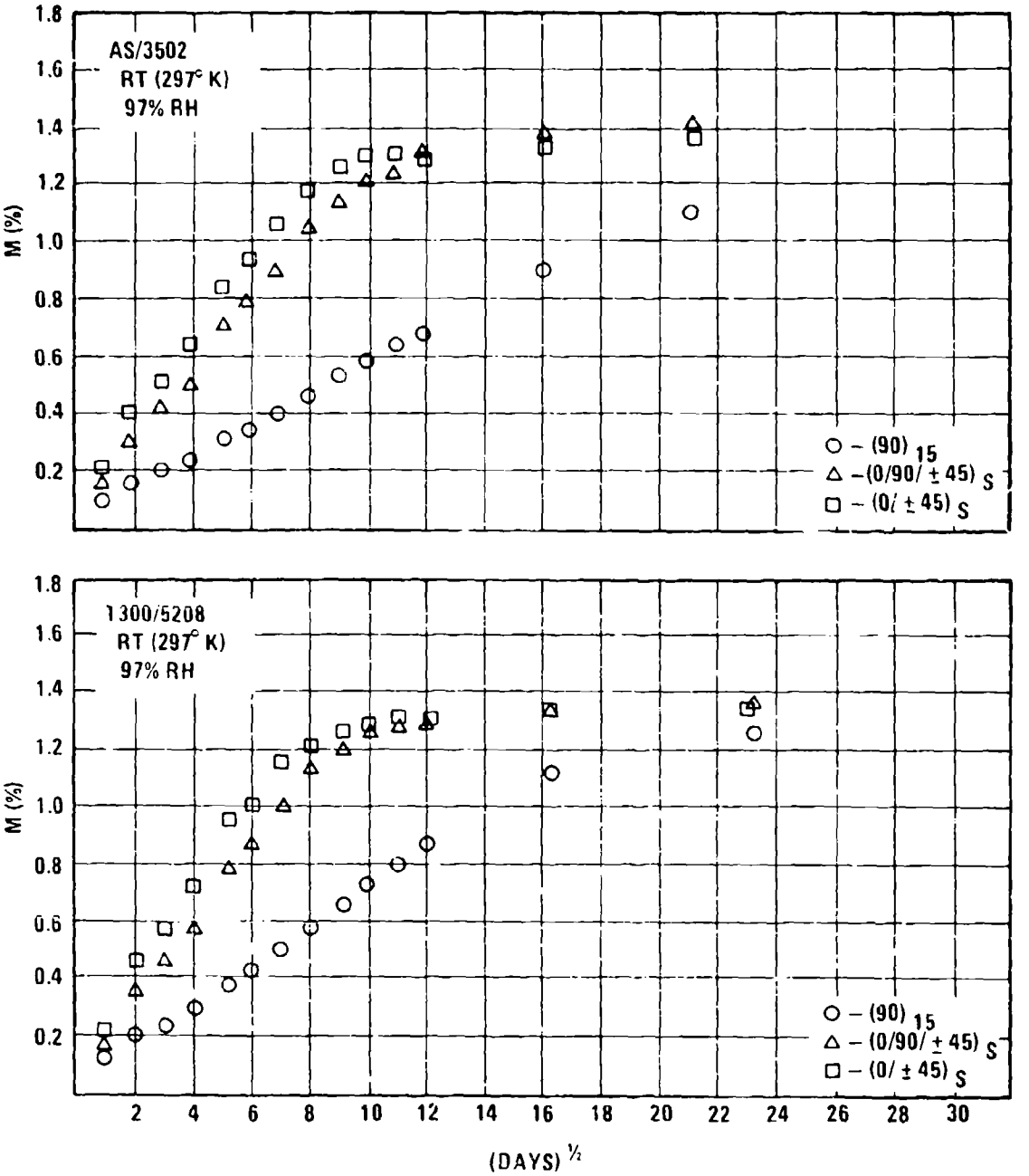

Figure 33 Moisture-Induced Weight Gain at 297° K (RT), 97% RH, for Various Laminates

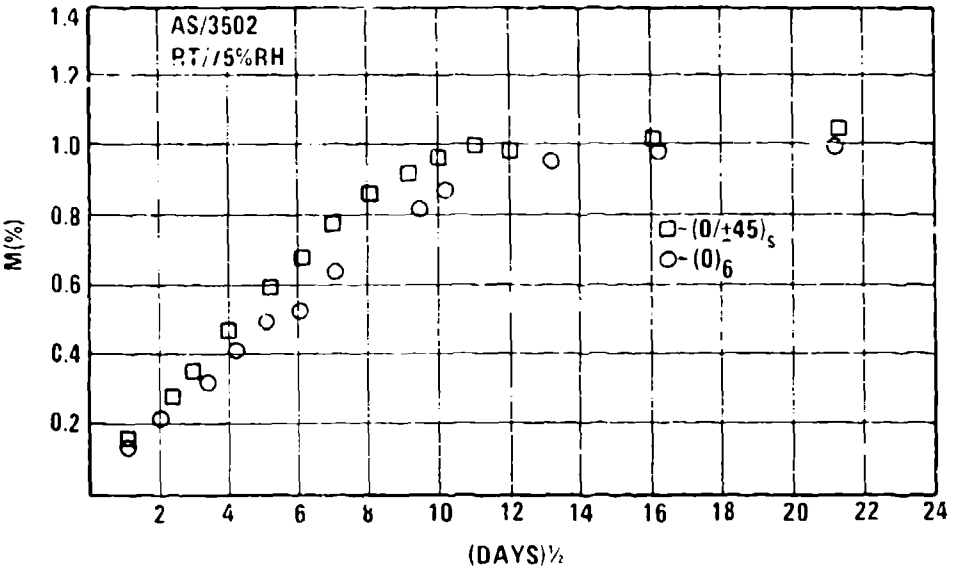

Figure 34 Comparision of Moisture Uptake In Different 6-Ply Layups

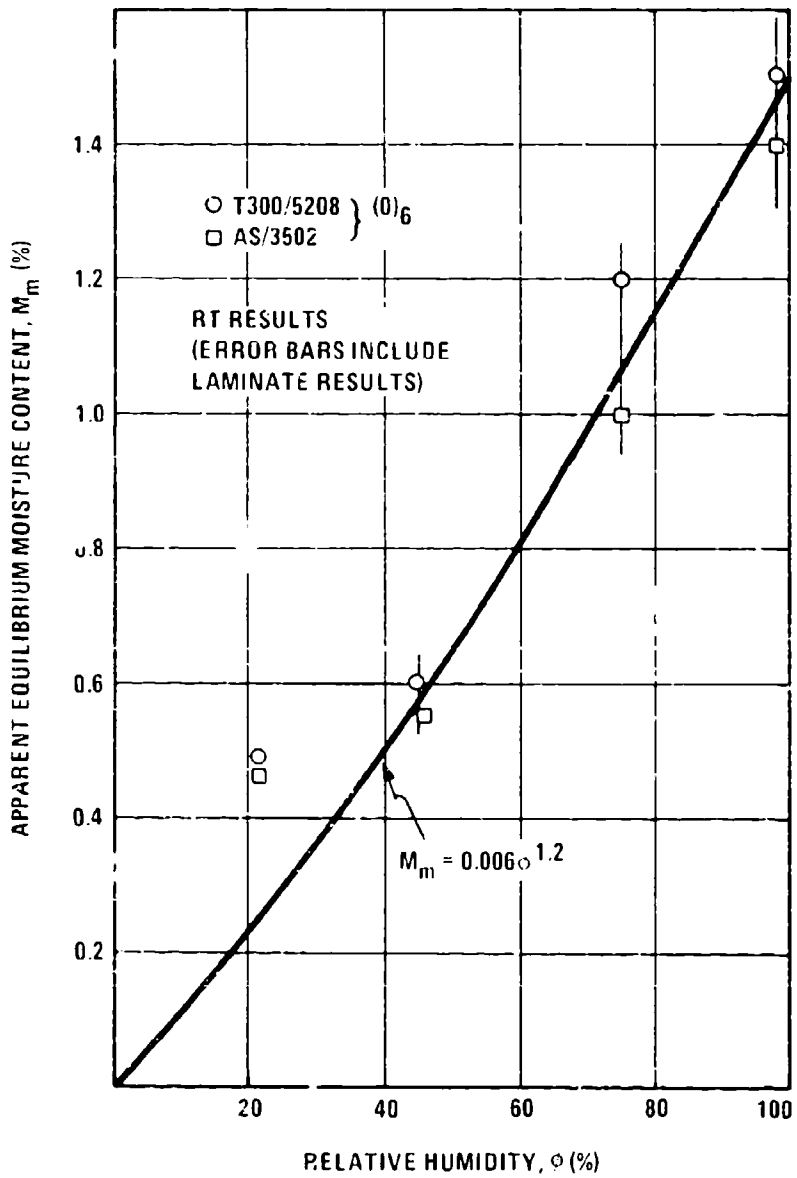

Figure 35 Variation of "Maximum" Moisture Level with Relative Humidity at Room Temperature

4.2 Moisture-Induced Swelling

At the same time each of the coupon weight gains was monitored, the specimen dimensions were measured using 4-place micrometers. This technique relies on the use of a fixture to hold both the micrometer and the specimens in a fixed relationship to one another, so that reproducible measurements are obtained on the specimen at the same reference position each time.

Swelling measurements were made on all three specimen dimensions. Within the limits of the measurements, however, no repeatable swelling was observed through the thickness (due to the 6 ply = .08 cm dimension). Along the fiber direction, a contraction of typically 0.01 -0.03% was usually observed, but such is probably not outside the data scatter.

Figure 36 shows the measured swelling in width (transverse to the fiber direction) for both materials at room temperature and at elevated temperature (322 and 339°K). The RT data are all quite similar for both materials, and are conveniently described by the equation given there. At elevated temperature we observe a trend toward somewhat greater expansional strain for a given moisture content.

As is used in such results, there is no observable swelling until a threshold moisture content is reached. The threshold here observed is at M(%)≃ 0.1, although at these very low swelling strains the threshold is somewhat indefinite and might be assigned somewhat higher. Crossman (Ref. 9 and 15) found the threshold at 0.4% for GY70/CE339 laminates, e.g.

During the course of the program, we also attempted to measure these swelling strains by two other methods, densitometric and via our thermo-mechanical analyzer (TMA). Since the TMA utilizes a highly precise probe and LVDT combination, we felt that this latter method held great promise. We were, however, not able to reproduce measurements due to the difficulty of repeatable positioning of the specimens. Both methods yielded unsatisfactory reproducibility and were abandoned in favor of the micrometer measurements described.

4.3 Thermal Expansion

Thermal expansion measurements on unidirectional $(90)_{15}$ composites were accomplished using a loaded column expansion method (Ref. 19) with a Perkin-Elmer TMS-1 thermomechanical analyzer (TMA). A schematic diagram of this test is shown in Figure 37.

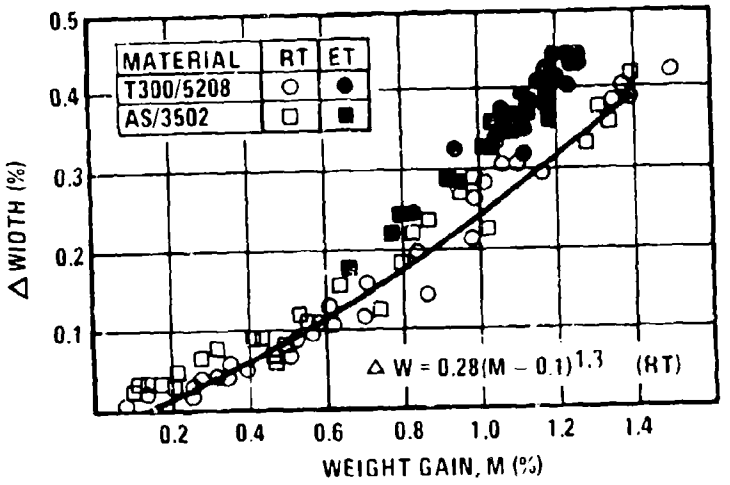

Figure 36 Moisture-Induced Swelling

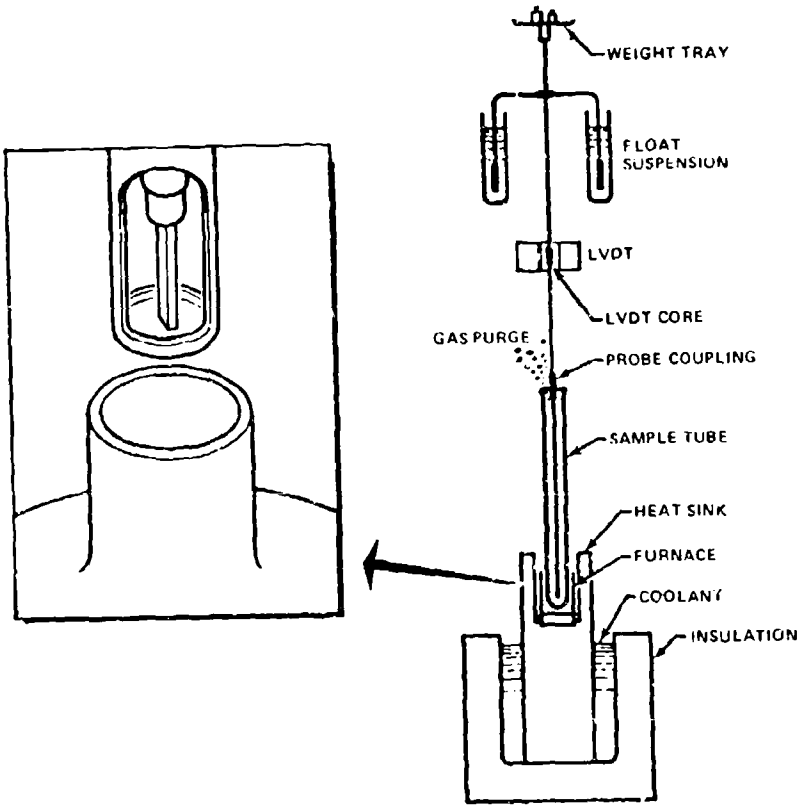

Figure 37. TMA Schematic for Loaded–Column Thermal Expansion Tests

Samples of dimension typically 1.27 cm x .64 cm x .20 cm were loaded parallel to the long dimension by placing 20-100 gm weights on top of the vertical quartz probe which rested on the test specimen. Changes in specimen length were then measured using a linearly variable differential transformer through which the probe moved. The probe used was a flat-bottomed quartz expansion probe with a diameter of approximately 0.25 cm. Further details of the technique and a specific discussion regarding measurements on moisture-saturated specimens may be found in Ref. 19.

For measurements of α_{11}, the thermal expansion coefficient parallel to the fibers, only one load/rate combination was used in the TMA apparatus, namely 100 gm and 20°K/min. Figures 38 and 39 summarize these measurements for dry and wet coupons. We note from those results that, as expected, α_{11} is negative for both materials due to the negative thermal expansion coefficient of graphite. The apparently large data scatter is to be expected however at these high TMA sensitivities ($0.1\mu\epsilon$).

The solid curves in each case represent a least squares fit to the data over the range indicated. It is interesting to observe the apparent slight differences in thermal characteristics of the T300 and AS fibers: α_{11} for T300 is about 2-3 times greater for T300 than for AS, i.e., typically $-0.6\mu\epsilon/^{\circ}K$ compared to $-0.25\mu\epsilon/^{\circ}K$. The fits would also suggest that α_{11} decreases slightly with increasing temperature for T300, while the opposite behavior occurs for AS fibers. Both curves suggest a dry glass transition temperature (T_g) in the 480-500°K range, which is somewhat higher than that inferred from the ensuing figures for α_{22}.

In order to examine possible load and rate effects during our measurements of α_{22} (thermal expansion coefficient transverse to the fibers), we employed the load/rate combinations indicated in Table VIII.

TABLE VIII LOAD/RATE PARAMETERS FOR α_{22} MEASUREMENTS

Scan Rate (°K/min) =	2.5	5	10	20
Load = 10 gm	X	X	X	X
= 100 gm		X		X

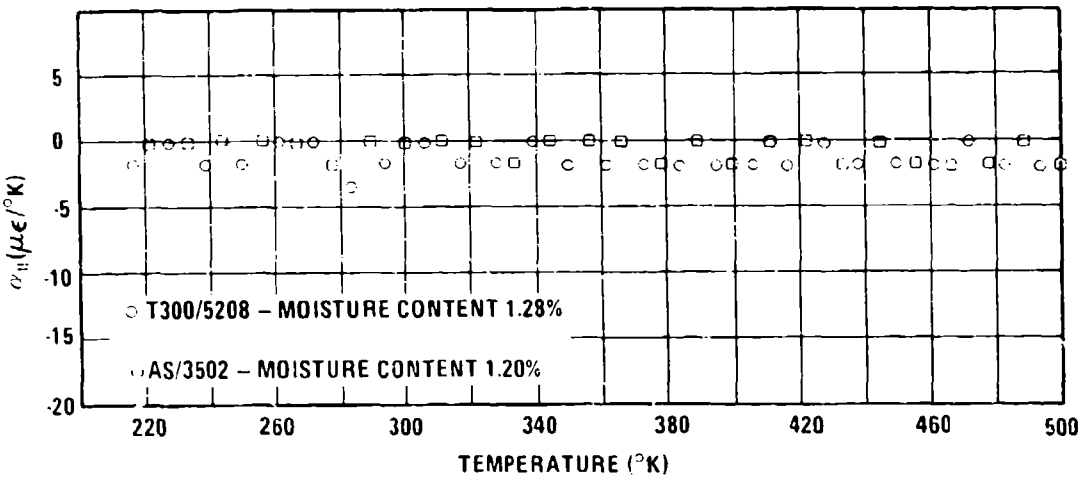

Figure 38 Longitudinal Thermal Expansion Coefficient $\alpha_{\parallel}$ for Both Materials Conditioned at 95% R.H.

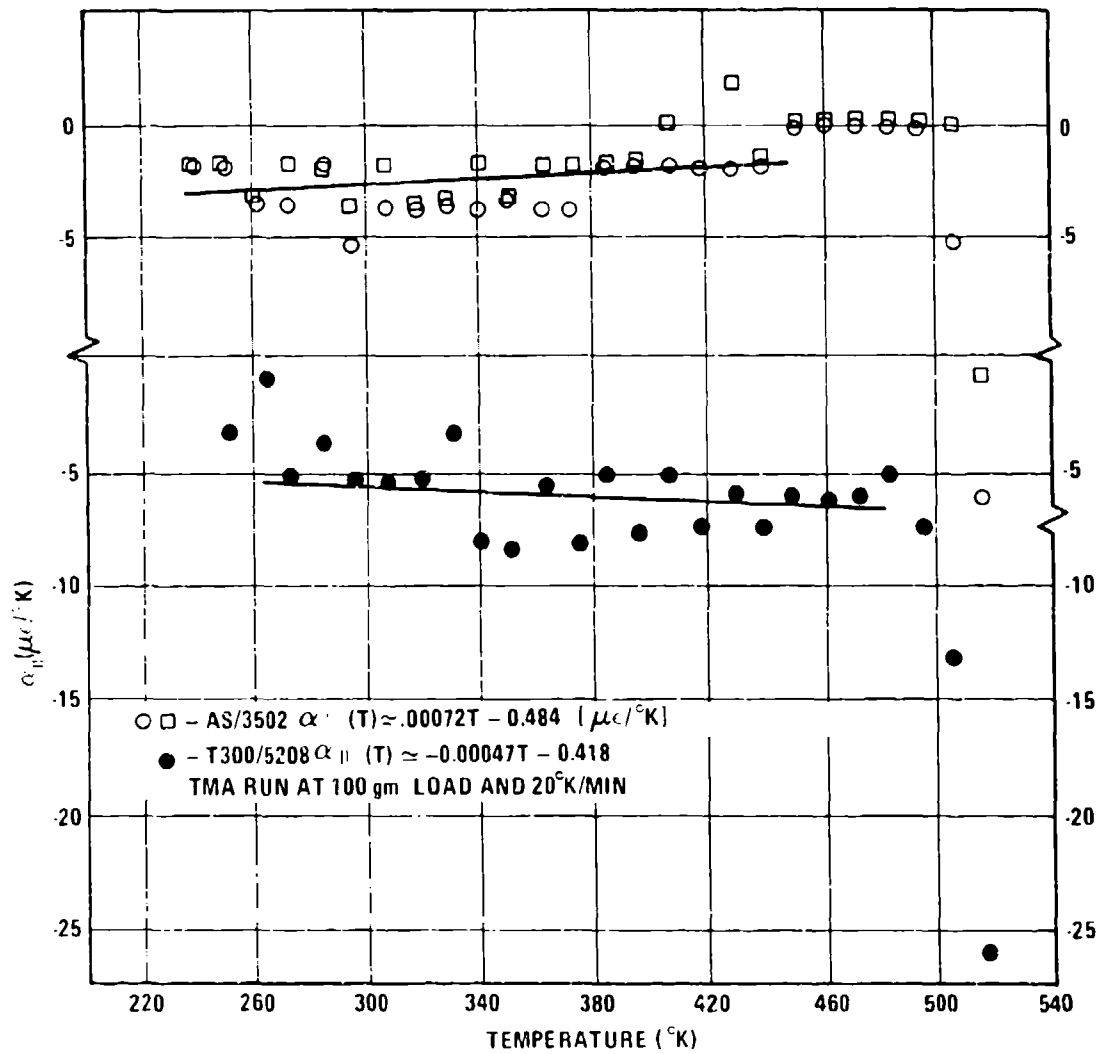

Figure 39 Longitudinal Thermal Expansion Coefficients $\alpha_{\parallel}$ for Dry Coupons

Figure 40 shows the measured α_{22} (dry) for the two materials. Although data for only four load/rate combinations are shown, the other results closely parallel those presented. The solid lines in the figures are again least squares fits to the data up to the cure/postcure temperature. The α_{22} values are quite similar for both materials (which is to be expected since the resin systems are similar) and the indicated T_g for each material is in the range of 450-480°K, at or slightly above the cure temperature.

Thermal expansion coefficients α_{22} for wet materials were run in the TMA at 20°K/min and 100 gm load. Such parameters have been found to yield valid measurements on moisture-saturated specimens, even though some drying occurs at the specimen surface (Ref. 19). Results for the two materials are shown in Figures 41 and 42 for specimens conditioned at 75% and 95% RH, respectively. Two specimens of each material were run in the TMA. We have plotted results for only one experiment in each case. The wet T_g values at 75% RH conditions would appear to be in the 375-385°K range (215-233°F); at 95% RH, the values are somewhat lower, namely 360-370°K (188-206°F).

As noted in the previous section, our test plan for time-dependent measurements on wet specimens was based on an expected wet T_g near the boiling point of water. Thus our highest test temperature for wet (creep) specimens of 372°K (210°F) was always at or slightly above the respective transition temperatures.

The glass transition values obtained from α_{22} measurements are summarized in Figure 43. We have there indicated the dry T_g to be at the postcure temperature, although our results may suggest a value somewhat higher.

4.4 Summary of Constants

In Table IX, following, are summarized the hygrothermal constants measured in this task for T300/5208 and AS/3502. Only one set of thermal expansion coefficients are given for wet (95% RH) coupons, since the results are quite similar for the two humidities investigated. The moisture-induced swelling parallel to fibers, β_{11}, is taken as zero from our results.

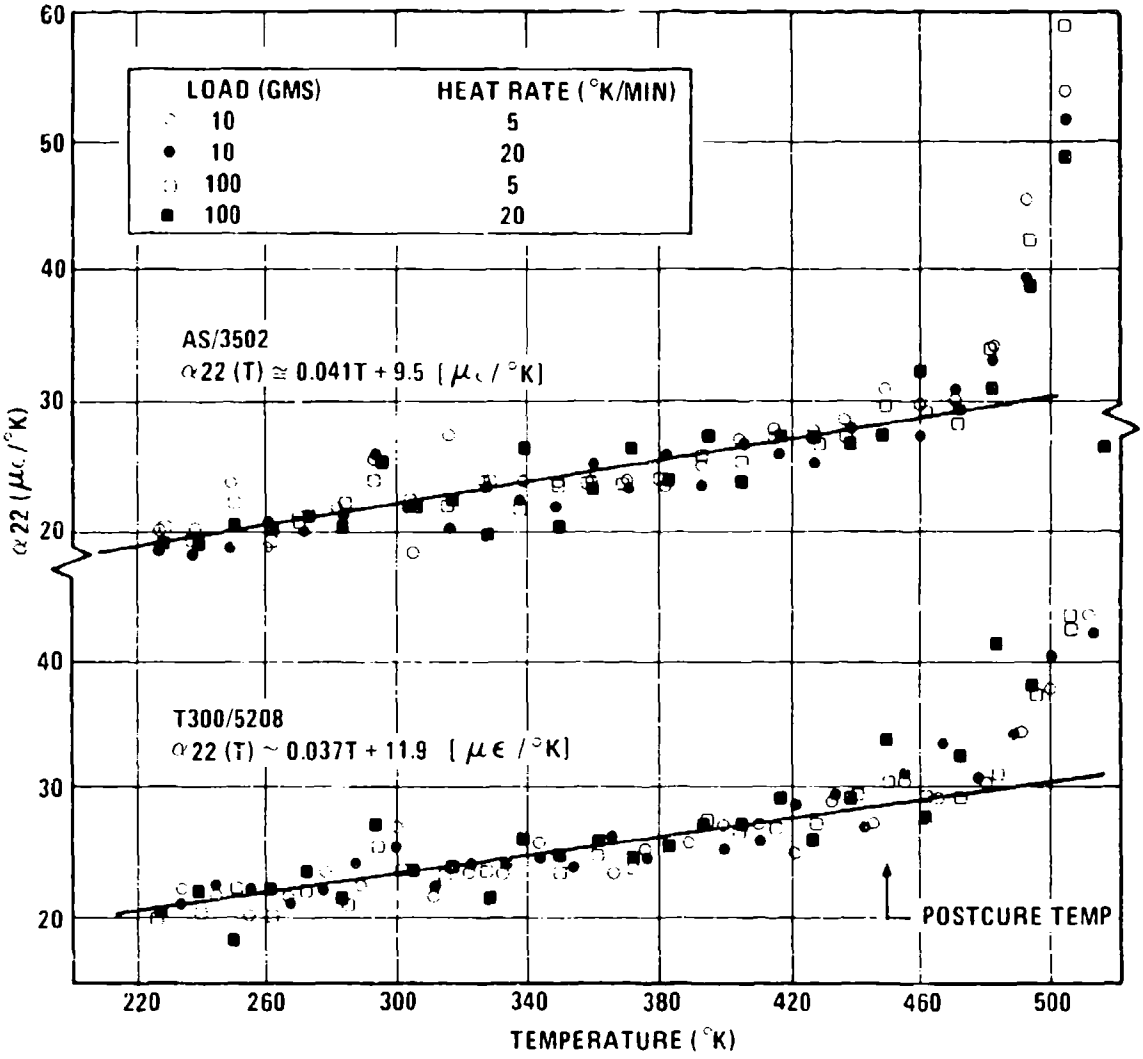

Figure 40 Transverse Thermal Expansion Coefficients α_{22} For Dry Coupons

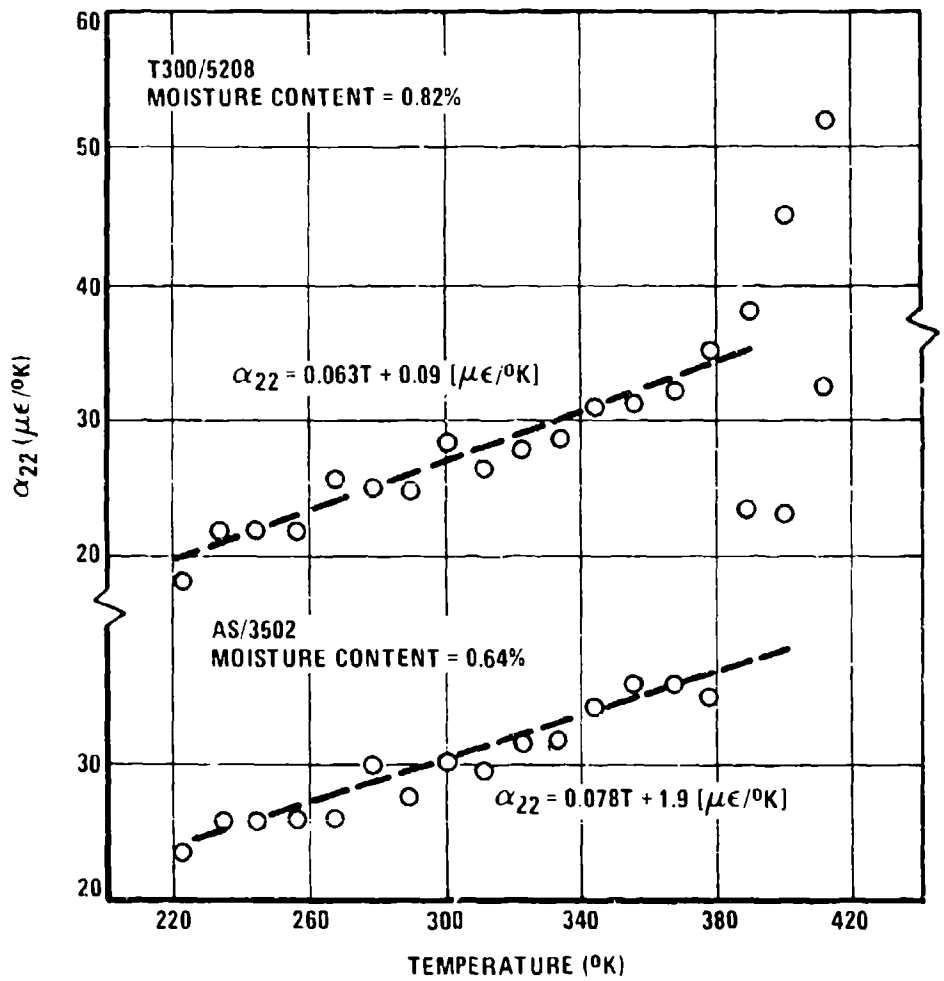

Figure 41 Transverse Thermal Expansion Coefficient α_{22} for Coupons Saturated at 75% LH

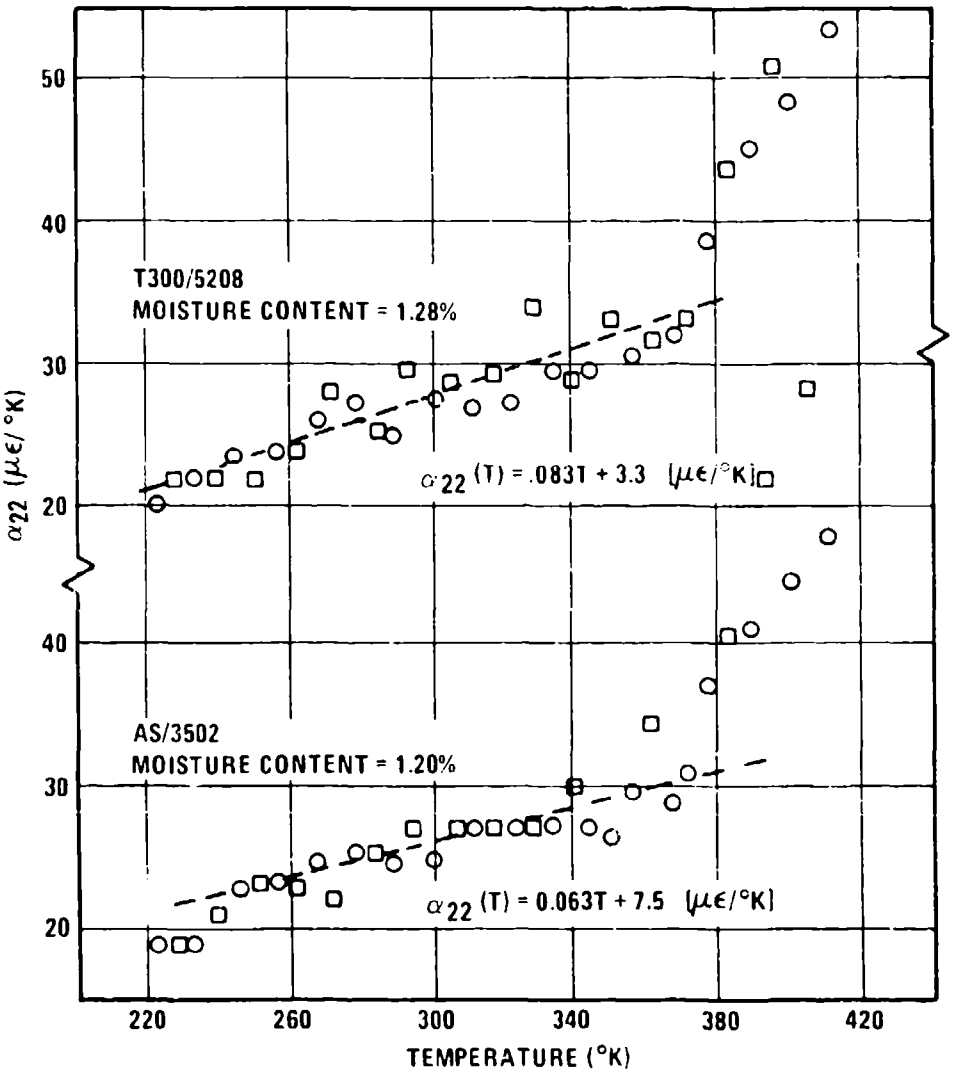

Figure 42 Transverse Thermal Expansion Coefficients α_{22} for Coupons Conditioned at 95% R.H.

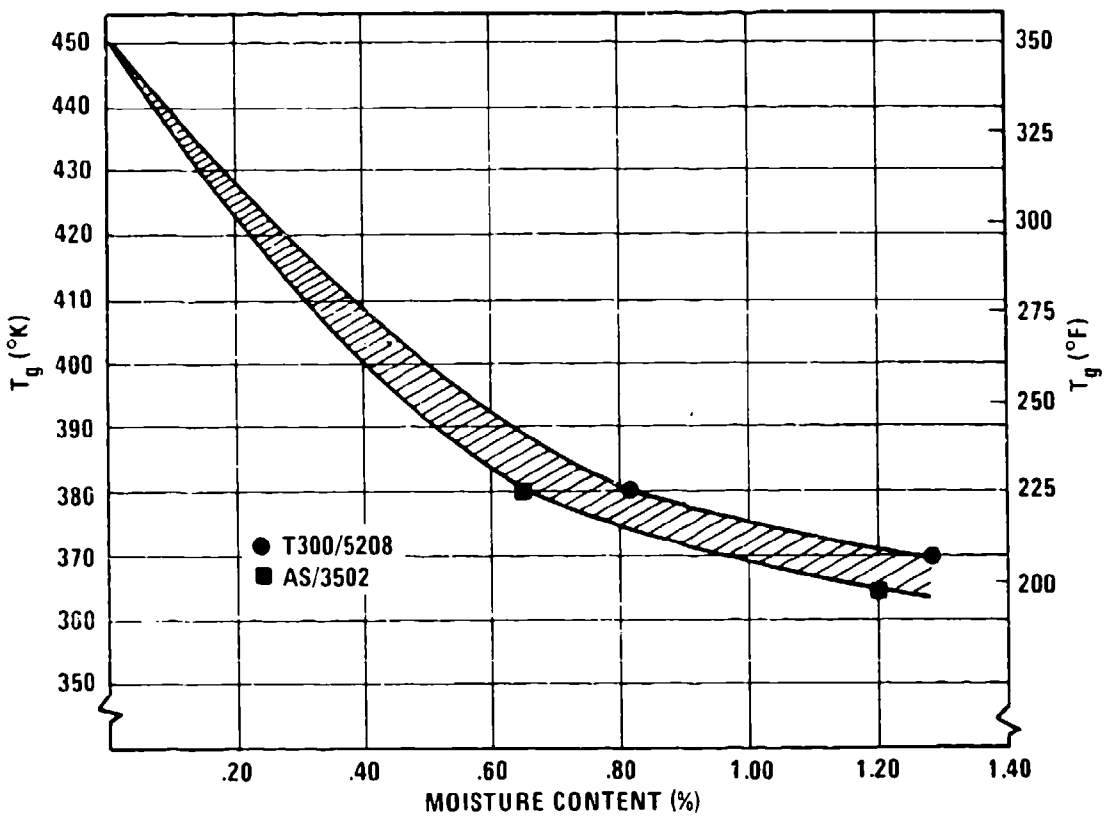

Figure 43 Glass Transition vs Moisture Content

TABLE IX. HYGROTHERMAL CONSTANTS

Coefficient	Environment	T300/5208	AS/3502
β_{22} ($\mu\epsilon/^{o}K$)	M(%)=0.5	1700	
	=1.0	2440	
	=1.4	2800	
D (cm^2/sec)	RT	17.0	12.0
α_{11}($\mu\epsilon/^{o}K$)	Dry, 300^{o}K	-0.56	-0.27
	400^{o}K	-0.61	-0.20
α_{11}($\mu\epsilon/^{o}K$)	95% RH	-1.0	
α_{22}($\mu\epsilon/^{o}K$)	Dry, 300^{o}K	23.0	21.8
	400^{o}K	26.7	25.9
	450^{o}K	28.6	28.0
α_{22}($\mu\epsilon/^{o}K$)	95% RH, 300^{o}K	28.2	26.4
	370^{o}K	34.0	30.8

SECTION V

5. ANALYTICAL METHODOLOGY

Using principal moduli derived from our compliance curves and quasielastic conversion, we have performed predictions of lamina and laminate behavior. Since we have shown that for many cases of practical interest the time-dependence is not particularly strong, we have stressed the use of simple predictive techniques already familiar in composite elastic analysis.

As an example, Figure 44 shows Halpin-Tsai predictions for E_m, the effective matrix modulus, and for E_{22}, based on our experimentally derived G_{12} master curve (wet and dry). We have used fiber properties essentially the same as those given in Ref. 20, and summarized below:

$G_{f_{LT}}$ = 3.5 MSI (24.1 GN/m^2)

$E_{f_{TT}}$ = 2.3 MSI (15.8 GN/m^2)

V_f = .68

ν_f = .20

ν_m = .37

ξ's = 1,2

The data points (o) in Figure 44 are our experimental data, while the solid curves are Halpin-Tsai results. The vertical bars on the E_{22} data represent typical scatter from our 90^o coupon results. The E_{22} data are those obtained as described in the previous section, i.e., by using the G_{12} shift factors. The data points (□) are results from Ref. 21 on neat 3502 resin, while the (▲) points are derived from results in Ref. 22 for 5208 resin.

We have based the Halpin-Tsai calculations on our G_{12} data. Given that (wet/dry) master curve, and using reasonable values for fiber properties and geometrical factors, with no unusual adjustment of parameters, we obtain a very reasonable description of E_{22} results. Additionally, the predicted matrix modulus agrees well with independent measurements on the cured resin material.

Using the time dependence for G_{12} and E_{22} shown in Figure 44, we have used our elastic code to calculate the average stiffness, stepwise in time, of a wet/dry $(90/\pm45)_S$ laminate. For these calculations we used E_{11} = 131 GN/m^2 (19 MSI), and ν_{12} = 0.31, which are "average" results from our measurements and assumed insensitive to time.

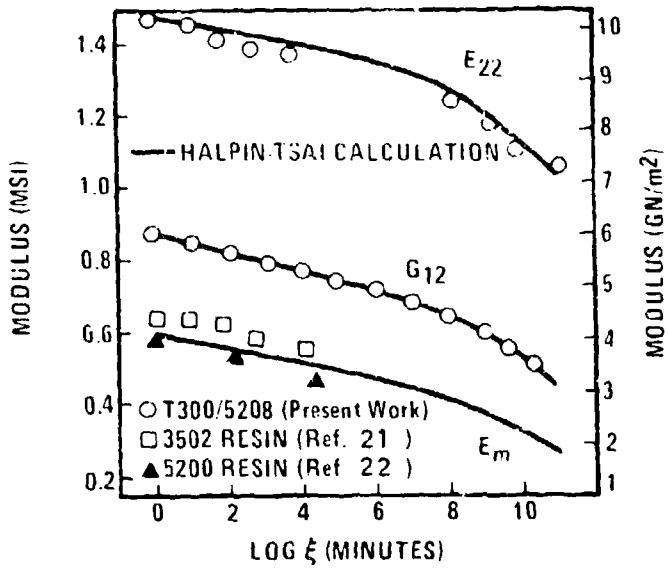

Figure 44 Measured and Predicted Lamina Properties

Figure 30 in the previous section presented the prediction obtained on this basis, along with the experimental master curve for this T300/5208 laminate. The agreement between measurement and prediction is within about 4% over the entire range of reduced time. This would seem to lend considerable weight to our conclusions that time-dependent tests on ±45 coupons, along with Halpin-Tsai predictions and conventional analysis procedures provide a good assessment of the expected material response to environment.

Also presented previously in Section III (Figure 29) were predictions for fiber-dominated laminate response. In that case, the measured values for all principal properties were used in the elastic code (rather than E_{22} derived from Halpin-Tsai computations). Equally good predictive descriptions of the experimentally-measured response were obtained.

For the cases we have studied, i.e., for constant loads and various constant tmeperature/humidity conditions, it is clear that commonly-used elastic techniques, when used with time-varying principal properties, provide excellent descriptions of laminate response.

In order to provide a more general framework for analyses, however, we have obtained exponential series fits to our time-dependent principal relaxation moduli (as in the case of Ref. 9, e.g.). Texas A&M University provided these collocation fits to our master curve results, and typical results for the T300/5208 ($\pm$45) coupons are shown in Figures 45 and 46.

In one case (Figure 45), ½-decade spacing was used and the fit is excellent. The slight oscillation at long times could be pushed off to longer times by including a "guessed" extrapolation of the data. One extra data point was in fact used at long time by assuming the log-log slope is constant between the actual last two points and an extra point ½ decade beyond the data. The same extrapolation method was used for 1-decade spacing in Figure 45, with an extra point one decade beyond the actual data.

The exponential series may be conveniently employed in hereditary integrals for predicting laminate behavior under time-varying loads and environments. A detailed discussion of this procedure, along with a general description of viscoelastic methodology for laminates, is presented in Appendix C, "Notes on Viscoelastic Analysis of Laminates", prepared for this program by R. A. Schapery.

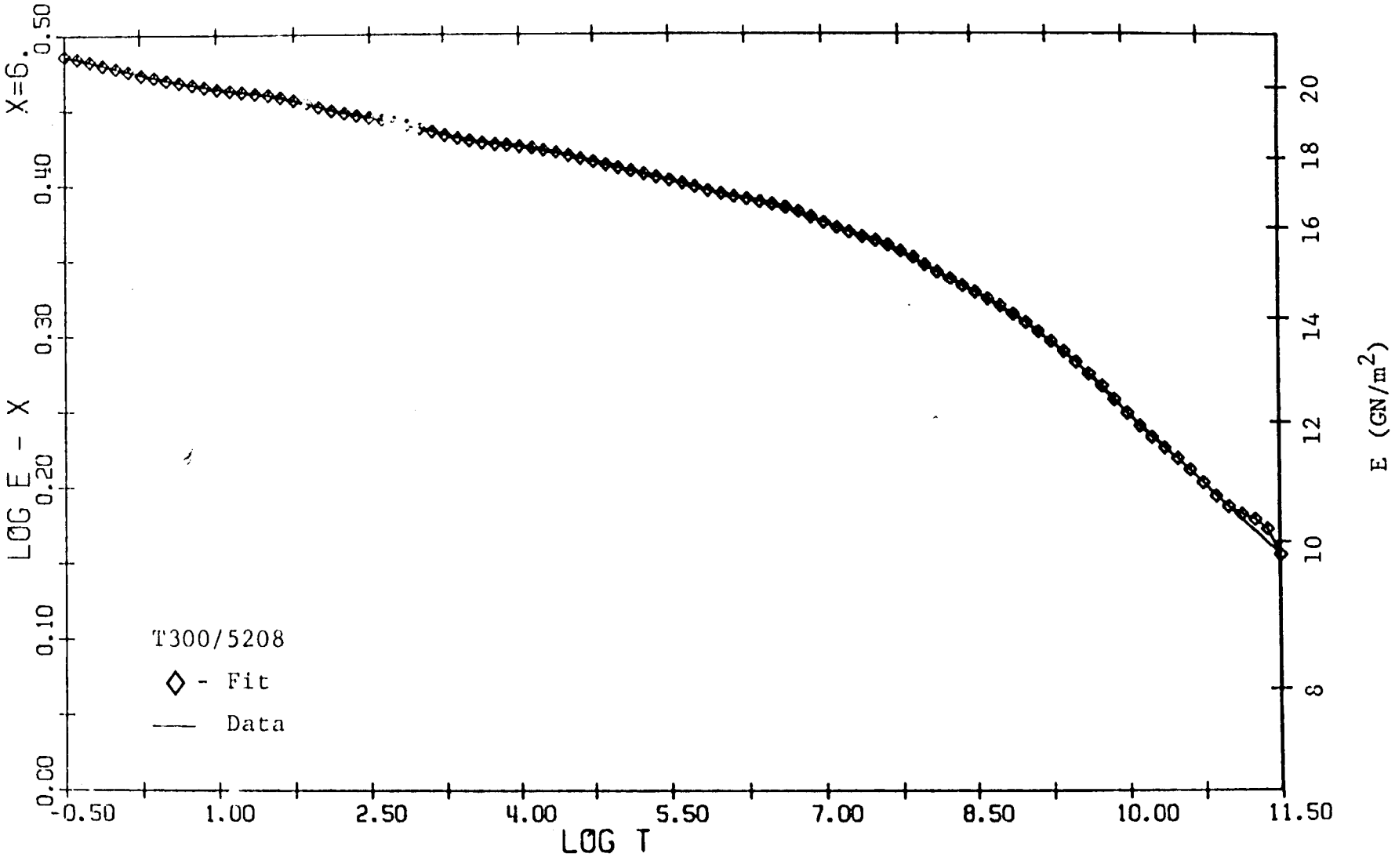

Figure 45. Exponential Series Fit (½ Decade) – ±45

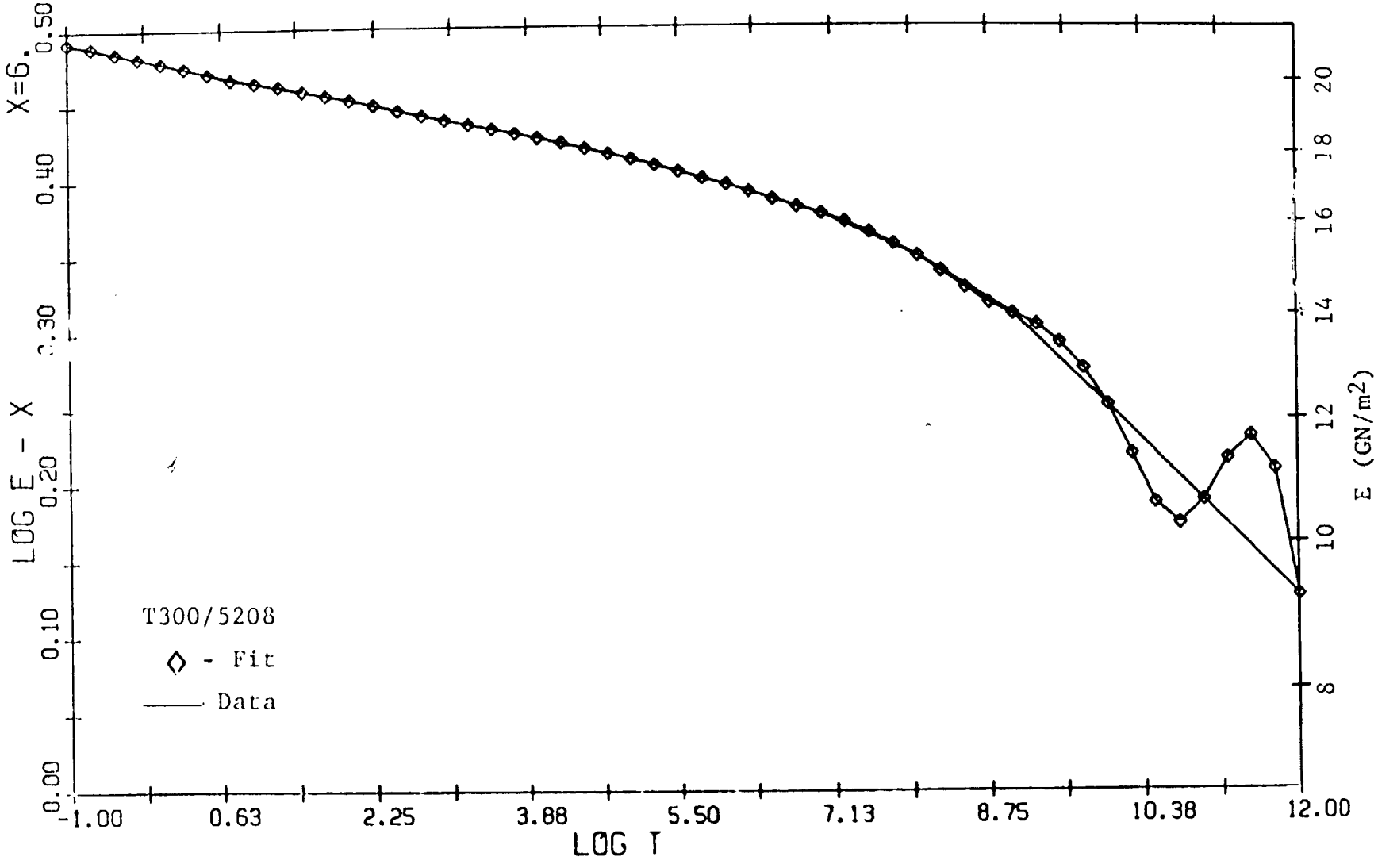

Figure 46. Exponential Series Fit (1 Decade) - ±45

SECTION VI

6. EFFECTS OF NON-UNIFORM MOISTURE DISTRIBUTION

In this task we set out to determine the effects of non-uniform moisture distribution, both experimentally and analytically, with the framework of methodology previously discussed. Our test coupons in this case were 24-ply layups, $(\pm 45)_{6S}$ and $(90/\pm 45)_{4S}$, of both materials.

Coupons were moisture conditioned at 333°K (140°F) for several days, at which time their total moisture content reached about 0.3-0.4%. Strain gages were then applied (and baked to cure the gage adhesive), and the specimens further moisture-soaked. Three coupons of this set were then stress-strain tested to failure at either RT or 339°K (150°F) for baseline values, while another set of three coupons were immersed in the wet creep chamber at the corresponding temperature. One-hundred minute creep tests were then performed once per day for 1-3 days. These creep specimens were subsequently tested (stress-strain to failure) for residual properties at RT. A moisture traveler followed the coupons at all times so that daily weight measurements could be compared with the predictions (both total moisture content and moisture distribution) of our finite difference moisture-diffusion code.

Figure 47 demonstrates the measured (data points) and predicted moisture content in a set of $(\pm 45)_{6S}$ T300/5208 coupons during this conditioning and test sequence. All specimens tested gave roughly equivalent results in terms of both the experimental and analytically-predicted data. We will, therefore, confine our remaining discussion to this particular set of coupons as representative of all our non-uniform moisture distribution data.

Figure 48 illustrates the analysis procedure used for these data. Beginning in the upper left corner and proceeding clockwise through the four items presented, we first observe the predicted moisture distribution through the thickness. Given this M(%) per ply, we proceed to our relationship between moisture content, M, and relative humidity, ϕ, determined in Section IV.

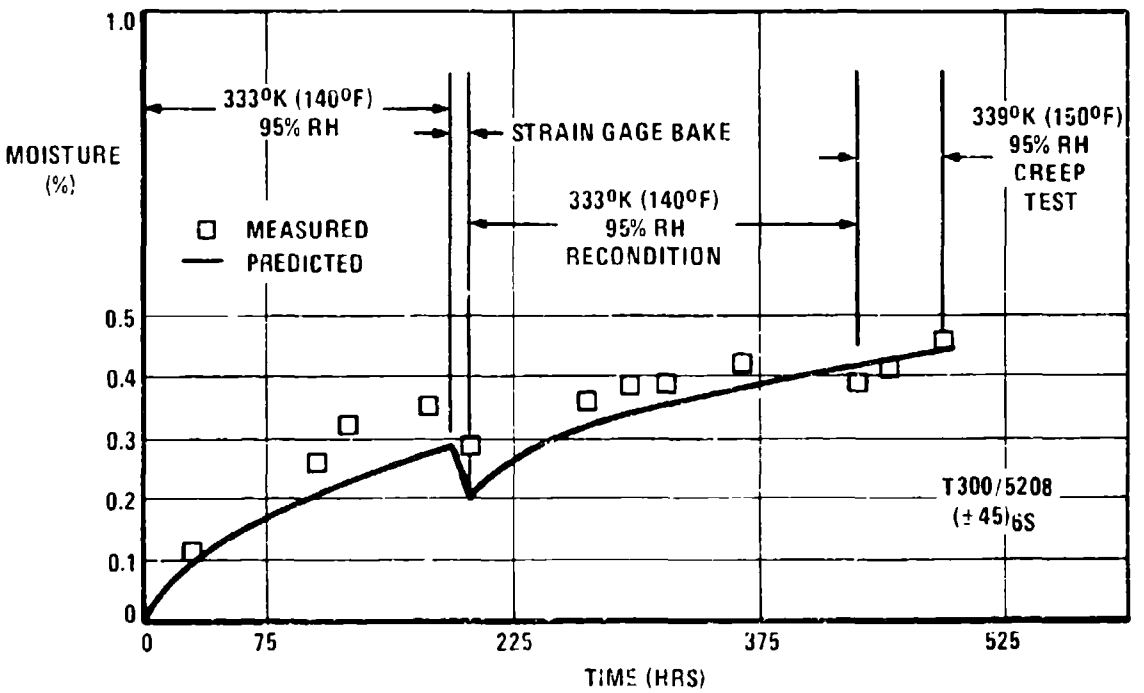

Figure 47 Conditioning/Test Sequence for Non Uniform Moisture Coupons

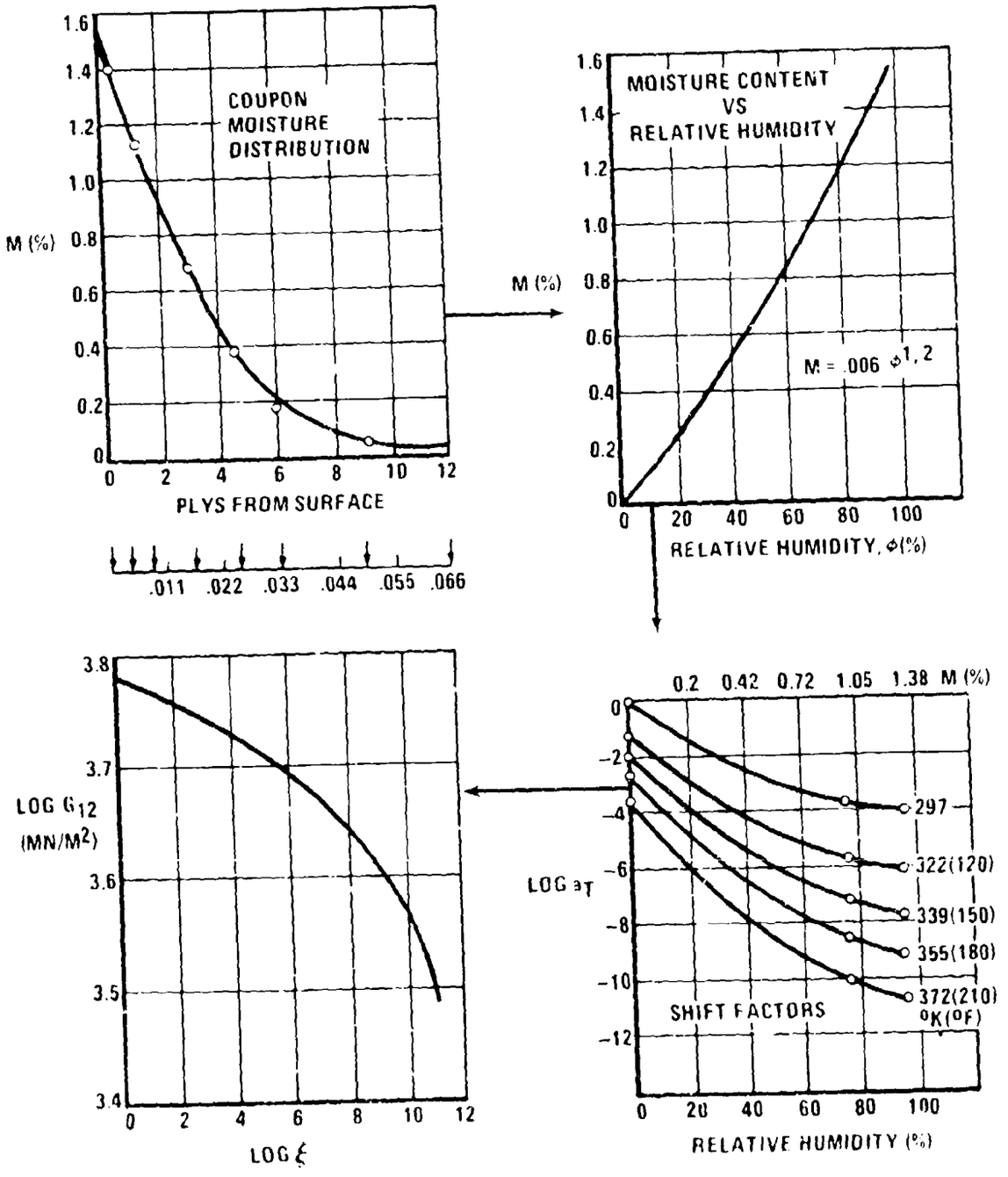

Figure 48 Schematic Procedure for Predicting Mechanical Response with Non Uniform Moisture Content

having thus a relative humidity ϕ corresponding to each ply, we can proceed to the shift factors, log a_T, presented in the lower right as a function of ϕ. For the ϕ representative of each ply, we read off (from the 339°K curve) the corresponding shift factor for that ply. Given the log a_T values, we simply enter the shear modulus master curve at the appropriate reduced time, obtaining a G_{12} for that ply. This procedure is thus repeated for discrete time steps during the duration of the (creep) loading.

Given then the $G_{12}(t)$ appropriate to each ply, we utilize the Halpin-Tsai relations to compute $E_{22}(t)$, and our previously measured values for the time-insensitive moduli E_{11} and ν_{12}. These principal properties are then used in a ply-by-ply elastic lamination code to predict the average tensile stiffness as a function of time.

Results of this procedure are given in Figure 49. We plot there the measured results for modulus (compliance^{-1}) on two successive days (essentially no change), the previously measured results for ($\pm$45) saturated at 75% RH, and the predicted response obtained as described above.

We note that the time-dependence is similar in each case, and the prediction is within about 6-7% in magnitude of the measured value.

Table X presents the strength tests obtained on these coupons with non-uniform moisture distribution. The 75% RH uniform moisture data are included for comparison. It is not clear that any substantial comments may be made about those results.

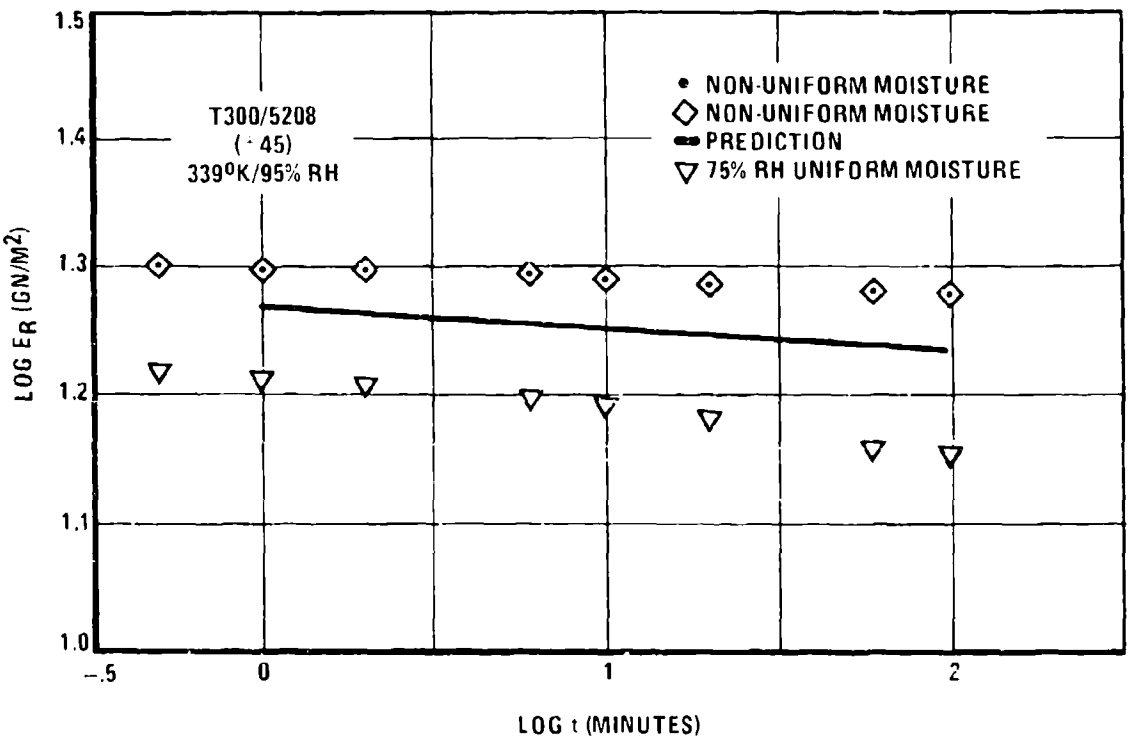

Figure 49 Non-Uniform Moisture Tests/Predictions

TABLE X RT STRENGTH TESTS

MATERIAL & LAYUP	MOISTURE CONDITION	STRESS ULTIMATE		STRAIN ULTIMATE %
		MN/m^2	KSI	
T300/5208 (±45)	DRY BASELINE	161 (6)	23 (1)	1.17 (.12)
	75% UNIFORM	160 (4)	23 (1)	1.69 (.20)
	NON UNIFORM	177 (1)	26 (.1)	1.91 (.53)
	NON UNIFORM (RESIDUAL)	178 (2)	26 (.3)	---(*) ---
AS/3502 (±45)	DRY BASELINE	165 (2)	24 (.3)	1.33 (.06)
	75% UNIFORM	154 (3)	22 (.4)	1.96 (.47)
	NON UNIFORM	171 (1)	25 (.2)	2.03 (.12)
	NON UNIFORM (RESIDUAL)	174 (2)	25 (.2)	2.07 (.39)
T300/5208 (90/±45)	DRY BASELINE	148 (6)	21 (1)	.63 (.02)
	75% UNIFORM	233 (112)	34 (16)	1.07 (.55)
	NON UNIFORM	193 (9)	28 (1)	.81 (.05)
	NON-UNIFORM (RESIDUAL)	219 (10)	32 (1)	.99 (.09)
AS/3502 (90/±45)	DRY BASELINE	188 (13)	27 (2)	.82 (.09)
	75% UNIFORM	213 (10)	31 (1)	.99 (.07)
	NON UNIFORM	239 (3)	35 (.4)	1.18 (.06)
	NON UNIFORM (RESIDUAL)	234 (3)	34 (.4)	1.16 (.07)

* Strain Gage Failure

SECTION VII

7. CURE CYCLE OPTIMIZATION

The intent of this task was to use existing and developed analytical tools in conjunction with our measured material properties to develop a procedure for minimizing residual stresses induced during the cure cycle.

This task was performed for this program by Y. Weitsman of Texas A&M University, and a complete description of his procedure is given as Appendix D to this report, entitled "Minimization of Residual Thermal Stresses in Cross Ply Laminates." That work presents an analytical-numerical scheme to minimize the residual thermal stresses due to cool-down of a cross ply laminate.

As an example of the application of the procedure described in Appendix D, Dr. Weitsman was provided with power law fits to our 90^{o} compliance results as described in Figure 50. In that figure we show our previous results for wet and dry 90^{o} coupons, in which the master curves for the two conditions were obtained by graphical (horizontal) shifting of the 90^{o} data. We used these results, rather than the more consistent data set which results from using G_{12}-derived shift factors, in order to examine the widest possible range of our data.

For each case shown in the figure, the data were fit with the power law form

$$D(\xi) = D_{o}(\xi+\xi_{o})^{q} \qquad (5)$$

and the four sets of fit parameters given correspond to the four indicated solid curves. Based on these sets of parameters, the optimized cooling paths (for AS/3502) derived are shown in Figure 51.

In each case, the cool-down path corresponds to an initial rapid temperature drop from T_{o} (cure temperature) to the indicated T_{1}, followed by a (nearly-linear) cool-down to a temperature T_{2}, the cool-down being constrained to occur with 100 minutes in this case. All cases shown yield similar residual stresses.

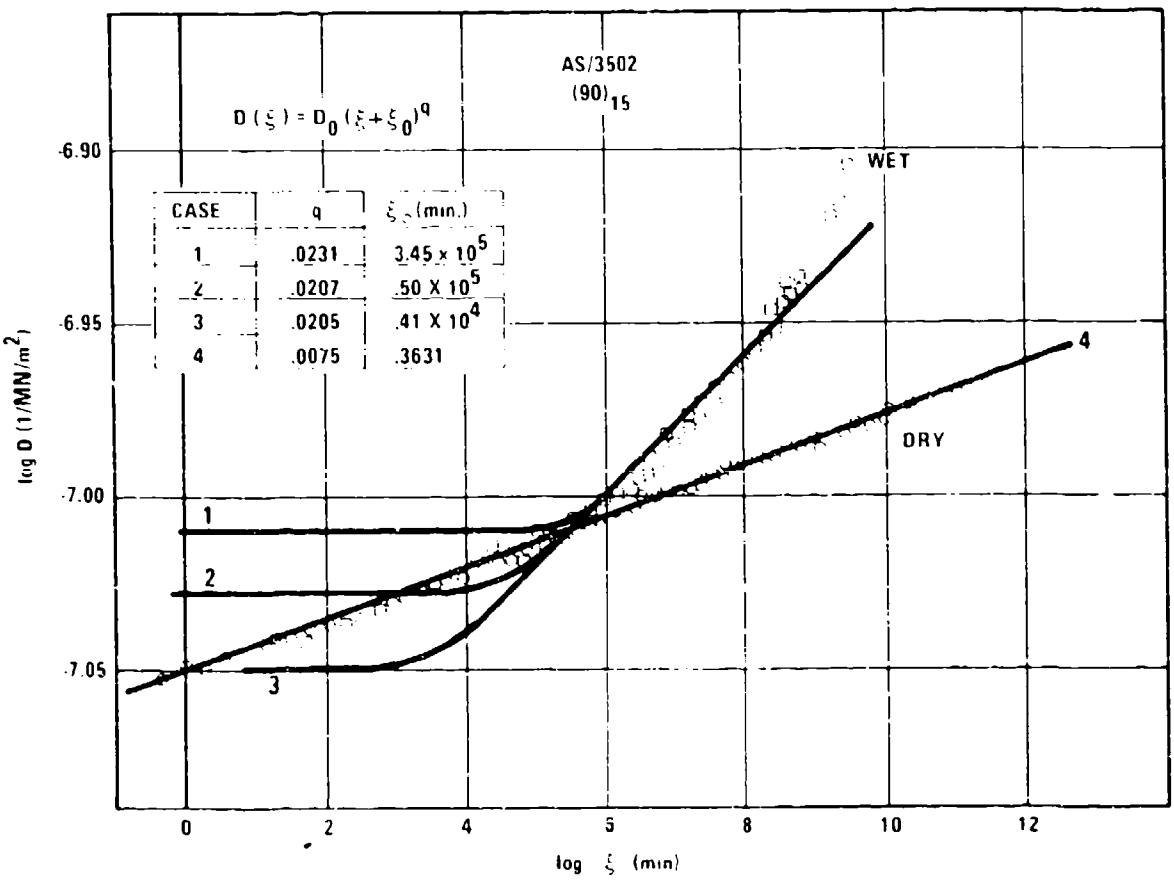

Figure 50 Power–Law Fits to 90° Compliance

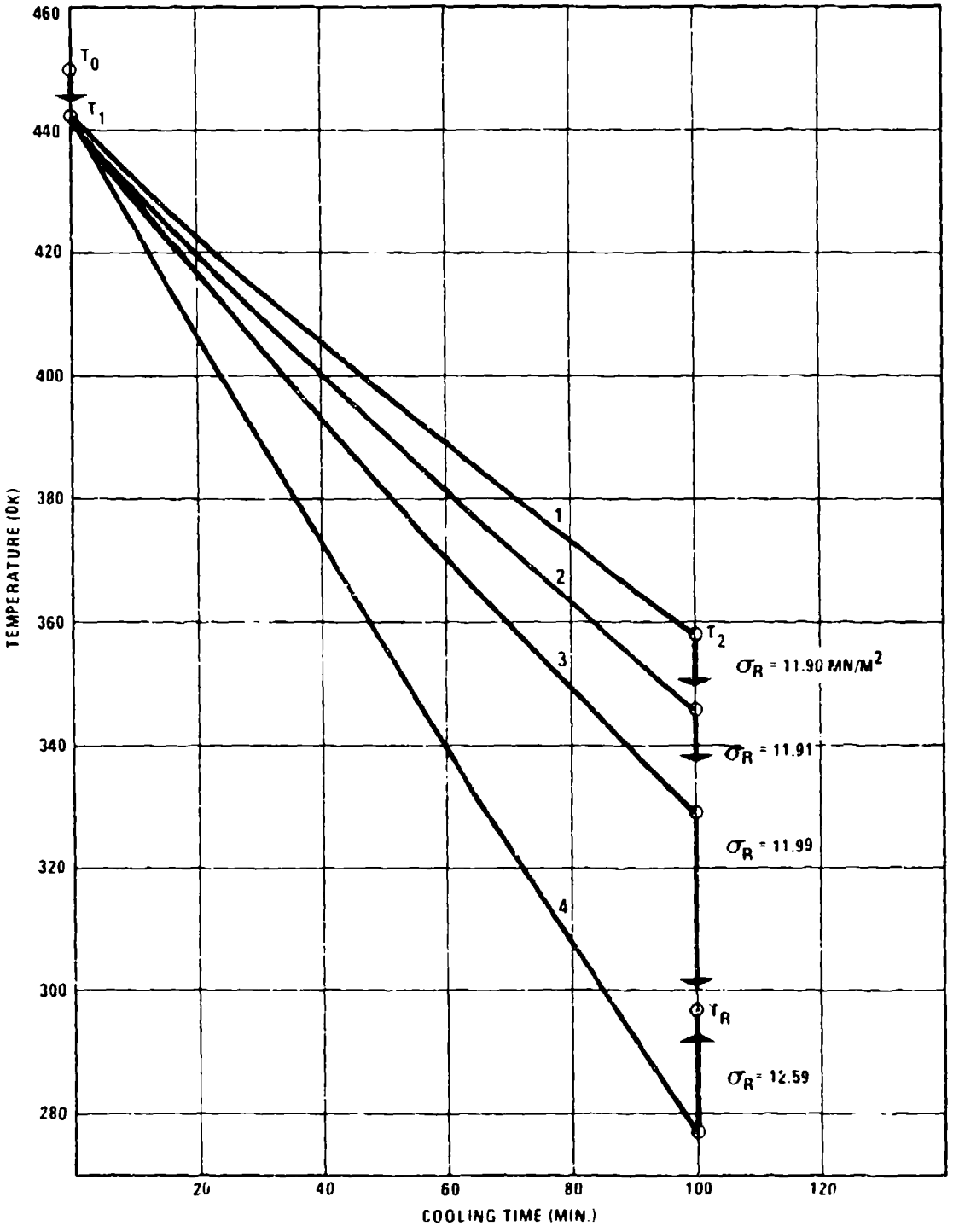

Figure 51 Optimized Cooling Paths for AS/3502

For comparison purposes, Table XI gives the calculated viscoelastic and elastic residual stresses for each of the four cases. The moduli used for the elastic computations were given by

$$E = \frac{1}{D(o)} = \frac{1}{D_o \xi_o q} \tag{6}$$

TABLE XI RESIDUAL STRESSES (MN/m^2)

Case No.	Viscoelastic	Elastic	% Difference
1	11.90	12.85	8
2	11.91	13.19	11
3	11.99	13.86	16
4	12.59	14.25	13

SECTION VIII

8. CONCLUSIONS AND RECOMMENDATIONS

We have obtained a rather complete linearly viscoleastic characterization of two graphite-epoxy material systems by measuring the principal properties as a function of time, temperature, and humidity. We have used this experimental characterization, along with slightly-modified, but conventional, analysis techniques to predict time-dependent laminate response. We believe the results are of general applicability for ascertaining the magnitude of time-temperature-humidity effects on structural composites. Specific conclusions and recommendations are summarized below.

- Immersion testing is a viable procedure for short-term experiments on "wet" specimens. The problem of specimen dryout is circumvented by such procedures, and a reasonable choice of fluids for the immersion, particularly those with high boiling points, allows simulation of any relative humidity.

- The principal properties E_{11} and ν_{12} are not sensitive to time, temperature, and moisture. This feature also appears to hold for the Poisson ratio ν_{xy} of $(\pm 45)_c$ coupons.

- Long-term results are predictable from short-term tests by simple horizontal superposition on a log-log scale. Master curves extending over 10 decades in reduced time were produced by such superposition of 2 decade tests in different environments. Verification of such master curves by longer term, elevated temperature tests extending for nearly 4 decades in time was accomplished for $(\pm 45)_c$ results.

- Moisture and temperature effects appear independently superposable from the $(\pm 45)_c$ results, that is, the combined shift factors may be represented by $a_{TH} = a_T a_H$. This is not necessarily a general result, but in the present case appears to provide a good overall description of the data.

- Prediction of laminate master curves is possible using conventional analysis procedures. That is, for the loads and environments tested, quasi-elastic analysis using stepped intervals in time to follow the measured principal properties provides excellent predictions of laminate time-dependent behavior.

- Time-dependent tests on ± 45 coupons for $G_{12}(t)$, with the Halpin-Tsai equations, provide an excellent assessment of the expected material response to environment. The derived $G_{12}(t)$ values, along with reasonable fiber and geometric factors, yield good agreement with both our measured $E_{22}(t)$ results and independent neat resin measurements. These $G_{12}(t)$ and $E_{22}(t)$, along with measured E_{11} and ν_{12} values then provide very acceptable laminate predictions when used with quasi-elastic lamination procedures.

- Considerable difficulty was encountered in obtaining consistent results with 90° coupons. Although damage effects were suspected, no evidence of such was found. These difficulties could perhaps be avoided by relying on $(\pm 45)_c$ measurements to obtain all time-dependent results, as summarized in the previous item.

- Evidence was found for possible physical aging phenomena in the 90° results. Specimens which had "aged" for about one year tended to give different time-dependent results than new specimens. The aged specimens exhibited less time dependence than expected on the basis of ± 45 results. If the specimens were "annealed" near the cure temperature briefly before test, however, their creep response was similar to that observed for the ± 45 coupons. This is a possible example of the aging effects noted in Ref. 16, by which the moduli of amorphous polymers changes due to a reduction in segmental mobility (decrease in free-volume) with time. If this effect is indeed significant, it implies that the usual superposition procedures will not apply. We, therefore, suggest some degree of caution in measurement and prediction of time-dependent properties. One should at least ensure that comparisons are made between materials similarly aged. Even better, however, the aging effects bear scrutiny in some detail. Since the materials are expected to become "stiffer" because of such aging, procedures such as we have here employed would tend to present a conservative prediction of long-term behavior.

- Shift factors derived for (dry) elevated temperature tests are correlatable with thermal expansion of the materials. This suggests that the shift factors (dry) are related to free volume. The equivalent correlation for moisture effects (swelling and shift factors) does not seem as simple.

- All master curves were derived by simple horizontal shifting on log-log scales. Although smooth and repeatable curves were derived, this does not address the possible requirements for vertical shifting. It is clear that combinations of vertical and horizontal shifting could probably produce equally good master curves, but the arbitrariness of such a procedure is questionable if the data set does not appear to require it.

- Although limited tests were performed on the rate dependence of tensile ultimate properties, it is clear that cognizance of such effects must be maintained. The rate used for tensile tests should be similar to any rate pertinent to use of the tensile properties, e.g., fatigue testing.

- In general, the time-dependence of these graphite-epoxy materials is not particularly strong, especially for a reference RT-dry condition, where significant effects occur only after many decades in time.

- For other conditions more representative of service, however, such as warm/wet environments, dramatic changes in matrix-dominated properties may be expected in times of the order of months or even weeks. At the very least, it would appear appropriate for the designer to have access to $G_{12}(t)$ master curves for various reference conditions, so that at least a preliminary assessment of potential property reduction might be made.

- The work reported here has been concentrated in the region of linear viscoelastic response. Further work should be conducted to examine the behavior in regions of nonlinearity.

- A general procedure for laminate analysis under conditions of transient and non-uniform temperature and moisture has been presented. (Appendix C)

- Certain minimization of residual stresses due to cure may result by employing an optimized cool-down path after cure (Appendix D). Although the reduction in residual stresses are not dramatic, they serve to indicate that additional benefits may accrue if a more scientific approach is taken toward the entire production cure process. It is hoped that future programs will address this area in more detail.

REFERENCES

1. J. C. Halpin, "Introduction to Viscoelasticity," Composite Materials Workshop, S. W. Tsai, J. C. Halpin, and N. J. Pagano, eds., Technomic Publishing Co., 1967.

2. J. E. Ashton, "Non-Linear Viscoelastic Response of Fibrous Composites," J. Composite Materials, Vol. 2, 1968, p. 116.

3. Y. C. Lou and R. A. Schapery, "Viscoelastic Characterization of a Non-linear Fiber-Reinforced Plastic," J. Composite Materials, Vol. 5, 1971, p. 208.

4. R. A. Schapery, S. W. Beckwith, and N. Conrad, "Studies on the Viscoelastic Behavior of Fiber-Reinforced Plastic," AFML-TR-73-179, Wright-Patterson AFB, OH, 1973.

5. A. S. D. Wang and P. K. Lin, "Humidity Effects on the Creep Behavior of an Epoxy-Graphite Material," AIAA/SAE 11th Propulsion Conference, Anaheim, CA, AIAA Paper No. 75-1341, 1975.

6. A. S. D. Wang, E. J. McQuillen, and A. S. Ahmadi, "Analytical and Experimental Investigation of Time-Temperature Creep of Graphite-Epoxy Composite Laminates," Mechanical Behavior of Materials, Vol. II, Soc. Mat. Sci., Japan, 1974.

7. S. W. Beckwith, "Viscoelastic Characterization of a Non-Linear, Glass/Epoxy Composite Including the Effects of Damage," Texas A&M University Report MM2895-74-8, 1974.

8. Y. T. Yeow, D. H. Morris, and H. F. Brinson, "Time-Temperature Behavior of a Unidirectional Graphite/Epoxy Composite," Composite Materials: Testing and Design (5th Conference), ASTM STP 674, S. W. Tsai, ed., American Society for Testing and Materials, 1979, pp. 263-281.

9. F. W. Crossman and D. L. Flaggs, "Dimensional Stability of Composite Laminates during Environmental Exposure," SAMPE Journal, July/August, 1979, pp. 15-20.

10. W. J. Renton and T. Ho, "The Effect of Environment on the Mechanical Behavior of AS/3501-6 Graphite/Epoxy Material," ATC Report No. B-92100/8CR-105, Vought Corporation, Dallas, TX, August 1978.

11. K. G. Kibler, "Time-Dependent Environmental Behavior of Epoxy Matrix Composites," Mechanics of Composites Review, AFML/MBM, Wright-Patterson AFB, OH, 30 Oct.-1 Nov., 1979, pp. 57-61.

12. S. Glasstone, Textbook of Physical Chemistry, D. Van Nostrand Co., 1946.

13. J. Romanko and W. G. Knauss, "On the Time-Dependence of the Poisson's ratio of a Commercial Adhesive Material," J. Adhesion 10, 1 (1979).

14. "Composite Materials for Structural Design," First Annual Technical Report, Contract No. F49620-78-C-0034, Texas A&M University Report No. MM3724-79-2, March 1979.

15. F. W. Crossman, R. E. Mauri, and W. J. Warren, "Moisture Altered Viscoelastic Response of Graphite/Epoxy Composites," ASTM STP 658, J. R. Vinson, ed., American Society for Testing and Materials, 1978, p. 205.

16. L. C. E. Struik, Physical Aging in Amorphous Polymers and Other Materials, Elsevier Scientific Publishing Co., New York, 1978.

17. J. M. Whitney and C. E. Browning, "Some Anomalies Associated with Moisture Diffusion in Epoxy Matrix Composite Materials," ASTM STP 658, J. R. Vinson, ed., American Society for Testing and Materials, 1978, p. 43.

18. H. G. Carter and K. G. Kibler, "Langmuir-Type Model for Anomalous Moisture Diffusion in Composite Resins," J. Composite Materials 12, 118 (1878).

19. E. L. McKague, J. D. Reynolds, and J. E. Halkias, "Swelling and Glass Transition Relations for Epoxy Matrix Material in Humid Environments," J. Applied Polymer Science 22, 1643 (1978).

20. R. D. Kriz and W. W. Stinchcomb, "Elastic Moduli of Transversely Isotropic Fibers and Their Composites," Experimental Mechanics, Feb. 1979, p. 41.

21. K. M. Liechti, V. H. Kenner, and W. G. Knauss, "Time Dependent Fracture Processes Relating to Service Life Predicting of Adhesive Joints and Advanced Composites, Progress Report No. 4," GALCIT SM 79-10, California Institute of Technology, Pasadena, CA, Oct. 1979.

22. K. G. Kibler and H. G. Carter, "Viscoelastic Parameters of Epoxy Resin from Thermomechanical and Electrical Conductivity Measurements," Composite Materials: Testing and Design (5th Conference), ASTM STP 674, S. W. Tsai, ed., American Society for Testing and Materials, 1979, p. 282.

APPENDIX A

BASELINE TENSILE DATA

BASELINE TENSILE DATA

MATERIAL T300/5208 LAYUP $(0)_6$

RELATIVE HUMIDITY %	TEMP °K (°F)	STRESS ULTIMATE MN/M²	STRESS ULTIMATE KSI	STRAIN ULTIMATE %	INITIAL MODULUS GN/M²	INITIAL MODULUS MSI	NUMBER OF COUPONS
DRY	RT	1494 (138)	217 (20)	1.03 (.08)	132.0 (6.3)	19.2 (.9)	3
	436 (325)	1159 (78)	168 (11)	.92 (.08)	138.8 (9.2)	20.2 (1.3)	4
75%	RT	1342 (1)	195 (.1)	.94 (.05)	137.8 (6.1)	20.0 (.9)	3
	372 (210)	1300 (192)	189 (28)	.83 (.11)	128.5 (.5)	18.7 (.1)	2
95%	RT	1313 (193)	191 (28)	.92 (.12)	133.2 (4.0)	19.3 (.6)	3
	372 (210)	1567 (16)	228 (2)	1.19 (.03)	125.6 (.4)	18.2 (.1)	3

BASELINE TENSILE DATA

MATERIAL T300/5208 LAYUP $(90)_{15}$

RELATIVE HUMIDITY %	TEMP °K (°F)	STRESS ULTIMATE MN/M²	STRESS ULTIMATE KSI	STRAIN ULTIMATE %	INITIAL MODULUS GN/M²	INITIAL MODULUS MSI	NUMBER OF COUPONS
DRY	RT	48 (11)	7 (2)	.50 (.11)	9.6 (.5)	1.4 (.1)	3
	436 (325)	34 (3)	5 (.4)	.39 (.04)	8.8 (.3)	1.3 (.04)	5
75%	RT	27 (6)	4 (1)	.24 (.06)	11.0 (.5)	1.6 (.1)	4
	372 (210)	20 (6)	3 (1)	.23 (.07)	10.4 (.3)	1.5 (.04)	3
95%	RT	28 (3)	4 (1)	.26 (.02)	11.0 (1.5)	1.6 (.2)	3
	372 (210)	16 (-)	2 (-)	.17 (-)	15.0 (-)	2.2 (-)	1

BASELINE TENSILE DATA

MATERIAL T300/5208 LAYUP $(\pm 45)_{2S}$

RELATIVE HUMIDITY %	TEMP °K (°F)	STRESS ULTIMATE MN/M²	STRESS ULTIMATE KSI	STRAIN ULTIMATE %	INITIAL MODULUS GN/M²	INITIAL MODULUS MSI	NUMBER OF COUPONS
DRY	RT	161 (6)	23 (1)	1.17 (.12)	20.4 (.5)	3.0 (.1)	4
	436 (325)	112 (2)	16 (.3)	2.30 (.30)	16.6 (.3)	2.4 (.04)	5
75%	RT	160 (4)	23 (1)	1.69 (.20)	17.6 (.6)	2.5 (.1)	4
	372 (210)	118 (2)	17 (.3)	2.85 (.27)	9.8 (.6)	1.4 (.1)	3
95%	RT	160 (5)	23 (1)	1.92 (.20)	17.5 (1.2)	2.5 (.2)	4
	372 (210)	119 (2)	17 (.3)	3.12 (.32)	9.2 (.3)	1.3 (.1)	3

BASELINE TENSILE DATA

MATERIAL T300/5208 LAYUP $(0/\pm 45)_S$

RELATIVE HUMIDITY %	TEMP °K (°F)	STRESS ULTIMATE MN/M²	STRESS ULTIMATE KSI	STRAIN ULTIMATE %	INITIAL MODULUS GN/M²	INITIAL MODULUS MSI	NUMBER OF COUPONS
DRY	RT	593 (30)	86 (4)	1.03 (.05)	57.2 (.7)	8.3 (.1)	5
	436 (325)	598 (35)	87 (2)	1.17 (.04)	54.3 (1.8)	7.9 (.3)	5
75%	RT	483 (43)	70 (6)	.92 (.07)	52.1 (1.0)	7.6 (.1)	4
	372 (210)	453 (6)	66 (1)	.93 (.02)	48.8 (.4)	7.1 (.1)	3
95%	RT	465 (112)	67 (16)	.85 (.18)	54.5 (2.3)	7.9 (.3)	3
	372 (210)	524 (71)	76 (10)	1.07 (.15)	49.3 (.5)	7.2 (.1)	3

BASELINE TENSILE DATA

MATERIAL T300/5208 LAYUP $(90/\pm45)_S$

RELATIVE HUMIDITY %	TEMP °K (°F)	STRESS ULTIMATE MN/M²	STRESS ULTIMATE KSI	STRAIN ULTIMATE %	INITIAL MODULUS GN/M²	INITIAL MODULUS MSI	NUMBER OF COUPONS
DRY	RT	148 (6)	21 (1)	.63 (.02)	25.1 (.6)	3.7 (.1)	4
	436 (325)	145 (10)	21 (2)	.70 (.05)	23.0 (.2)	3.3 (.03)	4
75%	RT	233 (112)	34 (16)	1.07 (.55)	25.6 (.7)	3.7 (.1)	4
	372 (210)	142 (3)	21 (.4)	.72 (.02)	22.0 (.4)	3.2 (.1)	3
95%	RT	178 (6)	26 (1)	.80 (.04)	25.8 (2.3)	3.7 (.3)	3
	372 (210)	132 (3)	19 (.4)	.63 (.01)	23.0 (1.1)	3.3 (.2)	3

BASELINE TENSILE DATA

MATERIAL T300/5208 LAYUP $(0/90/\pm45)_S$

RELATIVE HUMIDITY %	TEMP °K (°F)	STRESS ULTIMATE MN/M²	STRESS ULTIMATE KSI	STRAIN ULTIMATE %	INITIAL MODULUS GN/M²	INITIAL MODULUS MSI	NUMBER OF COUPONS
DRY	RT	515 (-)	75 (-)	1.02 (-)	51.1 (-)	7.4 (-)	1
	436 (325)	477 (13)	69 (2)	.94 (.02)	50.8 (.5)	7.4 (.1)	2
75%	RT	483 (43)	70 (6)	.92 (.07)	52.1 (1.0)	7.6 (.1)	4
	372 (210)	453 (6)	66 (1)	.93 (.18)	48.8 (.4)	7.1 (.1)	3
95%	RT	465 (112)	67 (16)	.85 (.18)	54.5 (2.0)	7.9 (.3)	3
	372 (210)	524 (71)	76 (10)	1.07 (.15)	49.3 (.5)	7.2 (.1)	3

BASELINE TENSILE DATA

MATERIAL AS/3502 LAYUP $(0)_6$

RELATIVE HUMIDITY %	TEMP ^{o}K (^{o}F)	STRESS ULTIMATE MN/M^2	STRESS ULTIMATE KSI	STRAIN ULTIMATE %	INITIAL MODULUS GN/M^2	INITIAL MODULUS MSI	NUMBER OF COUPONS
DRY	RT	1506 (190)	219 (28)	1.09 (.12)	124.7 (1.6)	18.1 (.2)	5
	436 (325)	1539 (54)	223 (8)	1.24 (.21)	124.0 (3.0)	18.0 (.4)	5
75%	RT	1595 (146)	231 (21)	1.23 (.09)	118.1 (11.9)	17.1 (1.7)	4
	372 (210)	1567 (16)	227 (2)	1.19 (.02)	125.6 (.4)	18.2 (.1)	3
95%	RT	1710 (65)	248 (9)	1.24 (.05)	128.0 (1.3)	18.5 (.2)	4
	372 (210)	1551 (137)	225 (20)	1.19 (.09)	124.0 (2.8)	18.0 (.4)	3

BASELINE TENSILE DATA

MATERIAL AS/3502 LAYUP $(90)_{15}$

RELATIVE HUMIDITY %	TEMP ^{o}K (^{o}F)	STRESS ULTIMATE MN/M^2	STRESS ULTIMATE KSI	STRAIN ULTIMATE %	INITIAL MODULUS GN/M^2	INITIAL MODULUS MSI	NUMBER OF COUPONS
DRY	RT	44 (7)	6 (1)	.41 (.07)	10.7 (.3)	1.6 (.1)	5
	436 (325)	36 (4)	5 (1)	.39 (.06)	9.3 (.6)	1.4 (.1)	5
75%	RT	27 (6)	4 (1)	.24 (.06)	11.0 (.5)	1.6 (.1)	4
	372 (210)	20 (6)	3 (1)	.23 (.07)	10.4 (.3)	1.5 (.04)	3
95%	RT	28 (3)	4 (.5)	.26 (.02)	11.0 (1.5)	1.6 (.2)	3
	372 (210)	16 (-)	2 (-)	.17 (-)	15.0 (-)	2.2 (-)	1

BASELINE TENSILE DATA

MATERIAL AS/3502 LAYUP $(\pm 45)_{2S}$

RELATIVE HUMIDITY %	TEMP °K (°F)	STRESS ULTIMATE MN/M²	STRESS ULTIMATE KSI	STRAIN ULTIMATE %	INITIAL MODULUS GN/M²	INITIAL MODULUS MSI	NUMBER OF COUPONS
DRY	RT	165 (2)	24 (.3)	1.33 (.06)	19.6 (.7)	2.9 (.1)	5
	436 (325)	127 (3)	18 (.4)	2.65 (.23)	16.0 (.5)	2.3 (.1)	4
75%	RT	154 (3)	22 (.4)	1.96 (.47)	17.6 (.5)	2.6 (.1)	4
	372 (210)	131 (1)	19 (.2)	3.75 (.48)	10.2 (.7)	1.5 (.1)	3
95%	RT	156 (1)	23 (.1)	3.08 (1.70)	17.3 (.7)	2.5 (.1)	4
	372 (210)	144 (6)	21 (1)	4.78 (1.15)	10.2 (1.0)	1.5 (.1)	3

BASELINE TENSILE DATA

MATERIAL AS/3502 LAYUP $(0/\pm 45)_S$

RELATIVE HUMIDITY %	TEMP °K (°F)	STRESS ULTIMATE MN/M²	STRESS ULTIMATE KSI	STRAIN ULTIMATE %	INITIAL MODULUS GN/M²	INITIAL MODULUS MSI	NUMBER OF COUPONS
DRY	RT	585 (75)	85 (11)	1.04 (.14)	55.7 (1.8)	8.1 (.3)	3
	436 (325)	552 (77)	80 (11)	1.15 (.12)	52.1 (.9)	7.6 (.1)	5
75%	RT	587 (33)	85 (5)	1.10 (.06)	54.6 (.2)	7.9 (.04)	4
	372 (210)	592 (14)	86 (2)	1.28 (.03)	48.7 (.9)	7.1 (.1)	3
95%	RT	507 (37)	73 (5)	.96 (.11)	55.0 (1.4)	8.0 (.2)	3
	372 (210)	602 (78)	87 (11)	1.27 (.14)	49.9 (1.3)	7.2 (.2)	3

BASELINE TENSILE DATA

MATERIAL AS/3502 LAYUP $(90/\pm45)_S$

RELATIVE HUMIDITY %	TEMP °K (°F)	STRESS ULTIMATE MN/M²	STRESS ULTIMATE KSI	STRAIN ULTIMATE %	INITIAL MODULUS GN/M²	INITIAL MODULUS MSI	NUMBER OF COUPONS
DRY	RT	168 (13)	27 (2)	.62 (.09)	25.3 (.8)	3.7 (.1)	5
	436 (325)	172 (5)	25 (1)	.82 (.07)	23.5 (.5)	3.4 (.1)	5
75%	RT	213 (10)	31 (1)	.99 (.07)	26.3 (1.5)	3.8 (.2)	4
	372 (210)	160 (7)	23 (1)	.79 (.07)	23.5 (1.0)	3.4 (.1)	3
95%	RT	212 (5)	31 (1)	.99 (.04)	26.3 (1.4)	3.8 (.2)	3
	372 (210)	156 (7)	23 (1)	.82 (.04)	23.4 (1.0)	3.4 (.1)	3

BASELINE TENSILE DATA

MATERIAL AS/3502 LAYUP $(0/90/\pm45)_S$

RELATIVE HUMIDITY %	TEMP °K (°F)	STRESS ULTIMATE MN/M²	STRESS ULTIMATE KSI	STRAIN ULTIMATE %	INITIAL MODULUS GN/M²	INITIAL MODULUS MSI	NUMBER OF COUPONS
DRY	RT	536 (42)	78 (6)	1.10 (.09)	49.3 (.5)	7.1 (.1)	4
	436 (325)	507 (2)	74 (.3)	1.04 (.07)	48.7 (.4)	7.1 (.1)	3
75%	RT	490 (30)	71 (4)	.96 (.07)	52.0 (1.7)	7.5 (.3)	4
	372 (210)	491 (14)	71 (2)	1.14 (.07)	46.4 (.8)	6.7 (.1)	3
95%	RT	481 (32)	70 (5)	.94 (.07)	51.7 (.7)	7.5 (.1)	3
	372 (210)	493 (30)	72 (4)	1.05 (.03)	47.8 (1.8)	6.9 (.3)	3

APPENDIX B

QUALITY ASSURANCE PLAN

General Dynamics Specifications FMS-2023A establishes the minimum requirements for graphite fiber-reinforced epoxy laminating materials for primary aircraft structure. Prepreg inspection and mechanical property requirements on the supplier and on GD for acceptance will be controlled by that specification and FPS-2003, "Advanced Composite Materials Test Specification."

General Dynamics Specification FPS-2021C establishes the requirements for lay-up, inspection, and cure of laminates using FMS-2023 materials. Ply inspection, lay up, preparation for cure, storage, cure cycle temperature and pressure profile control, and documentation will be controlled by that specification and FPS-2002B, "Process and Quality Control of Adhesive Bonded Boron and Graphite Composite Assemblies."

All laminates produced for this program will be monitored as outlined below to ensure the integrity of fabricated test specimens.

1. Incoming Prepreg Inspection and Basic Material Properties

   Per FMS-2023A, to include:

   - o Cured ply thickness
   - o Tack
   - o Mechanical properties:
     - 0° flexural strength at RT and $450^{\circ}K$ ($350^{\circ}F$)
     - 0° flexural modulus at RT
     - 90° flexural strength at RT and $450^{\circ}K$
     - Horizontal shear strength at RT and $450^{\circ}K$

2. Cure Cycle Parameter Control

   Per FPS-2021C, to include:

   - o Ply inspection, layup and cure preparation
   - o Cure cycle pressure and temperature profile control

   Additionally to include:

   - o Dielectric monitoring of cure for detection of irregularities by comparison with standard recordings of verified panels.

3. Cured Panel Inspection

- o Ultrasonic C-scan of panels prior to machining of specimens.
- o Mark reject areas to recover acceptable areas
- o Resin content measurement of questionable C-scan areas

4. Test Tabs

- o Standard unidirectional panel for mechanical properties as in (1) above.
- o Test tab of each layup for use in Task 3, moisture travelers for Task 1 and 2, and property recheck, as necessary.

5. Pretest NDI

- o Visual and optical examination of each test specimen for

  - General appearance:
    Scratch or scribe marks, cracks
    Peel ply removal
    Disfiguration or distortion
    Unusual discoloration
    Uniform thickness and width.

  - Edge conditions:
    Smooth and parallel
    Nicks, crack, scratches
    Fibers displaced or pulled out.

  - End tabs
    Proper taper
    Placement relative to specimen and each other
    Proper bonding.

- o Proper layup and number of plies
- o Random sampling of ultrasonic attenuation (low-level porosity)
- o Enhanced x-ray of questionable edge conditions

6. Dimensional Characterization

- o Width at three locations in gage section
- o Thickness at six locations.

7. Microphotographs

   - o 60 x for voids, cracks, delaminations, ply count and orientation on at least one specimen/group.

8. Fiber Volume

   - o Specific gravity of cured laminates
   - o Fiber and resin content.

9. History

   - o Complete material, panel, specimen history of above measurements.

APPENDIX C

NOTES ON VISCOELASTIC ANALYSES OF LAMINATES

R. A. Schapery*

* Director, Mechanics and Materials Research Center, Texas A&M University, College Station, TX 77840

1. EXPONENTIAL SERIES FIT TO RELAXATION MODULI

Let $D(\xi)$ denote a creep compliance, such as $S_{xx}(\xi)$ or $S_{22}(\xi)$. The relaxation modulus corresponding to $D(\xi)$ is denoted by $E(\xi)$; it can be calculated from the following simple relationship with negligible error (Ref. 1):

$$E(\xi) = \frac{\sin n\pi}{n\pi} \quad \frac{1}{D(\xi)} \tag{1}$$

where

$$n \equiv \frac{d \log D}{d \log \xi} \tag{2}$$

For all compliances obtained in this study, n is sufficiently small to permit use of

$$E(\xi) = \frac{1}{D(\xi)} \tag{3}$$

Stress analysis of laminates is facilitated if all time-dependent prinicpal lamina moduli are expressed in terms of a sum of exponentials in reduced time ξ. Namely, let E_M denote the so-called "Prony" series,

$$E_M(\xi) = E_e + \sum E_i e^{-\xi/\tau_i} \tag{4}$$

The constants E_e, E_i, and τ_i can be found by using the collocation method given in Ref. 2. The quantity E_e is equal to the equilibrium modulus,

$$E_e = E(\infty) \tag{5}$$

which can be taken as zero for the range of reduced time covered by our data. The series (4) is then equated to the given (measured) relaxation modulus $E(\xi)$ at a set of N values of ξ, denoted by ξ_i. The time constants τ_i are given as

$$\tau_i = 2\xi_i, \quad i = 1, \ldots, N \tag{6}$$

Table C-1 lists the values of the coefficients and time constants obtained from fitting (4) to $S_{22}^{-1}(\xi)$ for AS/3502 at points one-half decade apart in reduced time. For example, write

$$S_{22}^{-1}(\xi) \equiv E_{2e}^{0} + \sum_{i=1}^{N} E_{2i}\, e^{-\xi/\tau_i}$$

Then E_{2i} are the coefficients listed in Table C-1. Evaluation of the series at points intermediate to the fitted data points serves to check the accuracy of the series representation; we have found excellent agreement with the given function, such as $S_{22}^{-1}(\xi)$ which is plotted in Figure C-1.

Before turning to laminate stress analysis, it should be noted that the exponential series (4) enables one to calculate easily the complex modulus, which is useful in vibration analysis. Specifically, let E^* denote the complex modulus

$$E^* = E' + jE'' \tag{8}$$

where $j = \sqrt{-1}$. Then corresponding to an exponential series fit to the relaxation modulus,

TABLE C-1 Exponential Fit Parameters For E_{22} Master Curve (AS/3502)

EQUIL. MODULUS EE = 0.0

INDEX I	TIME TI	GIVEN MODULUS EM*10**(-X)	LOG10 EM-X	LOG10 TIME TI	X = 6.0
1	0.31623D+02	0.15985D+01	0.20100D+00	0.15000D+01	
2	0.10000D+03	0.15776D+01	0.19800D+00	0.20000D+01	
3	0.31623D+03	0.15668D+01	0.19500D+00	0.25000D+01	
4	0.10000D+04	0.15560D+01	0.19200D+00	0.30000D+01	
5	0.31623D+04	0.15311D+01	0.18500D+00	0.35000D+01	
6	0.10000D+05	0.15136D+01	0.18000D+00	0.40000D+01	
7	0.31623D+05	0.15031D+01	0.17700D+00	0.45000D+01	
8	0.10000D+06	0.14928D+01	0.17400D+00	0.50000D+01	
9	0.31623D+06	0.14791D+01	0.17060D+00	0.55000D+01	
10	0.10000D+07	0.14580D+01	0.16400D+00	0.60000D+01	
11	0.31623D+07	0.14289D+01	0.15500D+00	0.65000D+01	
12	0.10000D+08	0.13932D+01	0.14400D+00	0.70000D+01	
13	0.31623D+08	0.13521D+01	0.13100D+00	0.75000D+01	
14	0.10000D+09	0.13183D+01	0.12000D+00	0.80000D+01	
15	0.31623D+09	0.12794D+01	0.10700D+00	0.85000D+01	
16	0.10000D+10	0.12246D+01	0.88000D-01	0.90000D+01	
17	0.31623D+10	0.11482D+01	0.60000D-01	0.95000D+01	
18	0.10000D+11	0.10765D+01	0.32000D-01	0.10000D+02	

INDEX I	EXP. COEF. EI
1	0.16825D-01
2	0.18330D-01
3	-0.29130D-01
4	0.76309D-01
5	-0.11162D-01
6	0.26815D-01
7	-0.52657D-02
8	0.20088D-01
9	0.37843D-02
10	0.43091D-01
11	0.13589D-01
12	0.80031D-01
13	-0.33595D-02
14	0.79056D-01
15	-0.11261D+00
16	0.84722D+00
17	-0.15561D+01
18	0.22956D+01

INDEX K	TIME TK	PREDICTED MODULUS EA*10**(-X)	LOG10 EA-X	LOG10 TIME TK	X = 6.0
1	0.31623D+02	0.15985D+01	0.20100D+00	0.15000D+01	
2	0.42170D+02	0.15862D+01	0.20037D+00	0.16250D+01	
3	0.56234D+02	0.15836D+01	0.19964D+00	0.17500D+01	
4	0.74989D+02	0.15807D+01	0.19884D+00	0.18750D+01	
5	0.10000D+03	0.15776D+01	0.19800D+00	0.20000D+01	
6	0.13335D+03	0.15746D+01	0.19716D+00	0.21250D+01	
7	0.17783D+03	0.15717D+01	0.19637D+00	0.22500D+01	
8	0.23714D+03	0.15691D+01	0.19565D+00	0.23750D+01	
9	0.31623D+03	0.15668D+01	0.19500D+00	0.25000D+01	
10	0.42170D+03	0.15645D+01	0.19438D+00	0.26250D+01	
11	0.56234D+03	0.15622D+01	0.19373D+00	0.27500D+01	
12	0.74989D+03	0.15595D+01	0.19298D+00	0.28750D+01	
13	0.10000D+04	0.15560D+01	0.19200D+00	0.30000D+01	
14	0.13335D+04	0.15513D+01	0.19069D+00	0.31250D+01	
15	0.17783D+04	0.15453D+01	0.18900D+00	0.32500D+01	
16	0.23714D+04	0.15393D+01	0.18703D+00	0.33750D+01	
17	0.31623D+04	0.15311D+01	0.18500D+00	0.35000D+01	
18	0.42170D+04	0.15246D+01	0.18316D+00	0.36250D+01	
19	0.56234D+04	0.15196D+01	0.18172D+00	0.37500D+01	
20	0.74989D+04	0.15160D+01	0.18071D+00	0.38750D+01	

TABLE C-1 (Continued)

Exponential Fit Parameters For E_{22} Master Curve (AS/3502)

21	0.10000D+05	0.15136D+01	0.18000D+00	0.40000D+01
22	0.13335D+05	0.15114D+01	0.17938D+00	0.41250D+01
23	0.17783D+05	0.15090D+01	0.17868D+00	0.42500D+01
24	0.23714D+05	0.15062D+01	0.17787D+00	0.43750D+01
25	0.31623D+05	0.15031D+01	0.17700D+00	0.45000D+01
26	0.42170D+05	0.15002D+01	0.17615D+00	0.46250D+01
27	0.56234D+05	0.14975D+01	0.17538D+00	0.47500D+01
28	0.74989D+05	0.14951D+01	0.17468D+00	0.48750D+01
29	0.10000D+06	0.14928D+01	0.17400D+00	0.50000D+01
30	0.13335D+06	0.14902D+01	0.17323D+00	0.51250D+01
31	0.17783D+06	0.14870D+01	0.17232D+00	0.52500D+01
32	0.23714D+06	0.14833D+01	0.17123D+00	0.53750D+01
33	0.31623D+06	0.14791D+01	0.17000D+00	0.55000D+01
34	0.42170D+06	0.14745D+01	0.16866D+00	0.56250D+01
35	0.56234D+06	0.14697D+01	0.16723D+00	0.57500D+01
36	0.74989D+06	0.14645D+01	0.16569D+00	0.58750D+01
37	0.10000D+07	0.14588D+01	0.16400D+00	0.60000D+01
38	0.13335D+07	0.14524D+01	0.16209D+00	0.61250D+01
39	0.17783D+07	0.14452D+01	0.15994D+00	0.62500D+01
40	0.23714D+07	0.14373D+01	0.15756D+00	0.63750D+01
41	0.31623D+07	0.14289D+01	0.15500D+00	0.65000D+01
42	0.42170D+07	0.14202D+01	0.15234D+00	0.66250D+01
43	0.56234D+07	0.14113D+01	0.14963D+00	0.67500D+01
44	0.74989D+07	0.14024D+01	0.14687D+00	0.68750D+01
45	0.10000D+08	0.13932D+01	0.14400D+00	0.70000D+01
46	0.13335D+08	0.13834D+01	0.14094D+00	0.71250D+01
47	0.17783D+08	0.13731D+01	0.13769D+00	0.72500D+01
48	0.23714D+08	0.13625D+01	0.13433D+00	0.73750D+01
49	0.31623D+08	0.13521D+01	0.13100D+00	0.75000D+01
50	0.42170D+08	0.13424D+01	0.12787D+00	0.76250D+01
51	0.56234D+08	0.13336D+01	0.12504D+00	0.77500D+01
52	0.74989D+08	0.13258D+01	0.12248D+00	0.78750D+01
53	0.10000D+09	0.13183D+01	0.12000D+00	0.80000D+01
54	0.13335D+09	0.13102D+01	0.11733D+00	0.81250D+01
55	0.17783D+09	0.13010D+01	0.11427D+00	0.82500D+01
56	0.23714D+09	0.12906D+01	0.11081D+00	0.83750D+01
57	0.31623D+09	0.12794D+01	0.10700D+00	0.85000D+01
58	0.42170D+09	0.12675D+01	0.10294D+00	0.86250D+01
59	0.56234D+09	0.12548D+01	0.98587D-01	0.87500D+01
60	0.74989D+09	0.12409D+01	0.93726D-01	0.88750D+01
61	0.10000D+10	0.12246D+01	0.88000D-01	0.90000D+01
62	0.13335D+10	0.12055D+01	0.81180D-01	0.91250D+01
63	0.17783D+10	0.11845D+01	0.73529D-01	0.92500D+01
64	0.23714D+10	0.11641D+01	0.66006D-01	0.93750D+01
65	0.31623D+10	0.11482D+01	0.60000D-01	0.95000D+01
66	0.42170D+10	0.11345D+01	0.56348D-01	0.96250D+01
67	0.56234D+10	0.11221D+01	0.53870D-01	0.97500D+01
68	0.74989D+10	0.11175D+01	0.48233D-01	0.98750D+01
69	0.10000D+11	0.10765D+01	0.32000D-01	0.10000D+02
70	0.13335D+11	0.99032D+00	-0.42265D-02	0.10125D+02
71	0.17783D+11	0.95905D+00	-0.70553D-01	0.10250D+02
72	0.23714D+11	0.66477D+00	-0.17733D+00	0.10375D+02
73	0.31623D+11	0.46181D+00	-0.33553D+00	0.10500D+02

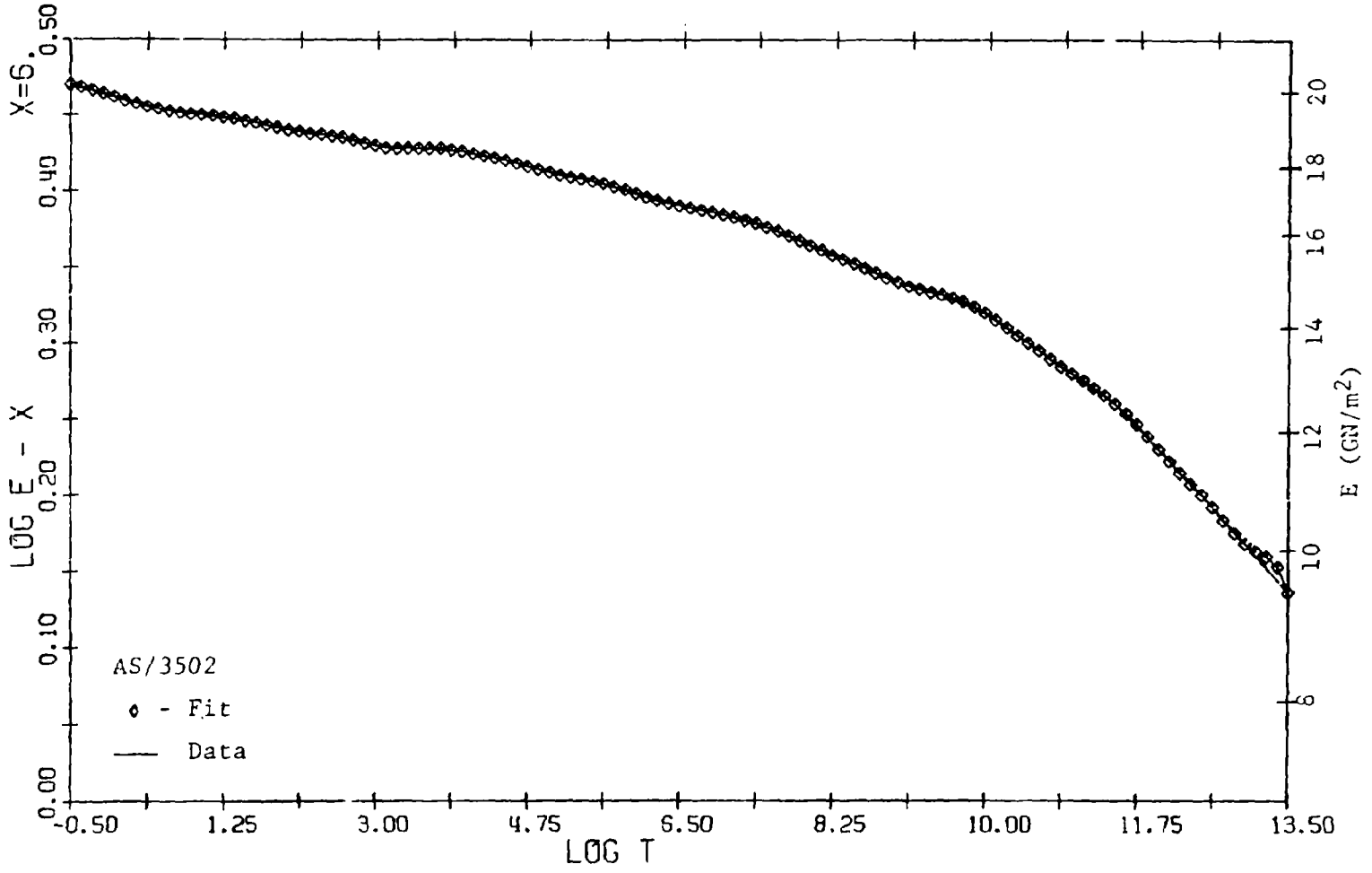

FIGURE C-1 EXPONENTIAL SERIES FIT (½ DECADE) TO E_{22} MASTER CURVE-$(90)_{15}$

$$E' = E_e + \sum_{i=1}^{N} \frac{\omega^2 \tau_i^2 E_i}{\omega^2 \tau_i^2 + 1} \tag{9}$$

and

$$E'' = \sum_{i=1}^{N} \frac{\omega \tau_i E_i}{\omega^2 \tau_i^2 + 1} \tag{10}$$

where w is the frequency and the constants (E_e, E_i, τ_i) are those found previously from the reciprocal of creep data.

2. STRESS ANALYSIS OF VISCOELASTIC LAMINATES

2.1 Lamina Constitutive Equations

By employing the accurate quasi-elastic method described in Ref. 1, the relaxation reduced lamina stiffness Q_{ij} and the laminate stiffness can be derived. Following the notation in Ref. 3, the so-called reduced stiffnesses are

$$Q_{11} = \frac{S_{22}}{S_{11}S_{22} - S_{12}^2} \tag{11}$$

$$Q_{12} = \frac{-S_{12}}{S_{11}S_{22} - S_{12}^2} \tag{12}$$

$$Q_{22} = \frac{S_{11}}{S_{11}S_{22} - S_{12}^2} \tag{13}$$

$$Q_{66} = \frac{1}{S_{66}} \tag{14}$$

where $S_{ij} = S_{ij}(\xi)$ are the principal creep compliances for the lamina. Exponential series can be fit to the $Q_{ij} = Q_{ij}(\xi)$ by the collocation method described above.

The full set of lamina constitutive equations in the lamina principal coordinate systems is

$$\sigma_1 = Q_{11}\{\epsilon_1 - \alpha_1\Delta T - \beta_1\Delta M\} + Q_{12}\{\epsilon_2 - \alpha_2\Delta T - \beta_2\Delta M\}$$

$$\sigma_2 = Q_{12}\{\epsilon_1 - \alpha_1\Delta T - \beta_1\Delta M\} + Q_{22}\{\epsilon_{22} - \alpha_2\Delta T - \beta_2\Delta M\}$$

$$\tau_{12} = Q_{66}\{\gamma_{12}\} \tag{15}$$

where $Q_{ij}\{\}$ is shorthand notation for the hereditary integral

$$Q_{ij}\{I\} \equiv \int_0^t Q_{ij}(\xi - \xi')\frac{\partial I}{\partial t'}\,dt' \tag{16}$$

and "I" represents any one of the arguments (e.g., ϵ, $-\alpha\Delta T$, $-\beta_1\Delta M$) appearing in (15). Also

$$\xi \equiv \int_0^t \frac{dt''}{a_{TM}} \quad , \quad \xi' \equiv \int_0^{t'} \frac{dt''}{a_{TM}} \tag{17}$$

where $a_{TM} = a_{TM}(T,M)$ is the temperature- and moisture-dependent shift factor. For time-independent moisture and temperature,

$$\xi = \frac{t}{a_{TM}} \quad , \quad \xi' = \frac{t'}{a_{TM}} \tag{18}$$

The expansion coefficients α_1, α_2, β_1, and β_2, in general may depend on reduced time (Ref. 1). If they are independent of reduced time, but are functions of temperature and moisture, they are properly interpreted as secant (not tangent) values.

Also, for this case, it can be shown that, without any loss of generality α_i can be taken as the coefficients in a reference moisture state; i.e., $\alpha_i = \alpha_i(T)$, but in general, $\beta_i = \beta_i(T,M)$.

2.2 Laminate Analysis for a Spacewise Uniform, Transient Temperature

For the case in which the temperature and moisture are either time-independent, or spacewise uniform or both, elastic solutions by means of the quasi-elastic method can be used to predict laminated stresses and deformations (Ref. 1). Each ply is assumed to depend on the same shift factor a_{TM}.

Let us illustrate the method by showing how laminate response can be calculated for the case of a time-dependent, spacewise-uniform temperature, in which stresses result from thermal expansion (or contraction) and external mechanical loading.

As the first step, we solve the problem for an elastic laminate using, for example, the equations in Ref. 3; in this step, the mechanical loads and temperature change ΔT are to be timewise constant. However, the reduced stiffnesses for each ply are to be those in Eqs. (11) - (14), which depend on reduced time. This so-called quasi-elastic solution should be evaluated at a series of reduced times; one or one-half decades spacing of the reduced time will normally suffice if an interpolation is used when performing the integrations described below.

Suppose the inputs are the forces N_x, N_y, N_{xy} and moments M_x, M_y, and M_{xy}, and temperature change ΔT. Consider any one response quantity of interest; say the stress $(\sigma_2)_k$ in the k-th ply. The quasi-elastic solution can always be written in the form,

$$(\sigma_2)_k = \lambda_1 N_x + \lambda_2 N_y + \lambda_3 N_{xy} + \lambda_4 M_x + \lambda_5 M_y + \lambda_6 M_{xy} + \lambda_7 \Delta T \tag{19}$$

where, in general, λ_i are functions of reduced time; they are simply the coefficients found from elastic analysis using time-dependent properties in Eqs. (11) - (14). For time-dependent inputs,

$$(\sigma_2)_k = \lambda_1\{N_x\} + \lambda_2\{N_y\} + \ldots + \lambda_7\{\Delta T\} \tag{20}$$

where, as before, $\lambda_i\{\}$ is shorthand for the integral

$$\lambda_i\{I\} \equiv \int_0^t \lambda_i(\xi - \xi')\frac{dI}{dt'}dt' \tag{21}$$

Thus the problem is reduced to elastic analysis plus numerical or analytical evaluation of the integrals (21). A numerically-efficient method for evaluating such integrals when λ_i is expressed in an exponential series is described below. For isothermal problems, the integration can often be accomplished analytically, depending, of course, on the time-dependence of the input.

2.3 Analysis for Transient and Nonuniform Temperature and/or Moisture

For the general class of problems considered here, quasi-elastic analysis cannot be used beyond the calculation of the Q_{ij} in Eqs. (11) - (14). Instead, an incremental time-marching numerical method of solution is required, such as used in Ref. 4 for cross-ply laminates.

A very efficient numerical solution for solving analogous problems involving isotropic viscoelastic materials was developed several years ago (Ref. 5) and is detailed in Ref. 6. It is based on the use of moduli which are represented in exponential series in reduced time. The shift factor a_{TM} may vary from point to point. For ease in reference, it is reproduced here, with an appropriate change of notation to treat anisotropic materials. The method is particularly suited to the finite element method. Basically, the lamina constitutive equations (15) and (16) are reduced to elastic equations for the current time step.

In order to illustrate the method, it will be sufficient to consider the numerical evaluation of an integral which is representative of those appearing in Eq. (15):

$$S = \int_0^t \phi(\xi - \xi') \frac{\partial \epsilon}{\partial t'} dt' \tag{22}$$

Let

$$\phi(\xi) = \phi_0 + \phi^*(\xi) \tag{23}$$

where $$\phi^*(\xi) = \sum_{m=1}^{M} \phi_m e^{-\beta_m \xi} \tag{24}$$

Then, Equ. (22) becomes

$$S = \phi\epsilon + \int_0^t \phi^*(\xi - \xi') \frac{\partial \epsilon}{\partial t'} dt' \tag{25}$$

The discussion deals explicitly with the effect of temperature in the equation. Moisture can be included in an analogous fashion.

2.3.1 Incremental Determination of the Constitutive Law

Subdivide the time span $\{o, t\}$ into N intervals such that $t_o = o, t_1 = t_o + \Delta t_1, \ldots, t_N = t_{N-1} + \Delta t_N = t$. For $S(x, t_N)$, $\epsilon(x, t_N)$ write S and ϵ respectively.

Assuming that $S(x\ o) = \epsilon(x\ o) = o$, Eq. (25) can be written as

$$S_N = \phi_o \epsilon_N + \int_o^{t_{N-1}} \phi^*(\xi_N - \xi') \frac{\partial \epsilon}{\partial t'} dt' + \int_{t_{N-1}}^{t_N} \phi^*(\xi_N - \xi') \frac{\partial \epsilon}{\partial t'} dt' \tag{26}$$

Now within each time interval approximate the time rate of change of each strain component using

$$\frac{\partial \epsilon}{\partial t} \doteq \frac{\epsilon_N - \epsilon_{N-1}}{\Delta t_N}, \quad t_{N-1} \le t \le t_N \tag{27}$$

Thus, Eq. (26) becomes

$$S_N = \phi_o \epsilon_N + \int_o^{t_{N-1}} \phi^*(\xi_N - \xi') \frac{\partial \epsilon}{\partial t'} dt' + \left(\frac{\epsilon_N - \epsilon_{N-1}}{\Delta t_N} \right) \int_{t_{N-1}}^{t_N} \phi^*(\xi_N - \xi') dt' \tag{28}$$

Define the quantity μ_N as

$$\mu_N = \frac{1}{\Delta t_N} \int_{t_{N-1}}^{t_N} \phi^*(\xi_N - \xi')\, dt' + \phi_0 \tag{29}$$

and let

$$L_N = \frac{1}{\Delta t_N} \cdot \epsilon_{N-1} \int_{t_{N-1}}^{t_N} \phi^*(\xi_N - \xi')\, dt' + \int_0^{t_{N-1}} \phi^*(\xi_N - \xi') \frac{\partial \epsilon}{\partial t'}\, dt' \tag{30}$$

or, using (29) in (30),

$$L_N = \left\{ \int_0^{t_{N-1}} \phi^*(\xi_N - \xi') \frac{\partial \epsilon}{\partial t'}\, dt' - (\mu_N - \phi_0)\epsilon_{N-1} \right\} \tag{31}$$

Using the definitions (29) and (36), the hereditary integral at time t_N is obtained from Eq. (28) as

$$\boxed{S_N = \mu_N \epsilon_N + L_N} \tag{32}$$

The analog of Eq. (32) appears in elasticity when considering a material subjected to thermal loading (L_N). μ_N represents the modulus for material point x at time t_N and reflects time-temperature dependence of relaxation behavior during the time interval $t_{N-1} \leq t \leq t_N$. L_N is the contribution of complete past strain and temperature history on current (t_N) response. The procedure for calculating the quantities μ_N, L_N is discussed below.

2.3.2 Determination of μ_N

Consider Eq. (29) and substitute in Eq. (24) for ϕ^*:

$$\mu_N = \frac{1}{\Delta t_N} \int_{t_{N-1}}^{t_N} \sum_{m=1}^{M} \phi_m e^{-\beta_m(\xi_N - \xi')}\, dt' + \phi_0 \tag{33}$$

The ϕ_m are time-independent material parameters; thus

$$\mu_N = \sum_{m=1}^{M} \phi_m \left\{ \frac{1}{\Delta t_N} \int_{t_{N-1}}^{t_N} e^{-\beta m(\xi_N - \xi')} \, dt' \right\} + \phi_o \tag{34}$$

Defining

$$J_{Nm} = \frac{1}{\Delta t_N} \int_{t_{N-1}}^{t_N} e^{-\beta_m(\xi_N - \xi')} \, dt' \tag{35}$$

we have

$$\boxed{\mu_N = \sum_{m=1}^{M} \phi_m J_{Nm} + \phi_o} \tag{36}$$

The problem of calculating μ_N is reduced to that of evaluating the integral J_{Nm}. The procedure for finding J_{Nm} is delayed at this point, and attention is now directed to the term L_N of Eq. (32), which is also shown to depend on the integral of Eq. (35).

2.3.3 Evaluation of L_N

Defining $\chi_N = \int_0^{t_{N-1}} \phi^*(\xi_N - \xi') \frac{\partial \epsilon}{\partial t'} \, dt'$ (37)

Eq. (31) can be written as

$$L_N = \left[\chi_N - (\mu_N - \phi_o) \epsilon_{N-1} \right] \tag{38}$$

Substitute Equ. (24) in Eq. (37) for ϕ^* and move ϕ_m from under the integral as before

$$\chi_N = \sum_{m=1}^{M} \phi_m \left\{ \int_0^{t_{N-1}} e^{-\beta_m(\xi_N - \xi')} \frac{\partial \epsilon}{\partial t'} \, dt' \right. \tag{39}$$

Let

$$C_{Nm} = \int_0^{t_{N-1}} e^{-\beta_m(\xi_N - \xi')} \frac{\partial \epsilon}{\partial t'} \, dt' \tag{40}$$

Hence

$$\boxed{\chi_N = \sum_{m=1}^{M} \phi_m C_{Nm}} \tag{41}$$

Now expand C_{Nm} as the sum of two integrals

$$C_{Nm} = \int_0^{t_{N-2}} e^{-\beta m(\xi_N - \xi')} \frac{\partial \epsilon}{\partial t'} dt' + \int_{t_{N-2}}^{t_{N-1}} e^{-\beta m(\xi_N - \xi')} \frac{\partial \epsilon}{\partial t'} dt' \tag{42}$$

or

$$C_{Nm} = e^{-\beta m \xi_N} e^{\beta m \xi_{N-1}} \left\{ \int_0^{t_{N-2}} e^{-\beta m(\xi_{N-1} - \xi')} \frac{\partial \epsilon}{\partial t'} dt' + \int_{t_{N-2}}^{t_{N-1}} e^{-\beta m(\xi_{N-1} - \xi')} \frac{\partial \epsilon}{\partial t'} dt' \right\} \tag{43}$$

From definition Eq. (40 it is seen that

$$\int_0^{t_{N-2}} e^{-\beta m(\xi_{N-1} - \xi')} \frac{\partial \epsilon}{\partial t'} dt' = C_{N-1,m} \tag{44}$$

Thus, Eq. (43) can be written as

$$C_{Nm} = e^{-\beta m(\xi_N - \xi_{N-1})} \left\{ C_{N-1,m} + \int_{t_{N-2}}^{t_{N-1}} e^{-\beta m(\xi_{N-1} - \xi')} \frac{\partial \epsilon}{\partial t'} dt' \right\} \tag{45}$$

Let $\xi_N - \xi_{N-1} = \Delta\xi_N$ and use the approximation Eq. (27) in Eq. (45):

$$C_{Nm} = e^{-\beta m \Delta \xi_N} \left\{ C_{N-1,m} + \frac{\epsilon_{N-1} - \epsilon_{N-2}}{\Delta t_{N-1}} \cdot \int_{t_{N-2}}^{t_{N-1}} e^{-\beta m(\xi_{N-1} - \xi')} dt' \right\} \tag{46}$$

But the integral appearing in Eq. (46) is defined previously in Eq. (35), hence

$$C_{Nm} = e^{-\beta m \Delta \xi_N} \left\{ C_{N-1,m} + (\epsilon_{N-1} - \epsilon_{N-2}) J_{N-1,m} \right\} \tag{47}$$

To summarize this section, the term L_N which represents a contribution of past strain-temperature-moisture history to Eq. (22) valid at time t_N, is found using Eqs. (38), (41), and (47). From the form of Eq. (47), it is seen that the effect of history is considered by means of recursive computation based on certain parameters known from the previous solution time point. In terms of numerical computation, this means that total history need not be retained for calculating a constitutive law governing current response.

In order to complete the calculations for μ_N and L_N a procedure for evaluating the integral (35) must be developed.

2.3.4 Evaluation of J_{Nm}

Recalling Eq. (35)

$$J_{Nm} = \frac{1}{\Delta t_N} \int_{t_{N-1}}^{t_N} e^{-\beta m (\xi_N - \xi)} \, dt \tag{35}$$

Now expand Eq. (35)

$$J_{Nm} = \frac{1}{\Delta t_N} \left\{ \int_{t_{N-1}}^{t_N} e^{-\beta m (\xi_N - \xi)} dt + \int_{t_{N-1}}^{t_N} e^{-\beta m a (t_N - t)} dt - \int_{t_{N-1}}^{t_N} e^{-\beta m a (t_N - t)} dt \right\} \tag{48}$$

or

$$J_{Nm} = \frac{1}{\Delta t_N} \left\{ \int_{t_{N-1}}^{t_N} e^{-\beta m a (t_N - t)} dt + \int_{t_{N-1}}^{t_N} \left[e^{-\beta m (\xi_N - \xi)} - e^{-\beta m a (t_N - t)} \right] dt \right\} \tag{49}$$

Let the change in reduced time $\Delta\xi_N$ during the time interval Δt_N be related to Δt_N through the parameter, a,

$$\xi_N - \xi_{N-1} = a(t_N - t_{N-1})$$

or

$$a = \frac{\Delta\xi_N}{\Delta t_N} \tag{50}$$

Define the quantity J^*_{Nm} as

$$J^*_{Nm} = \frac{1}{\Delta t_N}\int_{t_{N-1}}^{t_N}\left[e^{-\beta m(\xi_N - \xi)} - e^{-\beta m a(t_N - t)}\right]dt \tag{51}$$

Thus Eq. (49) becomes

$$J_{Nm} = \frac{1}{\Delta t_N}\cdot\frac{1}{a\beta_m}\cdot\left[e^{-\beta_m a(t_N - t)}\right]\Big|_{t_{N-1}}^{t_N} + J^*_{Nm} \tag{52}$$

Using Eq. (48) and performing the evaluation at the limits of integration, Eq. (52) reduces to

$$J_{Nm} = \frac{\left[1 - e^{-\beta_m \Delta\xi_N}\right]}{\beta_m \Delta\xi_N} + J^*_{Nm} \tag{53}$$

Finally consider J^*_{Nm} defined in Eq. (51)

$$J^*_{Nm} = \frac{1}{\Delta t_N}\int_{t_{N-1}}^{t_N}\left[e^{-\beta_m(\xi_N - \xi)} - e^{-\beta_m \Delta\xi_N \frac{(t_N - t)}{\Delta t_N}}\right]dt \tag{54}$$

Let

$$\tau = \frac{(t - t_N)}{\Delta t_N} + \frac{(t - t_{N-1})}{\Delta t_N}$$

which is to say that

$$\tau = \frac{\Delta t_n}{2}(\tau - 1) + t_N \;;\; t_{N-1} \le t \le t_N \tag{55}$$

Affecting a change of variable in Eq. (54),

$$J^{*}_{Nm} = \frac{1}{2}\int_{-1}^{1}\left[e^{-\beta_m(\xi_N-\xi)} - e^{-\beta_m\frac{\Delta\xi_N}{2}(1-\tau)}\right]d\tau \qquad (56)$$

Eq. (56) is in a form suitable for numerical evaluation using Gaussian Quadrature. One final step, however, must be developed in order to complete the determination of Eq. (56). Reduced time and real time must be functionally related over the interval $t_{N-1} \leq t \leq t_N$.

2.3.5 Evaluation of ξ

At a given point in space approximate the temperature as a linear function of time* within the interval Δt_N;

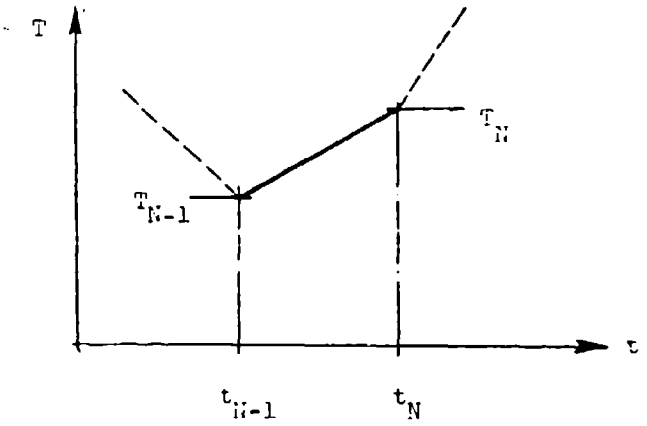

* The order of this approximation is consistent with that assigned for each strain component, see Eq. (27).

Thus

$$T(t) = A_{1N} + A_{2N} t \,, \qquad t_{N-1} \le t \le t_N \tag{57}$$

where

$$A_{1N} = \frac{T_{N-1} t_N - T_N t_{N-1}}{\Delta t_N}$$

$$A_{2N} = \frac{\Delta T_N}{\Delta t_N} \tag{58}$$

Recalling Eq. (17) and defining $\phi \equiv a_{TM}^{-1}$ and $f \equiv \ln \phi$,

$$\xi = \int_0^t \phi(T')dt' = \int_0^t e^{f(T')} dt \tag{59}$$

For the interval $t_{N-1} \le t \le t_N$ we have

$$\xi = \int_0^{t_{N-1}} e^{f(T')} dt + \int_{t_{N-1}}^{t} e^{f(T')} dt'$$

or

$$\xi = \xi_{N-1} + \int_{t_{N-1}}^{t} e^{f(T')} dt' \tag{60}$$

Now change the variable of integration to T';

$$dT' = A_{2N} dt' \,,$$

or

$$\xi = \xi_{N-1} + \int_{T_{N-1}}^{T} \frac{e^{f(T')}}{A_{2N}} d \tag{61}$$

which can be expanded to

$$\xi = \xi_{N-1} + \int_{T^*}^{T} \frac{e^{f(T')}}{A_{2N}} dT' - \int_{T^*}^{T_{N-1}} \frac{e^{f(T')}}{A_{2N}} dT' \tag{62}$$

where T* is an arbitrary value of temperature.

Define

$$Q(T) = \int_{T^*}^{T} e^{f(T')}\, dT' \tag{63}$$

Thus, using Eq. (63), Eq. (62) becomes

$$\xi = \xi_{N-1} + \frac{1}{A_{2N}} \left[Q(T) - Q(T_{N-1}) \right] \tag{64}$$

for $\xi_{N-1} \leq \xi \leq \xi_N$

Note that the change in reduced time in the interval Δt_N is found from Eq. (64) to be

$$\Delta \xi_N = \frac{1}{A_{2N}} \left[Q(T_N) - Q(T_{N-1}) \right] \tag{65}$$

Suppose that the temperature does not change in the interval Δt_N, then reduced and real time are proportional. Thus, when $A_{2N} = 0$, Eqs. (64) and (65) become

$$\xi = \xi_{N-1} + e^{f(T_{N-1})}(t - t_{N-1}) \tag{64a}$$

$$\Delta \xi_N = e^{f(T_{N-1})} \Delta t_N \tag{65a}$$

2.3.6 Summary of Computational Steps

The formulae presented in the preceding sections are for evaluating the hereditary law at time t_N for a linear viscoelastic material:

$$\boxed{S_N = \mu_N \epsilon_N + L_N}$$

Assuming that a solution has been obtained at time t_{N-1} and that the temperature and moisture distribution is known at t_N, then we can proceed to evaluating the response at t_N as follows.

$$\Delta t_N = t_N - t_{N-1} \qquad \Delta T_N = T_N - T_{N-1}$$

$$A_{1N} = \frac{T_{N-1} t_N - T_N t_{N-1}}{\Delta t_N} \qquad A_{2N} = \frac{\Delta T_N}{\Delta t_N}$$

Recalling the approximation for T(t) within Δt_N

$$T = A_{1N} + A_{2N}t,$$

Then reduced time is calculated using

$$\xi = \xi_{N-1} + \frac{1}{A_{2N}}\left[Q(T) - Q(T_{N-1})\right]$$

$$\left[\text{if } A_{2N}=0, \text{ then } \xi = \xi_{N-1} + e^{f(T_{N-1})}(t - t_{N-1})\right]$$

and

$$\xi_N = \xi_{N-1} + \frac{1}{A_{2N}}\left[Q(T_N) - Q(T_{N-1})\right]$$

$$\left[\text{if } A_{2N}=0, \text{ then } \xi_N = \xi_{N-1} + \Delta t_N e^{f(T_{N-1})}\right]$$

where

$$Q(T) = \int_{T^*}^{T} e^{f(T')}\, dT'$$

The shift function $\phi(t) = e^{f(T)}$ is conveniently defined in a numerical table (ϕ_i vs. T_i). Then Q(T) can be calculated using numerical integration at all points in T given by the input table (T^* is arbitrarily assumed to be the lowest temperature specified). The value Q(T) for $T \neq T_i$ is selected by interpolation once $Q(T_i)$ are established.

Recalling that

$$\Delta\xi_N = \xi_N - \xi_{N-1}$$

and that the relaxation function in distortion is known in terms of a Prony Series

$$\phi(t) = \phi_0 + \sum_{m=1}^{M} \phi_m e^{-\beta_m t}$$

we can evaluate the integral

$$J^*_{Nm} = \frac{1}{2}\int_{-1}^{1} \left[e^{-\beta_m(\xi_N - \xi(t'))} - e^{-\beta_m \frac{\Delta\xi_N}{2}(1-\tau)} \right] d\tau$$

$$\left[t' = \frac{\Delta t_N}{2}(\tau - 1) + t_N \right]$$

using Gaussian Quadrature.

Next form

$$J_{Nm} = \frac{\left[1 - e^{-\beta_m \Delta\xi_N}\right]}{\beta_m \Delta\xi_N} + J^*_{Nm}$$

which allows

$$\mu_N = \sum_{m=1}^{M} \phi_m J_{Nm} + \phi_0$$

to be calculated.

Using the response of the previous solution time interval, form

$$C_{Nm} = e^{-\beta_m \Delta\xi_N} \left[C_{N-1,m} + (\epsilon_{N-1} - \epsilon_{N-2}) J_{N-1,m} \right]$$

which leads directly to

$$\chi_N = \sum_{m=1}^{M} \phi_m C_{Nm}$$

which in turn allows

$$L_N = \left[\chi_N - (\mu_N - \phi_0)\epsilon_{N-1} \right]$$

to be evaluated.

The constitutive law governing each component of stress-strain is defined at this point for t_N. Thus,

$$S_N = \mu_N \epsilon_N + L_N$$

An equation of this type is to be derived for each integral in Eq. (15). The problem is thereby reduced to elastic analysis

for predictions of the current values of each S_N and ϵ_N (e.g., $\sigma_1, \sigma_2, \epsilon_1$, etc.)

REFERENCES

1. R. A. Schapery, "Viscoelastic Behavior and Analysis of Composite Materials," in Composite Materials, Vol. 2, G. P. Sendeckyj, ed., Academic Press, 1974.

2. R. A. Schapery, "A Simple Collocation Method for Fitting Viscoelastic Models to Experimental Data," Cal. Tech. Report GALCIT SM 61-23A, Nov. 1961.

3. R. M. Jones, Mechanics of Composite Materials, Scripta Book Co., Washington, D. C., 1975.

4. David Douglass, "Stresses Due to Environmental Conditioning of Graphite/Epoxy Laminates," Texas A&M University, M.S. Thesis, August 1979.

5. L. R. Herrmann and F. E. Pateroon, "A Numerical Procedure for Viscoelastic Stress Analysis," Proceedings ICRPG Mechanical Behavior Working Group, 7th Meeting, Nov. 1968.

6. K. W. Zills, Jr., F. E. Peterson, R. D. Steele, and R. C. Sampson, "Development of Criteria for Solid Propellant Screening and Preliminary Engineering Design," Aero Jet Report 1159-81F, 1968.

REFERENCES

1. R. A. Schapery, "Viscoelastic Behavior and Analysis of Composite Materials," in Composite Materials, Vol. 2, G. P. Sendeckyj, ed., Academic Press, 1974.

2. R. A. Schapery, "A Simple Collocation Method for Fitting Viscoelastic Models to Experimental Data," Cal. Tech. Report GALCIT SM 61-23A, Nov. 1961.

3. R. M. Jones, Mechanics of Composite Materials, Scripta Book Co., Washington, D. C., 1975.

4. David Douglass, "Stresses Due to Environmental Conditioning of Graphite/Epoxy Laminates," Texas A&M University, M.S. Thesis, August 1979.

5. L. R. Herrmann and F. E. Pateroon, "A Numerical Procedure for Viscoelastic Stress Analysis," Proceedings ICRPG Mechanical Behavior Working Group, 7th Meeting, Nov. 1968.

6. K. W. Zills, Jr., F. E. Peterson, R. D. Steele, and R. C. Sampson, "Development of Criteria for Solid Propellant Screening and Preliminary Engineering Design," Aero Jet Report 1159-31F, 1968.

APPENDIX D

MINIMIZATION OF RESIDUAL THERMAL STRESSES IN CROSS PLY LAMINATES

Y. Weitsman*

*Professor, Civil Engineering Department, Texas A&M Univ., College Station, TX 77840

Minimization of Residual Thermal Stresses In Cross Ply Laminates

by

Y. Weitsman*

Abstract

This work presents an analytical-numerical scheme to minimize the residual thermal stresses due to cool-down of cross ply laminates.

The analysis considers the time-dependent behavior of composites and the calculations are based upon recent data on the thermoviscoelastic response of graphite/epoxy laminates. It is shown that substantial reduction in the residual stresses can be achieved by following an optimal cool-down path.

*Professor, Civil Engineering Department, Texas A&M University, College Station, Texas 77840

1. Introduction

This work strives to apply some recent data on the time-temperature response of composites [1]*, [2] to achieve a reduction of the residual thermal stresses in composite laminates which arise upon cool-down from cure temperature to room temperature, by controlling the cool-down process.

An analytical-numerical scheme is presented whereby an optimal cool-down path is determined which minimizes the residual stresses. The analysis is based upon a recently developed scheme [3] - [5] and the numerical computations are conducted for material parameters that are representative of realistic properties.

The calculations are performed for symmetric, cross-ply laminates which contain equal numbers of 0° and 90° plies. When such laminates are subjected to fluctuating temperatures, the stiffer fibers within each ply restrain the transverse deformation of the adjacent laminas, and these mutual geometric constraints introduce substantial residual stresses in the laminate.

Since temperature causes thermal expansion, it can be considered as a stress inducing agent. On the other hand, temperature influences most significantly some of the material properties of fibrous laminates in a way which enhances the relaxation of stresses. The optimal time-temperature path achieves the best interplay among the above mentioned competing effects so as to minimize the residual thermal stress at the termination of the cool-down phase.

2. Elastic Analysis

Consider a symmetric cross-ply composite laminate, consisting of an equal number of 0° and 90° plies, exposed to fluctuating ambient temperature $T(t)$. For typical fiber-reinforced composites it is permissible to discard the precess of heat conduction and assume spatially uniform temperatures at all times t. Let C_L, C_T and C_{12}

*Numbers in brackets indicate reference listed at the end of this work.

denote ply moduli and α_L, α_T coefficients of thermal expansion, where subscripts L and T refer to the longitudinal (i.e. parallel to fiber) and transverse directions, respectively.

Consider first a geometrically constrained laminate which is subjected to a uniform temperature-increment ΔT. Elementary considerations yield the following expressions for the stress σ_x and σ_y:

$$\begin{aligned} \sigma_x^{0} &= \sigma_y^{90} = -(C_L\alpha_L + C_{12}\alpha_T)\Delta T \\ \sigma_y^{0} &= \sigma_x^{90} = -(C_T\alpha_T + C_{12}\alpha_L)\Delta T \end{aligned} \tag{1}$$

In (1) the superscripts "0" and "90" refer to the 0° and 90° laminas, respectively, assuming that the longitudinal (i.e. fiber) direction of the 0° ply coincides with the x direction of the underlying x, y Cartesian system. (Fig. 1).

Neglecting edge effects, the above stresses are relieved by spatially uniform strains ε_x and ε_y so as to yield null resultant forces F_x and F_y in the x and y directions.

Due to the assumed symmetric layup of equal numbers of 0° and 90° plies we have

$$\varepsilon_x = \varepsilon_y = \varepsilon \tag{2}$$

The strains (2) give rise to the following stresses:

$$\begin{aligned} \sigma_x^{0} &= \sigma_y^{90} = (C_L + C_{12})\varepsilon \\ \sigma_x^{90} &= \sigma_y^{0} = (C_T + C_{12})\varepsilon \end{aligned} \tag{3}$$

Combining (1) and (3) and requiring null resultant forces we get:

$$\sigma_x^{0} + \sigma_x^{90} = \sigma_y^{0} + \sigma_y^{90} = \tag{4}$$

$$= -(C_L\alpha_L + C_T\alpha_T + C_{12}\alpha_L + C_{12}\alpha_T)\Delta T + (C_L + C_T + 2C_{12})\varepsilon = 0$$

whereby

$$\varepsilon = \frac{C_L\alpha_L + C_T\alpha_T + C_{12}(\alpha_L + \alpha_T)}{C_L + C_T + 2C_{12}} \tag{5}$$

Insertion of (5) into (3) and superposition with (1) yield

$$\sigma_x^0 = \sigma_y^{90} = -\sigma_x^{90} = -\sigma_y^0 = \frac{(\alpha_T - \alpha_L)(C_L C_T - C_{12}^2)}{C_L + C_T + 2C_{12}} \Delta T \qquad (6)$$

or, in terms of compliances

$$\sigma_x^0 = \sigma_y^{90} = -\sigma_x^{90} = -\sigma_y^0 = \frac{\alpha_T - \alpha_L}{S_T + S_L - 2S_{12}} \Delta T \qquad (7)$$

3. Viscoelastic Formulation

It has been observed [1], [2] that the compliances S_L and S_{12} remain constant at all temperatures below the glass transition temperature T_g. In addition, it was possible to express the time dependent transverse compliance S_T in a "power law" form as follows

$$S_T = S_I + S_c t^q \qquad (8)$$

where S_I is the instantaneous compliance, S_c and q are material constants, and t is time.

At elevated temperatures S_T can be expressed by a thermorheologically complex relation

$$S_T(T) = S_I(T) + S_c[t/a(T)]^q \qquad (9)$$

In (9) $a(T)$ is the temperature dependent "shift-factor" function.

In the sequel we shall employ the average value of S_I over the range of temperatures relevant to our problem, thus approximating (9) by a "thermorheologically simple" expression.

Consequently, for the viscoelastic counterpart of (7), we express the compliances $(S_T + S_L - 2S_{12})$ in the form

$$B(t) = B_I + B_c t^q \qquad (10)$$

where

$$B_I = S_I^{avg.} + S_L - 2S_{12} \text{ and } B_c = S_c$$

The computation of stresses is greatly facilitated when a relaxation function $E(t)$ is employed in place of the compliance $B(t)$.

These two material properties are related by reciprocal relations in the Laplace transformed-time domain [6]

$$p\bar{E}(p) = [p\bar{B}(p)]^{-1}$$

Furthermore, an approximate inversion gives, to high degree of accuracy, the expression [7]

$$E(t) = \left.\frac{1}{p\bar{B}(p)}\right|_{p = \frac{1}{2t}} \tag{11}$$

Substitution of (10) into (11) yields

$$E(t) = \frac{1}{B_I(1 + At^q)} \tag{12}$$

where

$$A = 2^q\Gamma(q + 1)\frac{B_c}{B_I} .$$

In the subsequent analysis we shall further approximate (12) by the following expression

$$E(t) = E_0(t_0 + t)^{-q} \tag{13}$$

where E_0 and t_0 are chosen in such a manner that (13) provides good agreement with (12) over the time-span of interest.

The advantage of form (13) is that it is amenable to an analytic solution for the optimal cool-down path which, furthermore, is given by elementary functions.

Employment of (13) to represent the denominator in (7) gives the following expression for the stress $\sigma(t)$, accounting for transient viscoelastic behavior:

$$\sigma(t) = (\alpha_T - \alpha_L)E_0\int_0^t \left[\int_\tau^t \frac{ds}{a(T(s))} + t_0\right]^{-q} \frac{d\Delta T(\tau)}{d\tau}\, d\tau \tag{14}$$

In (14) $\sigma = \sigma_x^{\,0} = \sigma_y^{\,90} = -\sigma_x^{\,90} = -\sigma_y^{\,0}$

4. Optimal Cool-Down Path Which Minimizes Residual Thermal Stresses

Consider now the case of cooling from the initial cure temperature T_I down to room temperature T_R in a given time interval t_f. We search for an optimal temperature-time path $T(t)$ which minimizes $\sigma(t_f)$.

It has been shown [3], [5] that this optimal path consists of abrupt drops in temperature at $t = 0$ and at $t = t_f$. The initial drop, from T_I to T_0, is given by solving the the transcendental equation

$$T_0 - T_I = \frac{a(T_0)}{a'(T_0)} \tag{15}$$

In the open interval $0 < t < t_f$ the optimal path $T(t)$ was shown to be smooth and continuous, where it is governed by the nonlinear integro-differential equation

$$\frac{dT}{dt} = - \frac{E''(t,t_f)}{E'(t,t_f)} \frac{a'(T(t))}{a(T(t))a''(T(t))} \tag{16}$$

In (15) and (16) primes indicate derivatives with respect to the argument. Also

$$E(t_1, t_2) = E\left[\int_{t_1}^{t_2} \frac{ds}{a(T(s))}\right]$$

With given $E(t)$, $a(T)$ and T_I, the value of T_0 is determined by (15) and the optimal temperature path can be constructed by iteration through the employment of (16).

The iteration scheme consists of dividing the time interval t_f into, say, n equal sub-intervals Δt, and selecting a guess value for $T(t_f^-)$ denoted by $T_f^{(1)}$. Then, at $t = t_f^-$ (16) yields

$$\left.\frac{dT}{dt}\right|_{t = t_f^-} = - \frac{E''(0)}{E'(0)} \frac{a'(T_f)}{a(T_f)a''(T_f)} \tag{17}$$

The discretization of t_f into increments Δt gives

$$T(t_f - \Delta t) = T_f + \frac{E''(0)}{E'(0)} \frac{a'(T_f)}{a(T_f)a''(T_f)}$$

Now that both T_f and $T(t_f - \Delta t)$ are determined it is possible to extrapolate (16) back to $t = t_f - 2\Delta t$ and determine $T(t_f - 2\Delta t)$. The procedure extends backward up to $t = 0$. Obviously, it is to be expected that the value of $T(0)$, thus extrapolated, will not correspond to the value of T_0 as determined by (15). If $T(0) > T_0$ we must select another guess value $T_f^{(2)} < T_f^{(1)}$, and vice versa. The sequel of guess values for T_f are then iterated among themselves until a value of T_f is found which yields $T(0) = T_0$ to within a desired accuracy.

It is clear that the appropriate value of T_f will generally differ from the room temperature T_R. Consequently, a second abrupt variation in temperature is needed at time t_f to reach the prescribed value of T_R.

With the optimal temperature-path thus determined, the stresses at all times t, and in particular at $t = t_f^+$, can be determined by the numerical, time-discretized, evaluation of (14).

A particular simplification occurs for a "power law" response, as expressed in (12), when the shift-factor function is given by

$$a(T) = \exp\left(-\frac{T}{A} + B\right) \tag{18}$$

In this case it has been shown [5] that the optimal path is given by

$$T = \frac{1}{C} \ln \frac{L}{K + Ct} \tag{19}$$

where

$$C = \frac{q}{(q+1)A} \quad \text{and} \quad L = K \exp(CT_0)$$

while K is determined as the root of the transcendental equation

$$Ke^{CT_0} = \left[\frac{e^{B} t_0 (K + Ct_f)^{\frac{1}{q}}}{(q+1)A}\right]^{\frac{q}{q+1}}$$

Substitution of (18) and (19) into (14) yields, after several manipulations:

$$\sigma(t) = (\alpha_L - \alpha_T)E_0\left\{\int_0^t \left[Q\left[(K + C\tau)^{-\frac{1}{q}} - (K + Ct)^{-\frac{1}{q}}\right] + t_0\right]^{-q} \frac{d\tau}{K + C\tau}\right.$$

$$\left. + \left[Q\left[K^{-\frac{1}{q}} - (K + Ct)^{-\frac{1}{q}}\right] + t_0\right]^{-q} (T_I - T_0)\right\}. \qquad (20)$$

In (20) $Q = (q + 1)Ae^{-B}L^{\frac{q+1}{q}}$

At $t = t_f^-$, $\sigma(t_f^-)$ is obtained by setting t_f^- in place of t in (20).

At $t = t_f^+$:

$$\sigma(t_f^+) = \sigma(t_f^-) + (\alpha_L - \alpha_T)E_0 t_0^{-q}(T_f - T_R) \qquad (21)$$

5. Numerical Computations and Results

The numerical evaluation of (20) was obtained by discretizing the time t. For this purpose the interval t_f was divided into n equal sub-intervals $\Delta t = t_f/n$ and n intermediate values of time $t_j = (j - 1)\Delta t$, $j = 1,2,\ldots n+1$ were considered.

The temperatures $T_j = T(t_j)$ are obtained directly from (19).

The stress $\sigma_1 = \sigma(t_1) = \sigma(0^+)$, immediately after the initial drop from T_I to T_0, is given by

$$\sigma_1 = (\alpha_L - \alpha_T)E_0 t_0^{-q}(T_I - T_0) \qquad (22)$$

while the stresses at all subsequent times, during cool-down, are given by

$$\sigma_{j+1} = \sigma(t_{j+1})$$

$$= (\alpha_L - \alpha_T)E_0 \left\{ \frac{\Delta t}{2} \sum_{i=1}^{j} \left[\frac{[Q\left((K+Ct_{i+1})^{-\frac{1}{q}} - (K+Ct_{j+1})^{-\frac{1}{q}}\right) + t_0]^{-q}}{K + Ct_{i+1}} \right.\right.$$

$$\left.\left. + \frac{[Q\left((K+Ct_i)^{-\frac{1}{q}} - (K+Ct_{j+1})^{-\frac{1}{q}}\right) + t_0]^{-q}}{K+Ct_i} \right] \right.$$

$$\left. + [Q\left(K^{-\frac{1}{q}} - (K+Ct_{j+1})^{-\frac{1}{q}}\right) + t_0]^{-q} (T_I - T_0) \right\} \qquad (23)$$

with $j = 1,2,\ldots n$.

The stress at t_f^+, following the cool-down from $T_f = \frac{1}{C} \ln \frac{L}{K + Ct_f}$ to T_R, is obtained from (21).

Numerical computations were carried out for the following material parameters:

(a) Compliances and moduli:

$S_L = 0.5277 \times 10^{-7}\ (psi)^{-1}$ $\quad S_{12} = -0.1847 \times 10^{-7}\ (psi)^{-1}$

$S_T = S_I + S_c t^q$ $\quad S_I = 5.634 \times 10^{-7}\ (psi)^{-1}$ $\quad q = 0.18$

$S_c = 0.235 \times 10^{-7}\ (psi)^{-1}\ per(min)^{0.18}.$

These compliances were fitted into a relaxation-modulus given in (13), with $E_0 = 3.18 \times 10^7$ psi and $t_0 = 5.711 \times 10^7$ min.

(b) Coefficients of thermal expansion:

$\alpha_L = -0.17 \times 10^{-6}$ in/in/1°K $\quad \alpha_T = 7.94 \times 10^{-6}$ in/in/1°K

$T_I = 450°K(=350°F) \quad T_R = 297°K(=75°F)$

(c) Shift-factor function

$a(T) = \exp(-\frac{T}{A} + B)$ T in degrees Kelvin, A = 6.284

B = 47.265.

Results are shown in Figs. 2 and 3. In Fig. 2 the optimal temperature paths T(t) and the ensuing stresses $\sigma(t)$ are shown for cool-down times t_f = 31 min. (solid lines) and t_f = 100 min. (dashed lines).

Note the discontinuities in the paths T(t) and $\sigma(t)$ at t = 0 which are independent of t_f.

A second discontinuity occurs at the termination of cool-down when both optimal paths sustain sharp drops which lower the temperature down to T_R = 297°K. These drops are accompanied by sudden increases in $\sigma(t)$. Observe also the typical steepening of the path T(t), and the accompanying stress path $\sigma(t)$, for the shorter value of t_f. We also observe that while T(t) decreases monotonically during cool-down the stress $\sigma(t)$ oscillates at short times.

Fig. 3 demonstrates the reduction of residual thermal stress $\sigma(t_f^+)$ with cooling time t_f. Note that reductions of about 25% are attained.

6. Summary and Conclusions

The analysis presented herein, which draws upon relevant data for graphite-epoxy laminates, indicates that substantial reductions in the residual thermal stress due to cool-down can be achieved by following an optimal cooling path in time. Several approximations were employed in modeling the visco-elastic response of the laminate. These include the averaging of the initial compliance, the utilization of an approximate form for the relaxation modulus, and the assumption that data from aged composites applies to freshly cured laminates. Those approximations and assumptions will merit more careful consideration in the future.

References

[1] "Time-Dependent Environmental Behavior of Graphite/Epoxy Composites". General Dynamics Corp., Fort Worth Division. Quarterly Reports Nos. 1 - 7. (Oct. 1977 - May 1979).

[2] Renton, W.J. and Ho, T.: "The Effect of Environment on the Mechanical Behavior of AS/3501-6 Graphite Epoxy Material". Final Report, Vought Corp., August 1978.

[3] Weitsman, Y. and Ford, D.: "On the Optimization of Cool-Down Temperatures in Viscoelastic Resins". Recent Advances in Engineering Science". Proc. 14th Annual Meeting of SES, Nov. 1977. G.C. Sih, Editor, pp. 323-339.

[4] Weistman, Y.: "Residual Thermal Stresses due to Cool-Down of Epoxy-Resin Composites". J.App. Mechanics, ASME, Sept. 1979 (Forthcoming).

[5] Weitsman, Y.: "Discontinuous Temperature Paths Which Minimize Residual Thermal Stresses in Linear Viscoelastic Materials". (Forthcoming)

[6] Fung, Y.C.: "Foundations of Solid Mechanics" Prentice-Hall, 1965, p. 917.

[7] Schapery, R.A.: "Stress Analysis of Viscoelastic Composite Materials". J. Composite Materials, Vol. 1, 1967, pp. 228 - 266.

Figure Titles:

Fig. 1: A Symmetric Laminate Consisting of Equal Number of 0° and 90° Plies.

Fig. 2: Optimal Cool-Down Paths T(t), and the Accompanying Values of the Thermal Stress $\sigma(t)$, Vs. Time t During Cool-Down, for Two Values of Cool-Down Time, t_f = 31.6 min. (Solid Lines) and t_f = 100 min. (Dashed Lines) T in °K and σ in psi. Note the Sudden Drop at t = 0 from T_I = 450° K to T_0 = 443.72° K Accompanied by a Sudden Rise in Stress to 65.1 psi.

Fig. 3: The Residual Stress $\sigma(t_f^+)$, at Termination of Cool-Down, Along Optimal Path, Vs. Cooling Time t_f (in Minutes). Note the Logarithmic Scale for t_f. σ in psi. The Elastic Value of 1900 psi is shown by a Dashed Horizontal Line.

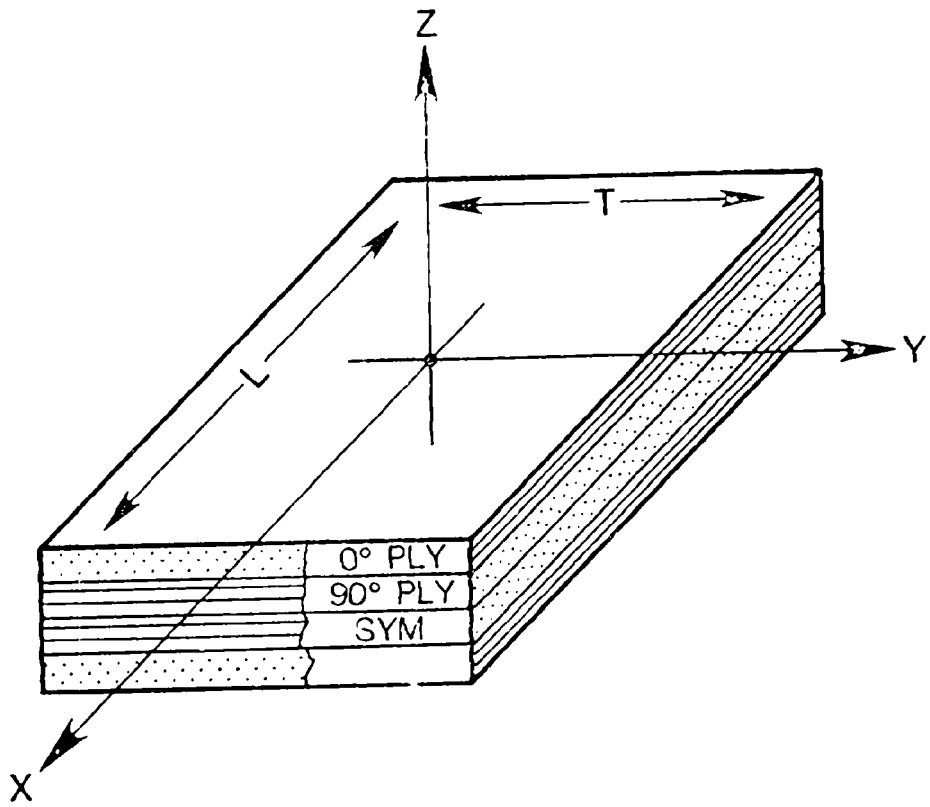

Figure 1. Symmetric Laminate With Equal Number of 0° and 90° Plies.

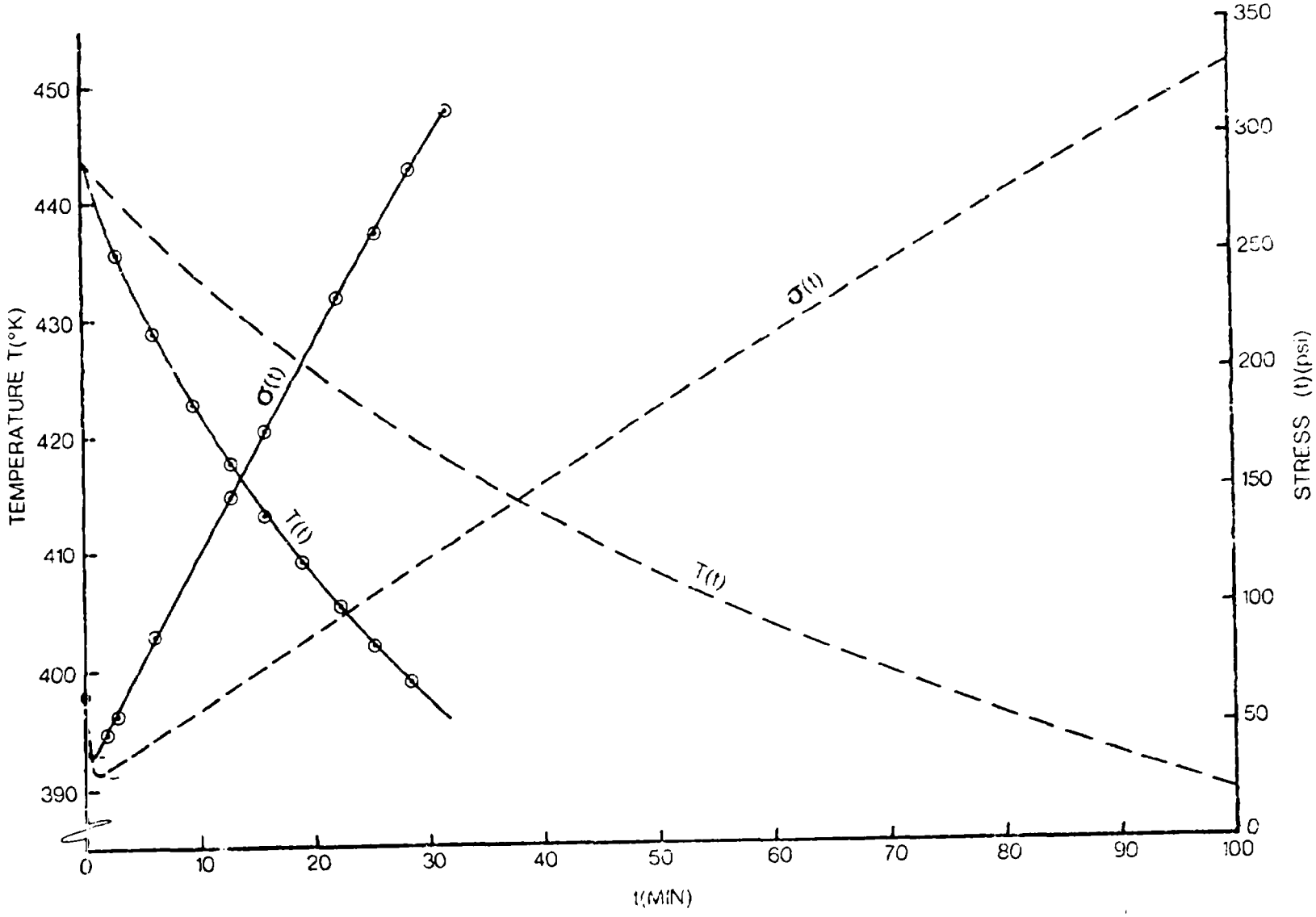

Figure 2. Optimal Cool-Down Paths T(t) for Two Values of Cool-Down Time.

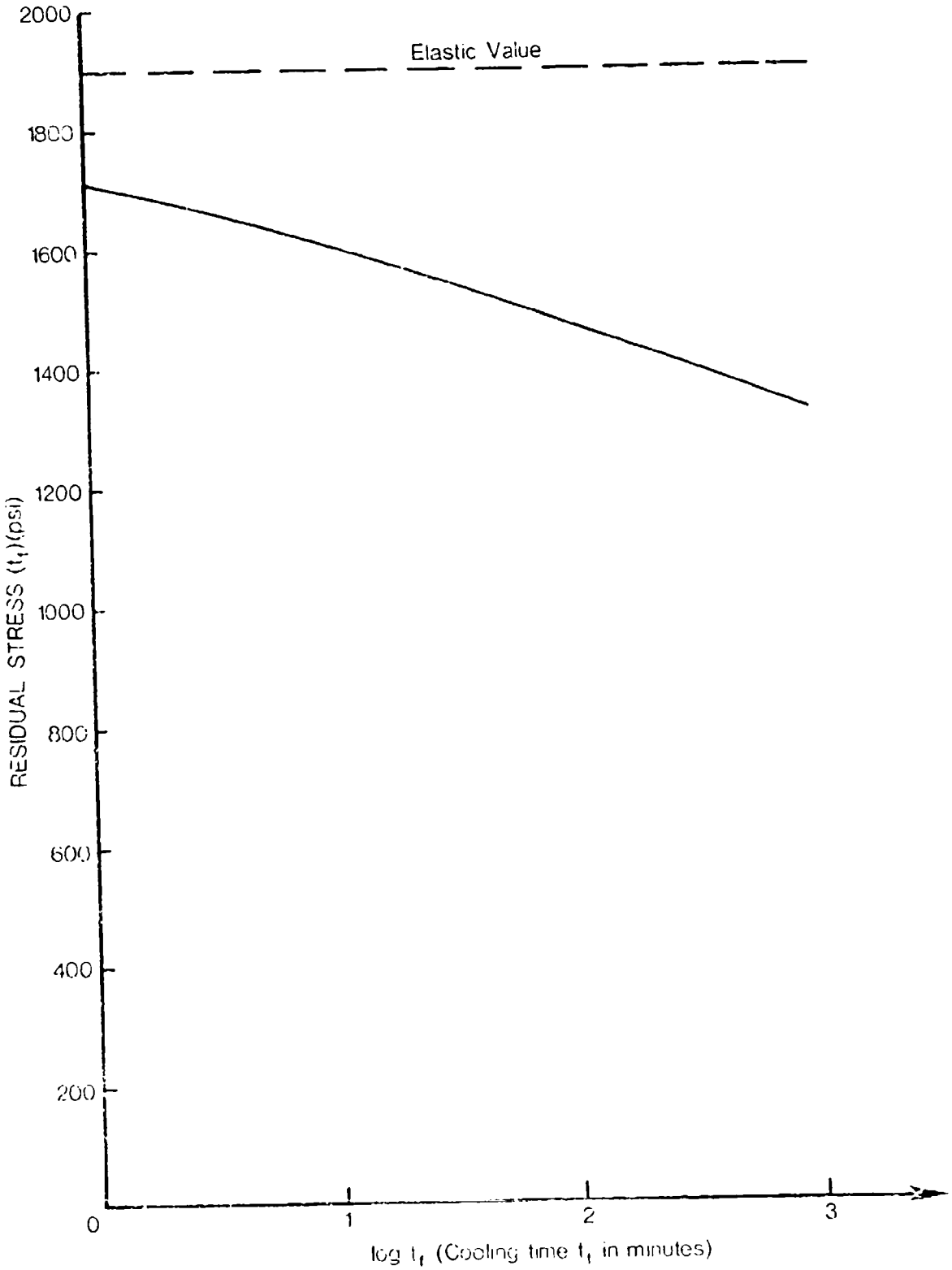

Figure 3. Residual Stress at Termination of Cool-Down Along Optimal Path.

*U.S.Government Printing Office: 1980 – 657-084/122